

PL-TR-97-2094

CALCULATIONS OF SELF-BROADENED LINE WIDTHS AND DATABASE MAINTENANCE FOR HITRAN

Robert R. Gamache

Department of Environmental, Earth, and Atmospheric Sciences
University of Massachusetts Lowell
1 University Avenue
Lowell, MA 01854

AUGUST 1997

Final Report

May 6, 1992 to August 6, 1997

19980122 088

Approved for public release; distribution unlimited.



PHILLIPS LABORATORY
Directorate of Geophysics
AIR FORCE MATERIEL COMMAND
HANSCOM AFB, MA, 01731-3010

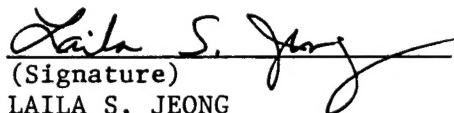
DTIC QUALITY INSPECTED 3

"This technical report has been reviewed and is approved for publication"



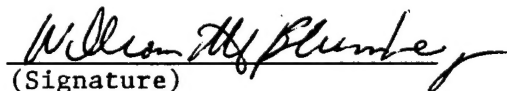
(Signature)

ROBERT L. HAWKINS
Contract Manager



(Signature)

LAILA S. JEONG
Branch Chief



(Signature)

WILLIAM A.M. BLUMBERG
Division Director

This report has been reviewed by the ESC Public Affairs Office (PA) and is releasable to the National Technical Information Service (NTIS).

Qualified requestors may obtain additional copies from the Defense Technical Information Center (DTIC). All others should apply to the National Technical Information Service (NTIS).

If your address has changed, if you wish to be removed from the mailing list, or if the addressee is no longer employed by your organization, please notify PL/IM, 29 Randolph Road, Hanscom AFB, MA 01731-3010. This will assist us in maintaining a current mailing list.

Do not return copies of this report unless contractual obligations or notices on a specific document require that it be returned.

REPORT DOCUMENTATION PAGE

Form Approved
OMB No. 0704-0188

Public reporting burden for this collection of information is estimated to average 1 hour per response, including the time for reviewing instructions, searching existing data sources, gathering and maintaining the data needed, and completing and reviewing the collection of information. Send comments regarding this burden estimate or any other aspect of this collection of information, including suggestions for reducing this burden, to Washington Headquarters Services, Directorate for Information Operations and Reports, 1215 Jefferson Davis Highway, Suite 1204, Arlington, VA 22202-4302, and to the Office of Management and Budget, Paperwork Reduction Project (0704-0188), Washington, DC 20503.

1. AGENCY USE ONLY (Leave Blank)		2. REPORT DATE August 1997		3. REPORT TYPE AND DATES COVERED Final (6 May 1992 - 6 August 1997)	
4. TITLE AND SUBTITLE Calculations of Self-Broadened Line Widths and Database Maintenance for HITRAN				5. FUNDING NUMBERS PE 61102F PR 2310 TA G1 WU BS Contract F19628-92-K-0018	
6. AUTHOR(S) Robert R. Gamache				8. PERFORMING ORGANIZATION REPORT NUMBER	
7. PERFORMING ORGANIZATION NAME(S) AND ADDRESS(ES) University of Massachusetts Lowell Dept. of Environmental, Earth & Atmospheric Section One University Avenue Lowell, MA 01854				10. SPONSORING/MONITORING AGENCY REPORT NUMBER PL-TR-97-2094	
9. SPONSORING/MONITORING AGENCY NAME(S) AND ADDRESS(ES) Phillips Laboratory 29 Randolph Road Hanscom AFB, MA 01731-3010 Contract Manager: Robert L. Hawkins / GPOS				10. SPONSORING/MONITORING AGENCY REPORT NUMBER PL-TR-97-2094	
11. SUPPLEMENTARY NOTES					
12a. DISTRIBUTION/AVAILABILITY STATEMENT Approved for public release; distribution unlimited				12b. DISTRIBUTION CODE	
13. ABSTRACT (Maximum 200 words) Total internal partition functions were calculated and polynomial coefficients determined for all species present on the 1992 HITRAN database and for some of the additional species on the 1996 HITRAN database. All spectroscopic parameters for the oxygen molecule have been recalculated and files created for HITRAN96. Halfwidths and line shifts for a number of bands of water vapor have been calculated using the Complex Robert-Bonamy Formalism (CRBF) method developed at UMass Lowell and a comparison with experimental measurements made. The results of the calculations are summarized. The calculations of spectral parameters for other species on HITRAN are discussed. These include work done on ozone, hydrogen halides, carbon monoxide, NH ₃ , H ₂ O ₂ , Transition moment squared, the addition of other molecules to the database, and degeneracy factors. A discussion of the work done on the high temperature molecular database, HITEMP, is discussed. Finally, important relationships between the Einstein coefficients, line intensities, integrated line intensities, transition moments squared, oscillator strengths, and degeneracy factors are derived and presented. Warnings of numerous errors in the literature for these factors are discussed and corrections issued.					
14. SUBJECT TERMS Total internal partition sum, CRBF calculations, halfwidth, line shift, intensity, spectral parameters, transition moment squared, atmospheric molecular species, Einstein-A coefficient, degeneracy factors.				15. NUMBER OF PAGES 136	
17. SECURITY CLASSIFICATION OF REPORT Unclassified				18. SECURITY CLASSIFICATION OF THIS PAGE Unclassified	
19. SECURITY CLASSIFICATION OF ABSTRACT Unclassified				20. LIMITATION OF ABSTRACT SAR	

TABLE OF CONTENTS

	Page
1.0 TOTAL INTERNAL PARTITION FUNCTIONS	1
2.0 SPECTROSCOPIC PARAMETERS FOR THE OXYGEN MOLECULE	18
2.1 General Theory	19
2.2 Line Intensity	23
2.3 Halfwidths	31
2.4 Updates to the Oxygen Data for the 1996 HITRAN Database	33
2.4.1 The principal isotopic species, $^{16}\text{O}_2$.	35
2.4.2) The $^{16}\text{O}^{18}\text{O}$ species	45
2.4.3) The $^{16}\text{O}^{17}\text{O}$ species	46
2.5 Other Changes	47
2.6 O_2 Continuum Absorption	47
3.0 HALFWIDTHS AND LINE SHIFTS OF H_2O TRANSITIONS	49
3.1 Complex Robert-Bonamy Formalism	53
3.2 Calculations	63
3.3 Results and Discussion	67
4.0 PROGRAMS FOR THE HITRAN DATABASE	81
4.1 Transition Moment Squared	82
4.2 State Independent Degeneracy Factors	83
5.0 SPECTRAL PARAMETERS FOR SPECIES THE DATABASE	85

5.1	Errors in the 1992 data for Hydrogen Halides and Carbon Monoxide	85
5.2	Vibrational Band Centers	86
5.3	Other Species Data for HITRAN	87
5.4	Ozone Data for the 1996 Edition of HITRAN	89
5.5	NH ₃ for HITRAN96	89
5.6	Transition Moment Squared for Ozone Molecule	93
5.7	Halfwidths for Transitions of H ₂ O ₂	95
5.8	State Independent Degeneracy Factors for New Species on the Database	96
6.0	EINSTEIN A COEFFICIENT, INTEGRATED BAND INTENSITY, AND DEGENERACY FACTORS.	97
7.0	HITEMP	107
8.0	REFERENCES	110
9.0	ACKNOWLEDGMENTS	125

LIST OF TABLES

Table		Page
1.	Ranges, temperatures, grid spacing of fits and final range of application of the polynomial.	6
2.	Percent Error across the Temperature Range Boundaries.	6
3.	Comparison of the TIPS values with literature values	9
4.	Species for which Coefficients are Set to Default Values	17
5.	Species for which Coefficients are Reported and Error>1%	17
6.	Q(296K) from Interpolating Polynomial	18
7.	Electronic-vibrational bands of O ₂ in the 1996 HITRAN data.	20
8.	Vibrational band intensities and Einstein-A coefficients for the $b^1\Sigma^+_g \leftarrow X^3\Sigma^-_g$ band of O ₂ .	29
9.	Halfwidths for the A- and B-bands of O ₂ .	34
10.	Measured intensities (Brault and Brown ⁶⁸) of the $a^1\Delta_g (v=0) \leftarrow X^3\Sigma^-_g (v=0)$ band, final HITRAN96 values, ratios, and final average ratio.	41
11.	Measured band intensities, derived Einstein-A coefficients, and statistical degeneracy factors for the $a^1\Delta_g (v=0) \leftarrow X^3\Sigma^-_g (v=0)$ band.	42
12.	Values of electrostatic moments for the water vapor, N ₂ , O ₂ , CO ₂ , H ₂ .	64
13.	Values of the heteronuclear atom-atom Lennard-Jones (6-12) parameters for the collision pairs	

	considered in this work.	65
14.	Values of the isotropic atom-atom parameters used to define the trajectories of the collision systems considered in this work.	65
15.	Values of the polarizability and ionization potential for N ₂ , O ₂ , CO ₂ , H ₂ .	66
16.	Average percent differences between the measured ¹¹⁹ and CRBF calculated halfwidths and line shifts for the water vapor-nitrogen system.	78
17.	Average percent differences between the measured ¹¹⁹ and CRBF calculated halfwidths and line shifts for the water vapor-oxygen system.	79
18.	Average percent differences between the measured ¹¹⁶ and CRBF calculated halfwidths and line shifts for the water vapor-carbon dioxide system.	79
19.	Average percent differences between the measured ¹²² and CRBF calculated halfwidths and line shifts for the water vapor-hydrogen system.	80
20.	State Independent Degeneracy Factors	84
21.	New Molecules and Isotopomers Added to the HITRAN Database since the 1986 Edition.	88
22.	Ozone Files for the 1996 HITRAN Compilation	90
23.	NH ₃ Data Files	91
24.	Coefficients of Polynomial in Eq. (1) for N ₂ - and O ₂ -Broadening of NH ₃	93
25.	Partition Functions at 296K for Ozone Molecule	94
26.	Transition Moment Squared for O ₃ Transitions in the	

	990-1010 cm^{-1} region from the 1992, scaled 1992, and 1996 HITRAN Databases	94
27.	Measured band intensities, derived Einstein-A coefficients, and statistical degeneracy factors for the $a^1\Delta_g (v=0) \leftarrow X^3\Sigma^-_g (v=0)$ band.	98

LIST OF FIGURES

Figure		Page
1.	Q(T) for H ₂ O, CH ₄ , and HNO ₃ vs. T in the range 70-500 K.	15
2.	Q(T) for H ₂ O, CH ₄ , and HNO ₃ vs. T in the range 500-1500 K.	15
3.	Q(T) for H ₂ O, CH ₄ , and HNO ₃ vs. T in the range 1500-3000 K.	16
4.	State diagram for the 3 lowest electronic levels of the oxygen molecule, X ³ Σ ⁻ _g , a ¹ Δ _g , and b ¹ Σ ⁺ _g , and their statistical weights.	23
5.	Halfwidth data cm ⁻¹ atm ⁻¹ at 296K for the A-, B- and γ-bands of O ₂ according to branches as a function of N.	32
6.	A-band halfwidths cm ⁻¹ atm ⁻¹ at 296K, RR and RQ values are shifted, N'' → N''+2.	32
7.	Energy difference in cm ⁻¹ between the formalism of Rouillé et al. ⁵³ and Ref. 57 versus N for the v''=0 band of X ³ Σ ⁻ _g of ¹⁶ O ₂ .	36
8.	Energy difference in cm ⁻¹ between the formalism of Rouillé et al. ⁵³ and Ref. 57 versus N' for the v''=1 band of X ³ Σ ⁻ _g of ¹⁶ O ₂ .	38
9.	Geometry for H ₂ O-A ₂ system. R is the center of mass separation and ω is the relative orientation. The molecular fixed axis's are defined relative to the space fixed axis by Euler angles.	56
10.	Halfwidth in units of cm ⁻¹ atm ⁻¹ for water vapor transitions in the 3ν ₁ +ν ₃ vibrational band perturbed by O ₂ versus energy ordered index (see text). Measurements of Grossmann and Browell ¹¹⁹ are plotted with error bars, 0 th order calculations with diamond symbols, 4 th order calculations with	

- circle symbols, and 8th order calculations with triangle symbols (order refers to the expansion of the atom-atom potential). 68
11. Line shifts in units of $\text{cm}^{-1} \text{ atm}^{-1}$ for water vapor transitions in the $3\nu_1 + \nu_3$ vibrational band perturbed by O_2 versus energy ordered index (see text). Measurements of Grossmann and Browell¹¹⁹ are plotted with error bars, 0th order calculations with diamond symbols, 4th order calculations with circle symbols, and 8th order calculations with triangle symbols (order refers to the expansion of the atom-atom potential). 69
12. Line shifts in units of $\text{cm}^{-1} \text{ atm}^{-1}$ for water vapor transitions in the $3\nu_1 + \nu_3$ vibrational band perturbed by nitrogen versus energy ordered index (see text). Calculations with various levels of the imaginary terms: RS_2 calculated values (diamond symbols), RS_1 calculated values (circle symbols), CRBF calculated values (triangle symbols) compared with the experimental data of Grossmann and Browell.¹¹⁹ 72
13. Line shifts for H_2O transitions broadened by CO_2 . Plotted are line shifts in units of $\text{cm}^{-1}/\text{atm}$ versus transition number from Table I of Ref. 116; Measurements with error bars, CRBF as solid circles, RS_2 as solid triangles, and RS_1 as solid squares. 73
- 14.. Halfwidths in units of $\text{cm}^{-1} \text{ atm}^{-1}$ for water vapor transitions in the $3\nu_1 + \nu_3$ vibrational band perturbed by

- oxygen. Measurements of Grossmann and Browell¹¹⁹ are plotted with error bars, results by RRB calculations with circle symbols, and results by CRBF calculations with triangle symbols. 75
15. Halfwidths for H₂O transitions broadened by CO₂. Plotted are halfwidths in units of cm⁻¹ atm⁻¹ vs. transition number from Table I of Ref. 116; Measurements with error bars, CRBF as solid circles, RS₂ as solid triangles, and RRB as solid squares. 76
16. Percent difference between CRBF and RRB calculations, (CRBF-RRB)/CRBF, vs. transition number from Table I of Ref. 116. 77
17. Linear fit in J" to halfwidths of H₂O₂ 95

1.0 TOTAL INTERNAL PARTITION FUNCTIONS

The knowledge of the total internal partition sum (TIPS) is useful for a number of reasons. For a system in thermodynamic equilibrium, the states obey a Boltzmann distribution. Hence, the number density of molecules in a particular state at a given temperature can be obtained from the total internal partition function. Relationships between the intensity of a spectral line, the transition moment squared, Einstein coefficients, or oscillator strengths require the partition sum be known.^{1,2} If the intensity of a spectral line is known, the intensity at other temperatures can be obtained knowing the partition sum at both temperatures. This has important consequences when studying systems that are not isothermal, e.g. the terrestrial atmosphere. Having a database of spectral lines of all important atmospheric species^{3,4} and knowing the partition sum at atmospheric temperatures, atmospheric spectra can be inverted to obtain concentration profiles. Note, in the literature, the term partition function is synonymous with the term partition sum.

The calculations of the total internal partition sums for the list of species taken from the HITRAN database³ were made under this project. However, the determination of the TIPS is not enough. In order to be useful for reduction of spectra a rapid yet accurate means of determining the partition sum is needed.

The total internal partition sum is defined as a direct sum over all states of the molecule of the factor $\exp(-E_i/kT)$. This can be simplified by accounting for degenerate states by the formula

$$Q(T) = \sum_{\text{all states}} d_i d_j e^{-E_i/kT} \quad (1)$$

where d_i accounts for degeneracies which are state dependent. An example of such degeneracies can be found using H_2^{16}O . Because of the C_{2v} symmetry of the molecule there is a coupling between nuclear states of the hydrogens and rotational states. In the ground vibrational state, the states of odd and even K_a+K_c have degeneracy factors of 3 and 1, respectively. Thus, the degeneracy factor depends on the rotational state. The factor d_j accounts for state independent degeneracy factors. An example of such factors are the nuclear degeneracy factor that do not couple with rotational motion (e.g. non-symmetrical molecule such as CO). This gives rise to a degeneracy factor given by the product of $(2I_j+1)$, where I_j is the nuclear spin of nuclei j . Thus, for $^{12}\text{C}^{16}\text{O}$ the state independent degeneracy factor is $(2 \cdot 1/2+1)(2 \cdot 0+1)=2$. The other terms in the equation are: E_i is the total energy (electronic, vibrational, rotational, and any other quantized motion) of state i , k is the Boltzmann constant, and T is the temperature in K.

In order to calculate the partition sum the degeneracy factors and energy levels of the species in question are needed. As the energy of the state increases, the exponential factor approaches zero and the sum can be truncated with no loss of accuracy. Where this occurs depends on the temperature since kT divides the energy of the state. Accurate calculations of the partition sum can only be made by summing over all energy levels until the exponential factor no longer contributes to the sum. This can be determined by

considering $Q(T)$ versus energy and noting where $Q(T)$ does not change as additional energies are summed over. At this point the calculation of the partition sum is said to have converged.

There are many conditions for which energy levels are not known to high enough levels to calculate accurate partition sums. For these cases approximations must be made. One, called the product approximation, can be made when many energy levels are available for the ground rotational state but those for excited vibrational states are not known. The assumption amounts to expressing the energy for the excited vibrational states as the sum of the vibrational and rotational energies, $E_{vJ} = E_v + E_J$. Thus, Eq. (1) can be written

$$Q(T) = \sum_{\substack{\text{vibrational} \\ \text{states}}} d_{\text{vib}} e^{-E_{\text{vib}}/kT} \sum_{\substack{\text{rotational} \\ \text{states}}} d_{\text{rot}} e^{-E_{\text{rot}}/kT} = Q_{\text{vib}} Q_{\text{rot}} \quad (2)$$

where d_{vib} and d_{rot} are the degeneracies, and E_{vib} and E_{rot} are the energies of the vibrational and rotational states, respectively. When the energies of the rotational states are not known to high enough levels for the temperatures in question, there are a number of analytical formulas of varying degrees of accuracy that can be used. These range from crude classical formulas⁵ to sophisticated analytical developments.⁶⁻¹¹ For the species under question the following approach was taken. When all energy levels are available such that the partition sums are converged, the direct sum is used. When the energy levels of the upper vibrational states are not known but the rotational levels for the ground vibrational state are, the product

approximation is used. Finally, when there are a significant number of energy levels missing for the temperature under consideration, the best analytical formulas are used.

Once the partition functions are calculated, it is useful to organize them in a form that is convenient for rapid accurate recall. While interpolation methods can accomplish this, they require the storage of many data and can be quite slow. A polynomial expression in T has been found to reproduce the partition sums to high accuracy for most of the species on the HITRAN database and provides a rapid means of retrieving the partition sum. The expression is 3rd order in temperature and requires the storage of 4 coefficients for a given temperature range, i.e.

$$Q(T) = a + b T + cT^2 + dT^3. \quad (3)$$

The temperature range for the polynomial fit was determined by requiring that the expression reproduce the calculated partition sum to better than 1% for most of the species in the atmosphere. For heavy systems with many vibrational degrees of freedom this is not always possible, see discussion below. From test calculations the temperature ranges in Table 1 were adopted.

The procedure is as follows. First the total internal partition sums are calculated. This is done by one of several methods depending on the species in question. If all the energy levels are known to high values such that the calculation of the partition sum has converged, a direct sum over the energy levels with appropriate degeneracy factors is made. When the rotational energies of the

ground vibrational state are known but not those of the excited vibrational states, the product approximation is used. And last, conditions for which the energies are not known to high enough states for the partition sums to converge, the best available analytical formula is used. The partition sums are calculated at the temperature spacing given in Table 1 and these data are then fit to the polynomial expression of Eq. (3) where the coefficients are determined by fitting to the data using a Simplex nonlinear minimization algorithm.¹² The fitting is based on minimizing the sum of the eighth powers of the percentage differences between the model and the calculated partition functions. The use of the percentage differences reflects the way partition functions are used in calculations, as well as the accuracy of the calculations, better than absolute differences would. The use of least-eighth powers as a fitting criterion yields almost a minimax fit. A true minimax fit would produce insignificantly smaller maximum differences, but larger average differences in many cases. The resulting coefficients are then stored in a BLOCKDATA routine for recalculating the total internal partition sum by a FORTRAN program, TIPS95.FOR, which is distributed with the HITRAN database.³

Several tests were performed to insure the quality of the partition functions. The first test was to calculate the TIPS across the fitting boundaries and at 296 and 300K to compare with literature values. Calculations were made at 296, 300, 499.99, 500.01, 1499.99, 1500.01, 2000, and 2500K. In Table 2 the boundaries that have error greater than 1% across the boundary are listed, these only occurred at the 1500K boundary.

Table 1. Ranges, temperatures, grid spacing of fits and final range of application of the polynomial.

Range	Temperatures used in fit	Temperature Grid	range of polynomial
1	70-565 K	5 K	$70 \leq T \leq 500$
2	465-1565 K	20 K	$500 < T \leq 1500$
3	1465-3005 K	20 K	$1500 < T \leq 3005$

Table 2 Percent Error across the Temperature Range Boundaries.

Molecule	Isotope	1500K boundary
CO	3 8	1.3%
O ₂	6 6	1.1%
O ₂	6 8	2.0%
O ₂	6 7	1.4%

The calculated partition sums are also compared with values found in the literature. This is limited to molecules and isotopic species that have been published. Note also that in the comparisons we often need to remove the state independent nuclear factor to compare with literature values. The reason for this is that in most applications the ratio of the partition sums are used thus the state independent nuclear factors cancel so many authors leave this out. The results are presented in Table 3 and notes on these results are given below.

H₂O - In addition, for 181, 171, and 162, the state independent nuclear factors are 1, 6, and 6 and the TIPS are 179.7, 1074.6, and 882.95, respectively. The scaled values for 171 and 162 are 179.1 and 147.2 respectively.

CO₂ - State independent nuclear factor removed.

O₃ - Possibly a sum over all levels which is incorrect for ¹⁶O₃, a Bose Particle; Energies to J=69 only.

N₂O - no notes.

CO - no notes.

CH₄ - no notes.

O₂ - no notes.

NO - neglects factor of 3 from F states

SO₂ - I am not sure why this value is low.

NO₂ - no notes.

NH₃ - I am not sure why this value does not agree with other references.

HNO₃ - We give the total partition sum compared with Ref. 13 who report only Q_r. For most molecules there is only a small difference; however, for HNO₃ there are 9 vibrational fundamentals some of which are low lying, Thus, the vibrational part contributes significantly at 300K. The JPL value agrees well with the classical rotational partition sum of 27346.5.

OH - 2 F levels per J level omitted

HF - State independent nuclear factor removed.

- HCl - State independent nuclear factor removed. We note that the classical partition sums are 19.7 for both isotopomers.
- HBr - We note that the classical partition sums are 24.6 for both isotopomers.
- HI - State independent nuclear factor removed.
- ClO - Burkholder et al.'s value¹⁴ was corrected by the vibrational partition sum ($Q_v=1.017$) and multiplied by 4 to account for the F states. The JPL (Ref. 13) values do not have Q_v contained in them.
- OCS - $Q_v=1.208$ at 300K; When this is included with the JPL value the result is 1241.82, in agreement with our value.
- H₂CO - no notes.
- HOCl - no notes.
- N₂ - no notes.
- HCN - Values in the table have been multiplied by $Q_v=1.069$ to compare with the TIPS value directly.
- CH₃Cl - no notes.
- H₂O₂ - The JPL value was multiplied by $Q_v(300K)=1.02$ to compare with the TIPS value.
- C₂H₂ - The value of McDowell was multiplied by $Q_v(300K)=1.186$ to compare with the TIPS value.
- C₂H₆ - Both values contain the state independent nuclear factor ($g_j=64$), the TIPS value is for $T=296K$.

- PH₃ - The JPL value, 405.64, has been multiplied by the symmetry factor of McDowell,⁸ 8/3, and the state independent nuclear factor ($g_j=2$).
- COF₂ - The value from Ref. 23, $Q_r=59715$, was multiplied by $Q_v(296K) = .163$ to give the value in the table.
- SF₆ - The TIPS value is at 296K.
- H₂S - no notes.
- HCOOH - The JPL value, 8883.82, has been multiplied by $Q_v(300)=1.123$ and the state independent nuclear factor ($g_j=4$).
- HO₂ - The state independent nuclear factor is contained in both values.
- ClONO₂ - The JPL values for the ³⁵Cl and ³⁷Cl species, 100540 and 103108, were multiplied by $Q_v(300)=1.831$ and the state independent nuclear factor ($g_j=12$).
- NO⁺ - The state independent nuclear factor is contained in both values.

Table 3. Comparison of the TIPS values with literature values

Temp K	Ref.	Q(Ref)	Q(TIPS)
H ₂ ¹⁶ O			
300	13	178.15	178.20
225	13	116.017	115.72
150	13	63.677	63.63
75	13	23.170	23.16
296	15	174.6	174.63
420	15	295.6	294.16

Table 3. continued

Temp K	Ref.	Q(Ref)	Q(TIPS)
$^{12}\text{C}^{16}\text{O}_2$			
296	16	286.11	286.22
500	16	625.76	625.36
800	16	1625.3	1608.00
$^{13}\text{C}^{16}\text{O}_2$			
296	16	288.34	288.47 ^a
500	16	637.93	638.37
800	16	1665.3	1664.45
$^{16}\text{O}^{12}\text{C}^{18}\text{O}$			
300	17	618.41	618.47
$^{16}\text{O}_3$			
300	13	6084.16 ^b	3562.7
225	13	4563.52 ^b	2219.
296	18 ^b	3473	3481.9
$^{16}\text{O}^{18}\text{O}^{16}\text{O}$			
296	18	3599	3645
$^{16}\text{O}^{16}\text{O}^{18}\text{O}$			
296	18	7385	7462
$^{14}\text{N}^{14}\text{N}^{16}\text{O}$			
200	19	342.00	342.9
300	19	564.08	564.8
$^{12}\text{C}^{16}\text{O}$			
225	13	81.708	81.72
300	13	108.787	108.878

Table 3. continued

Temp K	Ref.	Q(Ref)	Q(TIPS)
$^{12}\text{C}^1\text{H}_4$			
300	20	598.639	602.52
$^{13}\text{C}^1\text{H}_4$			
300	20	598.600	602.50
$^{12}\text{C}^1\text{H}_3\text{D}$			
300	20	1613.818	1624.27
$^{16}\text{O}_2$			
300	13	218.655	218.65
294	21	213.9	214.26
$^{14}\text{N}^{16}\text{O}$			
300	13	1159.46	1151.38
296	22	380.03 ^b	1132
$^{32}\text{S}^{16}\text{O}_2$			
300	13	5899.297 ^b	6497.5
296	23	6345	6244.5
$^{14}\text{N}^{16}\text{O}_2$			
296	24	13618	13631
$^{14}\text{N}^1\text{H}_3$			
296	25	1057.9 ^b	570.3
300	26	580.616	581.9
300	27	589.26	581.9
$\text{H}^{14}\text{N}^{16}\text{O}_3$			
300	13	27938	35779
$^{16}\text{O}^1\text{H}$			
220	28	27.7 ^b	58.6
300	13	81.494	81.5
300	29	40.75	81.5
$^1\text{H}^{19}\text{F}$			
300	30	39.8	32.85 ^a
$^1\text{H}^{35}\text{Cl}$			
300	13	81.232	20.35 ^a

Table 3. continued

Temp K	Ref.	Q(Ref)	Q(TIPS)
$^1\text{H}^{37}\text{Cl}$ 300	13	81.352	20.38 ^a
$^1\text{H}^{79}\text{Br}$ 300	13	101.2045	25.36 ^a
$^1\text{H}^{81}\text{Br}$ 300	13	101.2511	25.36 ^a
$^1\text{H}^{127}\text{I}$ 300	30	32.025	32.85 ^a
$^{35}\text{Cl}^{16}\text{O}$ 296 300	14 13	3291 ^b 3291.54	3288 3347.4
$^{37}\text{Cl}^{16}\text{O}$ 296 300	14 13	3348 ^b 3348.11	3345 3406.0
$^{16}\text{O}^{12}\text{C}^{32}\text{S}$ 300	13	1028.25 ^b	1242
$^1\text{H}_2^{12}\text{C}^{16}\text{O}$ 300	13	2876.7	2742
$^1\text{H}_2^{13}\text{C}^{16}\text{O}$ 300	13	2949.7	2811
$^1\text{H}^{16}\text{O}^{35}\text{Cl}$ 300	13	2380	2468
$^1\text{H}^{16}\text{O}^{35}\text{Cl}$ 300	13	2422.5	2512
$^{14}\text{N}_2$ 298	31	469.7	470.28
$^1\text{H}^{12}\text{C}^{14}\text{N}$ 300 300 300	13 6 30	424.154 151.2 ^b 150.73 ^b	151.3 151.3 151.3

Table 3. continued

Temp K	Ref.	Q(Ref)	Q(TIPS)
$^{12}\text{C}^1\text{H}_3^{35}\text{Cl}$ 300	30	14770	14831
$^1\text{H}_2^{16}\text{O}_2$ 300	13	7804 ^b	7850
$^{12}\text{C}_2^1\text{H}_6$ 300	8	55940	54627 ^b
$^{31}\text{P}^1\text{H}_3$ 300	13	3226 ^b	3322
$^{12}\text{C}^{16}\text{O}^{19}\text{F}_2$ 296	32	69448	69763
$^{32}\text{S}^{19}\text{F}_6$ 300	7	1.719 E6	1.62 E6 ^c
$^1\text{H}_2^{32}\text{S}$ 296	33	505.6	503.2
$^1\text{H}_2^{33}\text{S}$ 296	33	506.2	504.5
$^1\text{H}_2^{34}\text{S}$ 296	33	506.9	503.9
$^1\text{H}^{12}\text{C}^{16}\text{O}^{16}\text{O}^1\text{H}$ 300	13	39906 ^b	39960
$^1\text{H}^{16}\text{O}_2$ 300	30	2191	2196
$^{35}\text{Cl}^{16}\text{O}^{14}\text{N}^{16}\text{O}_2$ 300	13	2209064 ^b	2208960
$^{37}\text{Cl}^{16}\text{O}^{14}\text{N}^{16}\text{O}_2$ 300	13	2265489 ^b	2265182
$^{14}\text{N}^{16}\text{O}^+$ 300	30	311.8	313.0

^a State independent nuclear factor removed.

^b See text for explanation.

^c The TIPS value is at 296K..

We have found that species with many low lying vibrational modes are not well represented by the polynomial expression. The reason is the vibrational partition sum increases very rapidly with temperature and thus the product of the rotational and vibrational partition sums increases more rapidly. The 4 term polynomial has difficulty fitting the data to the 1% uncertainty threshold. A number of the species do meet the 1% criterion; all species of CH₄ in temperature ranges 2 and 3 and all species of HNO₃ in all temperature ranges. This can be understood by looking at Figures 1, 2, and 3 which show $Q(T)$ vs. Temp for H₂O, CH₄, and HNO₃ in the three temperature ranges. HNO₃ has 9 vibrational modes starting at 458 cm⁻¹. H₂O has 3 vibrational modes starting at 1594 cm⁻¹ and CH₄ has 9 vibrational modes starting at 1311 cm⁻¹. In the range 70-500K (Figure 1), H₂O and CH₄ both rise slowly however HNO₃, because of 9 low-lying vibrational modes, is increasing rapidly. H₂O has a fit error of 0.37%, CH₄ a fit error of 0.92%, and HNO₃ a fit error of 3.6%. In Figure 2 the second temperature range is shown, HNO₃ is going off the scale and the fit error is 24%, H₂O is still relatively flat and the fit error is 0.14%, however CH₄ is starting to increase rapidly and the resulting fit error is 4.9%. In the high temperature range all the vibrational modes contribute to $Q(T)$ and in Figure 3 we see that HNO₃ is off scale and CH₄ is going off scale (6.9% fit error) but H₂O is still reasonable to fit giving an error of 0.03%. We must keep track of all species that do not meet the 1% fit criterion and make a decision on how these will be handled in the block data BD-QT.FOR routine. At present, my feeling is to flag these with negative

coefficients indication no polynomial fit was done. Other alternatives should be explored in the future.

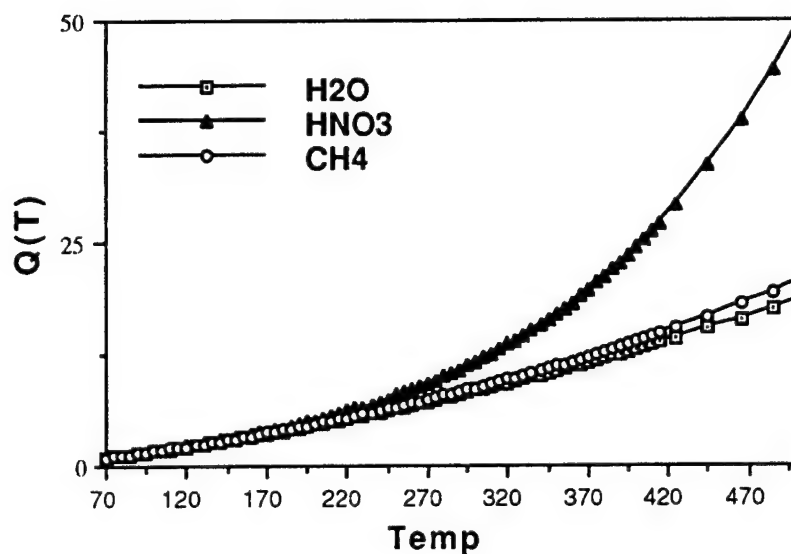


Figure 1. $Q(T)$ for H_2O , CH_4 , and HNO_3 vs. T in the range 70-500 K.

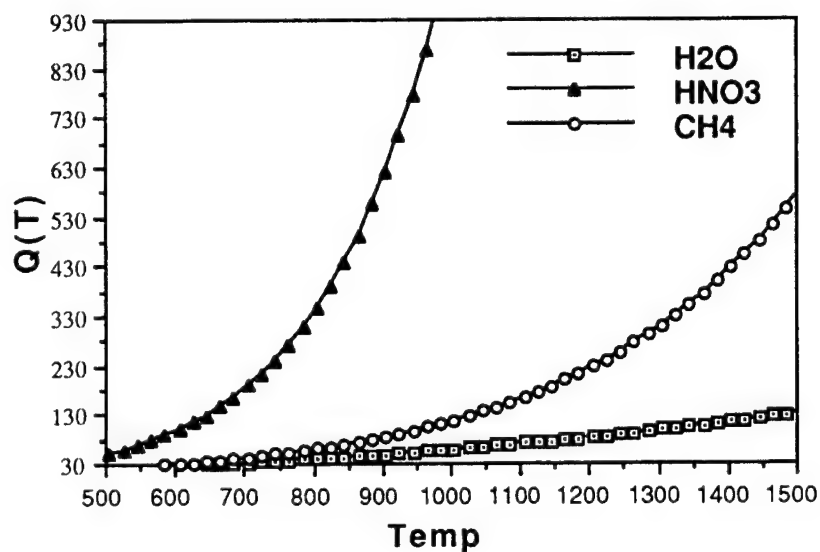


Figure 2. $Q(T)$ for H_2O , CH_4 , and HNO_3 vs. T in the range 500-1500 K.

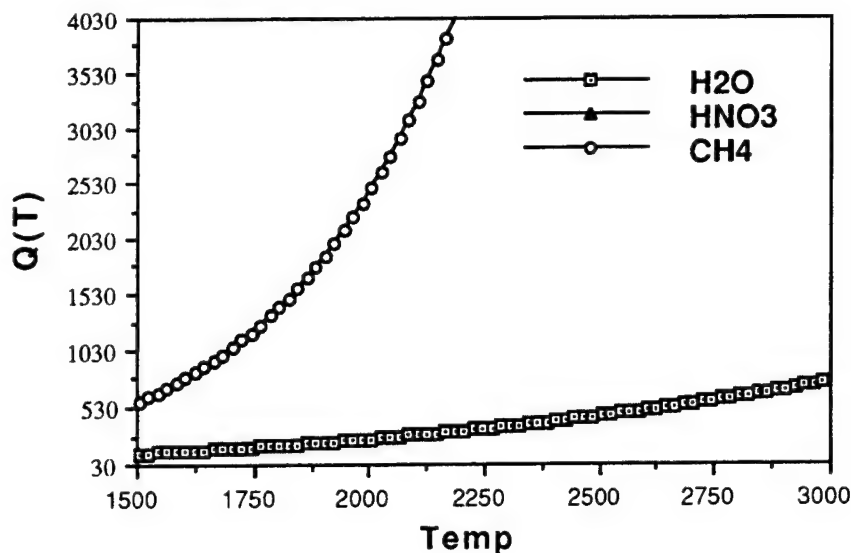


Figure 3. $Q(T)$ for H_2O , CH_4 , and HNO_3 vs. T in the range 1500-3000 K.

By studying the graphs of the error, we determined that some of the coefficients could be used for species where the error was greater than 1%. Table 4 list the species for which the coefficients were defaulted (-1, 0., 0., 0.) and Table 5 list those for which they were retained even though the error was larger than the criterion.

The routine also uses $Q(296K)$. For this the values of the partition sum at 296 K were calculated from the polynomial. For species where the polynomial fit was not good (SF_6 and $ClONO_2$) the $Q(296K)$ values were obtained by using an interpolating polynomial in Mathematica with the values of Q at 280 to 305 K in 5K steps. The values are in Table 6.

Table 4. Species for which Coefficients are Set to Default Values

Species	ISO	T Range
CH ₄	2 1 1	2 and 3
	3 1 1	2 and 3
	2 1 1	2 and 3
HNO ₃	1 4 6	1, 2, and 3
CH ₃ Cl	2 1 5	2 and 3
	2 1 7	2 and 3
C ₂ H ₆	1 2 2 1	1, 2, and 3
COF ₂	2 6 9	2 and 3
SF ₆	2 9	1, 2, and 3
HCOOH	1 2 6	2 and 3
ClONO ₂	5 6 4 6	1, 2, and 3
	7 6 4 6	1, 2, and 3

Table 5. Species for which Coefficients are Reported and Error>1%

Species	ISO	Fit Error		
		1	2	3
H ₂ CO	1 2 6		2.2	2.2
	1 3 6		2.2	2.2
	1 2 8		2.2	2.2
CH ₃ Cl	2 1 5	1.3		
	2 1 7	1.3		
PH ₃			2.7	2.5
COF ₂	2 6 9	1.7		
HCOOH	1 2 6	1.7		

Table 6 Q(296K) from Interpolating Polynomial

Species	ISO	Q(296K)
SF ₆	2 9	1.62242 x 10 ⁶
ClONO ₂	5 6 4 6	2.12829 x 10 ⁶
	7 6 4 6	2.18246 x 10 ⁶

2.0 SPECTROSCOPIC PARAMETERS FOR THE OXYGEN MOLECULE

Atmospheric spectra of oxygen are used for deducing information about properties of the atmosphere and other species in the atmosphere, for example, measurements of O₂ emission are used as a standard for O₃ profile analysis.^{34,35} There is a need to have available the most accurate parameters for this molecule. The spectrum of the oxygen molecule, even though O₂ is a simple diatomic, is unexpectedly complex. The oxygen molecule has two unpaired electrons with a total spin of 1 in the electronic ground state. There are two low-lying excited electronic states which give rise to near-IR and visible spectra, and the symmetries of the isotopomers, ¹⁶O₂, ¹⁶O¹⁸O, and ¹⁶O¹⁷O, affect the number of allowed states. In addition, both magnetic dipole and electric quadrupole transitions occur, the degeneracy of states needs to be carefully considered, and transitions occur from the microwave to the visible. Although the line intensities are usually small, the high mixing ratio and long optical path in the terrestrial atmosphere compensate to produce meaningful absorption.³⁶

In this work, the spectral parameters for the oxygen molecule are calculated for the electronic-vibrational bands listed in Table 7. These data represent an improvement to the data contained on the 1992 version of the HITRAN molecular absorption database,³ which are from calculations made in 1982.³⁷ The calculations consider the lower state energy, the wavenumber of the transition, the line intensity, and transition moment squared of the spectral lines. In addition, halfwidths as a function of transition quantum number are determined from the available experimental measurements. All fundamental physical constants used in the calculations are those reported by Cohen and Taylor.³⁸ The calculations were made in double precision on several different computer systems using codes written in FORTRAN. Below, we discuss the theory of molecular oxygen and describe the improvements to the data for each band.

2.1 General Theory

To understand the spectrum of the molecular oxygen in the atmosphere, one must consider the properties of the three most abundant isotopic species of oxygen and the structure of the three lowest-lying electronic states. An excellent review for this material can be found in Herzberg.^{5,39}

Table 7. Electronic-vibrational bands of O₂ in the 1996 HITRAN data.

Electronic Band	Isotopomer		
	¹⁶ O ₂	¹⁶ O ¹⁸ O	¹⁶ O ¹⁷ O
	v' ← v''	v' ← v''	v' ← v''
X ³ Σ _g ⁻ ← X ³ Σ _g ⁻	0 ← 0	0 ← 0	0 ← 0
	1 ← 0		
	1 ← 1		
a ¹ Δ _g ← X ³ Σ _g ⁻	0 ← 1	0 ← 0	
	0 ← 0		
	1 ← 0		
b ¹ Σ _g ⁺ ← X ³ Σ _g ⁻	0 ← 0	0 ← 0	
	1 ← 0	1 ← 0	1 ← 0
	2 ← 0	2 ← 0	
	1 ← 1		
	0 ← 1		

The theoretical treatment of the ground state of molecular oxygen was first given by Tinkham and Strandberg⁴⁰ and it was later clarified with the aid of the transformation theory of spherical tensors by Steinbach and Gordy.^{41,42} References 43 and 44 give excellent overviews of the theory. The ground electronic state of the oxygen molecule is the X³Σ_g⁻ state. There are also two low-lying electronic states, the a¹Δ_g state and the b¹Σ_g⁺ state at 7918 cm⁻¹ and 13195 cm⁻¹ above the ground state, respectively. Since the electronic ground state is the X³Σ_g⁻ state, the average electronic orbital angular momentum vanishes (Λ=0). Still, there is an instantaneous non-zero value of the orbital angular momentum which produces a precessing magnetic dipole moment of orbital

origin. The total electronic spin is $S=1$, so that molecular oxygen has a permanent magnetic dipole moment of approximately two Bohr magnetons. The energy is described in terms of the total electronic spin vector, S , and the rotational angular momentum, N . In the electronic ground state, Hund's coupling case (b) dominates³⁹ (more recent work shows the need for intermediate coupling) and the total angular momentum J is $J=N+S$. Thus, for each value of N there are 3 allowed values of J . The oxygen molecule can interact with an electromagnetic field via its magnetic dipole (md) moment or by its electric quadrupole (eq) moment. In this work, calculations are made for both md and eq lines of O_2 .

The principal isotopic species, $^{16}O_2$, is unique in that it is the only homonuclear diatomic molecule of the three isotopomers on the database. Because of this symmetry and the fact that the oxygen-16 nuclei have zero nuclear spin, the molecule behaves as a Bose particle. Thus, the total wavefunction must be symmetric with respect to inversion through the center. The spins of the individual electrons form a resultant $S=1$ that gives rise to a coupling of electronic (S) and rotational angular momentum (N) yielding a triplet of states labeled by J ; $J = N$, $J = N + 1$, and $J = N - 1$. The wavefunctions for the vibrational and nuclear motion are symmetric, whereas the electronic wavefunction for a Σ^-_g state is antisymmetric, indicating the only allowed rotational wave functions are those for odd (antisymmetric) N . The result is that one-half (all N even) of the states of $^{16}O_2$ are missing in the ground electronic state.

In the $a^1\Delta_g$ electronic state, the resultant of the individual electron spin is zero ($S=0$) giving $J=N$, but the rotational levels are

split into two, one symmetric (+) and one antisymmetric (-) state, by Λ -doubling. Because of the constraints placed on the wavefunction by Bose-Einstein statistics, only the (+) state is allowed and, although all N are occupied, only one-half of the states are realized. The $b^1\Sigma^+_g$ electronic state also has $S=0$ giving $N=J$ and the electronic wavefunction for the Σ^+_g state is symmetric as are Ψ_{nuc} and Ψ_{vib} ; thus, the only rotational wavefunctions are the symmetric (N even) ones. Because of the symmetry of the $^{16}\text{O}_2$ species and the nuclear spin $I(^{16}\text{O})=0$, one-half of the rotational states of *each* electronic level are missing.

For the two isotopic species on the database, $^{16}\text{O}^{18}\text{O}$ and $^{16}\text{O}^{17}\text{O}$, inversion through the center is no longer a valid symmetry operation. For this condition, all rotational levels of the molecule are allowed, both (+) and (-). The ground electronic state is a triplet, $J=N$ and $J=N\pm 1$, with all N allowed, $N=1,2,3,\dots$. The two low-lying electronic states, $a^1\Delta_g$ and $b^1\Sigma^+_g$ are singlets ($J=N$) with all values of N (even and odd) starting at $N_{\text{min}}=\Lambda$. Note that for the $a^1\Delta_g$ state there is Λ -type doubling, thus each N has two states.

Figure 4 is a rotational state diagram for the lowest three electronic states of O_2 . A note of caution here: the rotational states of a diatomic molecule are classified according to the behavior of the *total wavefunction* with respect to reflection at the origin and not of the rotational wavefunction alone (see pp 128-129 of Ref. 39). Thus in the diagram, the states labeled (+) in the $X^3\Sigma^-_g$ state correspond to $N=\text{odd}$ (antisymmetric) states; whereas the states labeled (+) in the $b^1\Sigma^+_g$ state correspond to $N=\text{even}$ (symmetric) states. The principal species of oxygen, $^{16}\text{O}_2$, follows Bose-Einstein statistics and as such

does not have any of the (-) symmetry levels. Thus, in the diagram all (-) states are eliminated, in the $X^3\Sigma^-_g$ state all even N levels are missing, in the $a^1\Delta_g$ state one level for each N is missing, and in the $b^1\Sigma^+_g$ state all odd N are missing. For the non-homonuclear species all levels are allowed. These symmetry factors have an important role in the statistics of the molecule. Taking the ratio of the number of levels in the $X^3\Sigma^-_g$ state to the $a^1\Delta_g$ state gives 3:2 regardless of the isotopomer (this is because for $^{16}\text{O}_2$ one-half of the levels are missing in each electronic state). Likewise the similar ratio of the $X^3\Sigma^-_g$ state to the $b^1\Sigma^+_g$ state is 3:1.

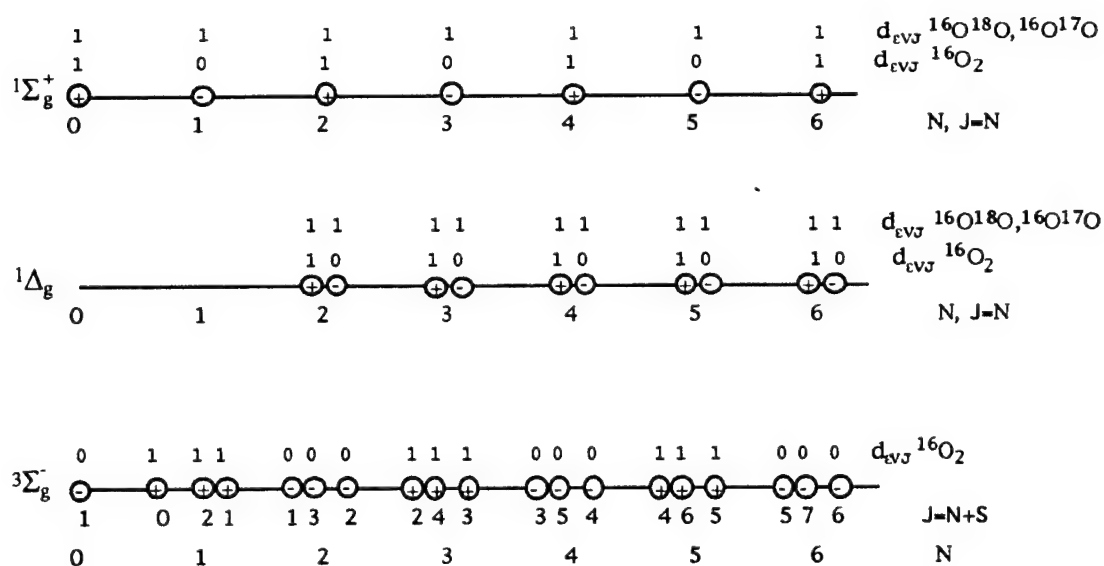


Figure 4. State diagram for the 3 lowest electronic levels of the oxygen molecule, $X^3\Sigma^-_g$, $a^1\Delta_g$, and $b^1\Sigma^+_g$, and their statistical weights.

2.2 Line Intensity

Various formulas are used to calculate the line intensities depending on the particular transition. Below these formulas are presented along with other relationships needed for the calculations.

Also presented are relationships to explain problems encountered in determining the Einstein-A coefficients for transitions in the $X^3\Sigma^-_g \rightarrow a^1\Delta_g$ band. The transitions involve, in general, different electronic, lambda doubling, vibrational, and rotational states which will be labeled by ϵ, Λ, v , and J, M , respectively with the usual spectroscopic notation of a single prime for the upper state and a double prime for the lower state. In the absence of an electric or magnetic field, the M states are degenerate and will be summed over to express the line intensity for the transition labeled by $\epsilon''\Lambda''v''J'' \rightarrow \epsilon'\Lambda'v'J'$. In the following, a shorthand notation will be adopted by substituting η for the set of quantum numbers $\epsilon\Lambda vJ$. Thus, $\eta'' \equiv \epsilon''\Lambda''v''J''$ and $\eta' \equiv \epsilon'\Lambda'v'J'$. The line intensity in units of ($\text{cm}^{-1}/\text{molec}\cdot\text{cm}^{-2}$) for a transition $\eta'' \rightarrow \eta'$ is (see Refs. 1 and 45)

$$S_{\eta'' \rightarrow \eta'} = \frac{8\pi^3}{3hc} I_a \frac{(d_{\eta''} e^{-E_{\eta''}/kT})}{d_{J''} Q(T)} \frac{\nu_{(\eta'')(\eta')}}{c} \times (1 - e^{-h\nu_{(\eta'')(\eta')}/kT}) \sum_{M'', M'} |\mathbf{R}_{(\epsilon''\Lambda''v''J''M'')(\epsilon'\Lambda'v'J'M')}|^2 10^{-36}, \quad (4)$$

where the total internal partition sum, $Q(T)$, is

$$Q(T) = \sum_{\epsilon\Lambda vJ} d_{\epsilon} d_{\Lambda} d_v d_J d_{\text{sym}} e^{-E_{\epsilon\Lambda vJ}/kT}, \quad (5)$$

and I_a is the isotopic abundance of the species, the factor 10^{-36} is needed for the units chosen, $|\mathbf{R}_{(\epsilon''\Lambda''v''J''M'')(\epsilon'\Lambda'v'J'M')}|^2$ is the transition-moment squared and has units of Debye squared/molec, $d_{\eta''}$ is the degeneracy and $E_{\eta''}$ the energy of the state η'' , $\nu_{(\eta'')(\eta')}/c = \omega_{(\eta'')(\eta')}$ is the wavenumber of the transition, and all other symbols

are the usual constants. (Note, in Eq. (4) and in a few expressions that follow we have not canceled some of the degeneracy factors in order to emphasize the fractional number of molecules in the state η'' , $N_{\eta''}$.) In this report we use the "regular" matrix elements while in the Gamache and Rothman 1992 paper¹ we used the "weighted" ones. The degeneracy factors given by the product of the degeneracy factors for the quantized motions, $d_{\eta}=d_{\epsilon}d_{\Lambda}d_{\nu}d_Jd_{\text{sym}}$ with $d_{\epsilon}=(2S+1)$, $d_{\Lambda}=(2-\delta_{\Lambda,0})$, $d_{\nu}=1$, $d_J=(2J+1)$, and d_{sym} is one for the heteronuclear species and the (+) states of the homonuclear species and zero for the (-) states of the homonuclear species. This factor accounts for the symmetry restrictions for the homonuclear diatomics (note, this gives an overall factor of 1/2 in the partition sum).

This expression can be written in terms of the Einstein-A coefficient by making use of the relationship^{4,5}

$$A_{\eta' \rightarrow \eta''} = \frac{64\pi^4}{3h} \frac{10^{-36}}{\omega_{(\eta'')(\eta')}}^3 \frac{1}{d_{J'}} \sum_{M'', M'} |R_{(\epsilon''\Lambda''\nu''J''M'')(\epsilon'\Lambda'\nu'JM')}|^2, \quad (6)$$

whence the line intensity is

$$S_{\eta' \rightarrow \eta''} = \frac{I_a}{8\pi c} \frac{(d_{\eta''} e^{-E_{\eta''}/kT})}{Q(T)} \frac{1}{\omega_{(\eta'')(\eta')}}^2 (1 - e^{-h\nu_{(\eta'')(\eta'')}/kT}) \frac{d_{J'}}{d_{J''}} A_{\eta' \rightarrow \eta''}. \quad (7)$$

The Einstein-A coefficient is usually determined from a measurement of a vibrational band intensity, $S_{\epsilon''\Lambda''\nu''}^{\epsilon'\Lambda'\nu'}$ so it is useful to formulate Eqs. (4) and (7) in terms of this quantity. The integrated intensity for an electronic-vibration-rotation band in units of $\text{cm}^{-1}/(\text{molec} \cdot \text{cm}^{-2})$ is given by^{4,5}

$$S_{\epsilon'\Lambda'v'}^{\epsilon''\Lambda''v''} = \frac{8\pi^3 10^{-36}}{3hc} \omega_{(\epsilon''\Lambda''v'')(\epsilon'\Lambda'v')} \frac{(d_{\epsilon''\Lambda''v''} e^{-E_{\epsilon''\Lambda''v''}/kT})}{Q_{\epsilon\Lambda v}} |R_{(\epsilon''\Lambda''v'')(\epsilon'\Lambda'v')}|^2 \quad (8)$$

(Note, this is similar to α/N_L (Ref. 45, p153 with $\alpha = \sum_{J''J'} S_{\epsilon''\Lambda''v''J'' \rightarrow \epsilon'\Lambda'v'J'}$) with the exception that the radiation field term, $(1 - e^{-h\nu(\eta'')(\eta')/kT})$, is explicitly retained in the rotational part of the intensity formula. Thus, our definition of $S_{\epsilon'\Lambda'v'}^{\epsilon''\Lambda''v''}$ does not contain the approximate factor $(1 - e^{-h\nu(\epsilon''\Lambda''v'')(\epsilon'\Lambda'v')/kT})$.) To implement Eq. (8), the electronic-vibration and rotation parts are separated using the product approximation for the total partition sum and the transition-moment squared, and the assumption of additivity of energy

$$\begin{aligned} Q_{\text{tot}} &= Q_{\epsilon\Lambda v} \cdot Q_{\text{rot}} , \\ \sum_{M'', M'} |R_{(\eta'')(\eta')}|^2 &= |R_{(\epsilon''\Lambda''v'')(\epsilon'\Lambda'v')}|^2 \cdot |R_{(J'')(J')}|^2 , \\ E_{\eta''} &= E_{\epsilon''\Lambda''v''} + E_{J''} . \end{aligned} \quad (9)$$

Inserting these into Eq. (4) and rearranging terms yields

$$\begin{aligned} S_{\eta'' \rightarrow \eta'} &= \frac{8\pi^3 10^{-36}}{3hc} \frac{(d_{\epsilon''\Lambda''v''} e^{-E_{\epsilon''\Lambda''v''}/kT})}{Q_{\epsilon\Lambda v}} \omega_{(\epsilon''\Lambda''v'')(\epsilon'\Lambda'v')} |R_{(\epsilon''\Lambda''v'')(\epsilon'\Lambda'v')}|^2 \\ &\times I_a \frac{(d_{J''} d_{\text{sym}} e^{-E_{J''}/kT})}{d_{J''} d_{\text{sym}} Q_{\text{rot}}} \frac{\omega(\eta'')(\eta')}{\omega_{(\epsilon''\Lambda''v'')(\epsilon'\Lambda'v')}} (1 - e^{-h\nu(\eta'')(\eta')/kT}) |R_{(J'')(J')}|^2 . \end{aligned} \quad (10)$$

The first part of this expression is simply the band intensity as defined in Eq. (8); thus the line intensity can be written

$$S_{\eta'' \rightarrow \eta'} = S_{\epsilon'' \Lambda'' v''}^{\epsilon'' \Lambda'' v''} I_a \frac{(d_{J''} d_{\text{sym}} e^{-E_{J''}/kT})}{d_{J''} d_{\text{sym}} Q_{\text{rot}}} \frac{\omega_{(\eta'')(\eta')}}{\omega_{(\epsilon'' \Lambda'' v'')(\epsilon' \Lambda' v')}} (1 - e^{-h\nu_{(\eta'')(\eta')}/kT}) |R_{(J'')(J')}|^2 . \quad (11)$$

In what follows we will need the relationships between the Einstein coefficients and the electronic-vibrational transition-moment squared. They are

$$B_{\epsilon'' \Lambda'' v'' \rightarrow \epsilon' \Lambda' v'} = \frac{8\pi^3 10^{-36}}{3h^2} |R_{(\epsilon'' \Lambda'' v'')(\epsilon' \Lambda' v')}|^2 , \quad (12a)$$

$$B_{\epsilon' \Lambda' v' \rightarrow \epsilon'' \Lambda'' v''} = \frac{8\pi^3 10^{-36}}{3h^2} \frac{d_{\epsilon'' \Lambda'' v''}}{d_{\epsilon' \Lambda' v'}} |R_{(\epsilon'' \Lambda'' v'')(\epsilon' \Lambda' v')}|^2 , \quad (12b)$$

and

$$A_{\epsilon' \Lambda' v' \rightarrow \epsilon'' \Lambda'' v''} = \frac{64\pi^4 10^{-36}}{3h} \omega_{(\epsilon' \Lambda' v')(\epsilon'' \Lambda'' v'')}^3 \frac{d_{\epsilon'' \Lambda'' v''}}{d_{\epsilon' \Lambda' v'}} |R_{(\epsilon'' \Lambda'' v'')(\epsilon' \Lambda' v')}|^2 . \quad (12c)$$

Solving Eq. (12c) for the transition-moment squared and inserting into Eq. (8) gives the result

$$S_{\epsilon'' \Lambda'' v''}^{\epsilon'' \Lambda'' v''} = \frac{1}{8\pi c} \frac{(d_{\epsilon'' \Lambda'' v''} e^{-E_{\epsilon'' \Lambda'' v''}/kT})}{Q_{\epsilon \Lambda v} \omega_{(\epsilon' \Lambda' v')(\epsilon'' \Lambda'' v'')}^2} \frac{d_{\epsilon' \Lambda' v'}}{d_{\epsilon'' \Lambda'' v''}} A_{\epsilon' \Lambda' v' \rightarrow \epsilon'' \Lambda'' v''} . \quad (13)$$

This expression allows the Einstein-A coefficient to be determined by measuring the integrated band intensity. This relationship with Eq. (11) allows the $\epsilon'' \Lambda'' v'' J'' \rightarrow \epsilon' \Lambda' v' J'$ line intensity to be written in terms of the Einstein $A_{\epsilon' \Lambda' v' \rightarrow \epsilon'' \Lambda'' v''}$ coefficient

$$S_{\eta'' \rightarrow \eta'} = \frac{I_a}{8\pi c} \frac{(d_{\epsilon'' \Lambda'' v'' J''} e^{-E_{\epsilon'' \Lambda'' v'' J''}/kT})}{d_{J''} Q_{\text{tot}}} \frac{\omega_{(\epsilon'' \Lambda'' v'' J'')(\epsilon' \Lambda' v' J')}}{\omega_{(\epsilon'' \Lambda'' v'')(\epsilon' \Lambda' v')}}^3$$

$$\times (1 - e^{-h\nu(\eta')(\eta'')/kT}) L_J'' \frac{d_{\epsilon'\Lambda'v'}}{d_{\epsilon''\Lambda''v''}} A_{\epsilon'\Lambda'v' \rightarrow \epsilon''\Lambda''v''} \quad (14)$$

where the partition function and the energy are no longer approximated and the Hönl-London factor is inserted for the rotational transition-moment squared. Note that the degeneracy factors preceding the Einstein-A coefficient account for the number of J and M states in the upper and lower electronic-vibration states and the degeneracy factors with the partition function term are $d_{\epsilon\Lambda v} = (2S+1)(2-\delta_{\Lambda,0})(d_{\text{sym}})(2J+1)$. From the symmetry arguments presented above, it is clear that the ratio of the degeneracy factors, $d_{\epsilon'\Lambda'v'}/d_{\epsilon''\Lambda''v''}$, is 2/3 for $X^3\Sigma^-_g \rightarrow a^1\Delta_g$ transitions and 1/3 for the $X^3\Sigma^-_g \rightarrow b^1\Sigma^+_g$ transitions.

For several of the bands calculated, the program employs the Einstein-A coefficients in units of sec^{-1} . Often one must work from measured vibrational band intensities. In order to make use of these values, we must convert from vibrational band intensity to the Einstein-A coefficient. This relationship was presented in Eq. (13). However, quite often in the literature the vibrational band intensity is reported in units of $\text{cm}^{-1} \text{ km}^{-1} \text{ atm}^{-1} \text{ STP}$. The values must be converted to the HITRAN units of $\text{cm}^{-1}/(\text{molec} \cdot \text{cm}^{-2})$ to apply the equations presented here. This is accomplished by the relationship

$$S_{v'}^v \left(\frac{\text{cm}^{-1}}{\text{molec cm}^{-2}} \right) \times \frac{N_L}{p(\text{atm})} \times 10^5 \frac{\text{cm}}{\text{km}} = S_{v'}^v (\text{cm}^{-1} \text{ km}^{-1} \text{ atm}^{-1} \text{ STP}) \quad (15)$$

where N_L is Loschmidt's number, the number of molecules per cubic centimeter of perfect gas at STP. Thus, we have

$$S_v^v \left(\frac{\text{cm}^{-1}}{\text{molec cm}^{-2}} \right) \times 2.6867 \times 10^{24} \frac{\text{cm}}{\text{km}} = S_v^v (\text{cm}^{-1} \text{ km}^{-1} \text{ atm}^{-1} \text{ STP}) . \quad (16)$$

From Eq. (13), the Einstein-A coefficients used in the program have been updated using vibrational band intensities reported in the literature. The vibrational band intensities and Einstein-A coefficients used in the program are presented in Table 8 for the $b^1\Sigma^+_g \leftarrow X^3\Sigma^-_g$ band.

Table 8. Vibrational band intensities and Einstein-A coefficients for the $b^1\Sigma^+_g \leftarrow X^3\Sigma^-_g$ band of O_2 .

Band	S_v^v , a	S_v^v , b	A ^c	Ref.	A(ref.) ^c	A(O2CALC) ^c
A band	532.	1.9812-22	0.0770	46	0.077	0.077
(0-0)	582.	2.1712-22	0.084	47	0.084	NA
		2.2812-22	0.0887	21	0.0887	NA
B band	40.8	1.5212-23	0.00724	48	NG	0.00591*
(1-0)	38.8	1.4412-23	0.00689	47	0.0069	NA
γ band	1.52	5.6612-25	3.2412-4	49	NG	2.212-4*
(2-0)	1.50	5.5812-25	3.1912-4	47	3.212-4	NA
	1.26	4.7112-25	2.6912-4	50	NG	NA
(3-0)	0.0269	1.0012-26	6.7312-6	47	6.712-6	NA
(1-1)	0.136	5.0612-26	0.0701	47	0.0704	0.0704
(0-1)	0.0114	4.2412-27	0.00467	47	0.0047	0.0047

a units of $\text{cm}^{-1} \text{ km}^{-1} \text{ atm}^{-1} \text{ STP}$

b units of $\text{cm}^{-1}/(\text{molec cm}^{-2})$

c units of $\text{sec}^{-1}/\text{molec}$

* does not agree with literature value (see text)

NA not applicable

NG not given

The vibrational band centers are computed using the following expressions

$$G(v) = \omega_e (v+1/2) - \omega_e x_e (v+1/2)^2 + \omega_e y_e (v+1/2)^3 - \omega_e z_e (v+1/2)^4, (17)$$

$$G(v') = \omega'_e (v'+1/2) - \omega'_e x'_e (v'+1/2)^2 + \omega'_e y'_e (v'+1/2)^3 - \omega'_e z'_e (v'+1/2)^4, (18)$$

and

$$\omega_0 = T_e + G(v') - G(v). (19)$$

The constants (T_e , ω_e , $\omega_e x_e$, $\omega_e y_e$, $\omega_e z_e$, ω'_e , $\omega'_e x'_e$, $\omega'_e y'_e$, $\omega'_e z'_e$) are taken from Krupenie⁵¹ for both the $a^1\Delta^+_g$ and $b^1\Sigma^+_g$ electronic states.

The partition sums used in the program are those from the TIPS⁵² (Total Internal Partition Sum) program. Before addition to the HITRAN database, the line intensities are filtered through a wavenumber dependent cutoff given by

$$S_{\text{cut}} = S_{\omega_c} \left(\frac{\omega}{\omega_c} \right) \left(\frac{1 - e^{-\frac{h\nu}{kT}}}{1 + e^{-\frac{h\nu}{kT}}} \right) (20)$$

with $\omega_c = 2000 \text{ cm}^{-1}$ and $S_{\omega_c} = 3.7 \times 10^{-30} \text{ cm}^{-1}/(\text{molec} \cdot \text{cm}^{-2})$. All lines with an intensity less than the cutoff are not included in the database with the exceptions noted below.

2.3 Halfwidths

Measurements of the halfwidths are available for several bands of the O₂ molecule. The data of Krupenie⁵¹ are taken for the X³Σ^{-g} pure rotation bands, the A-band data are from Ritter and Wilkerson,²¹ the B-band data from Giver et al.,⁴⁸ and the γ-band data are from Mélières et al.⁵⁰ The data of Refs. 21,49-50 are plotted in Figure 5 as a function of N" for the various types of transitions. The transitions are labeled by ΔNΔJ N" J"; however with symmetry arguments the notation ΔNΔJ_{N"} is often used. For the A-band we find that if the R_R and R_Q values are shifted, (N" → N"+2), they agree with the P_P and P_Q values (see Figure 6), i.e.

$$\gamma(\text{PP}_{\text{N}''}) = \gamma(\text{RR}_{\text{N}''+2})$$

and

(21)

$$\gamma(\text{PQ}_{\text{N}''}) = \gamma(\text{RQ}_{\text{N}''+2})$$

For the B-band, the difference between the P_P, P_Q, R_R, and R_Q values for a given N" is small. The data of Mélières et al.⁵⁰ for the γ-band, however, show large variations in the halfwidth as a function of N" not seen in the other data (see open circles and triangles in Figure 5).

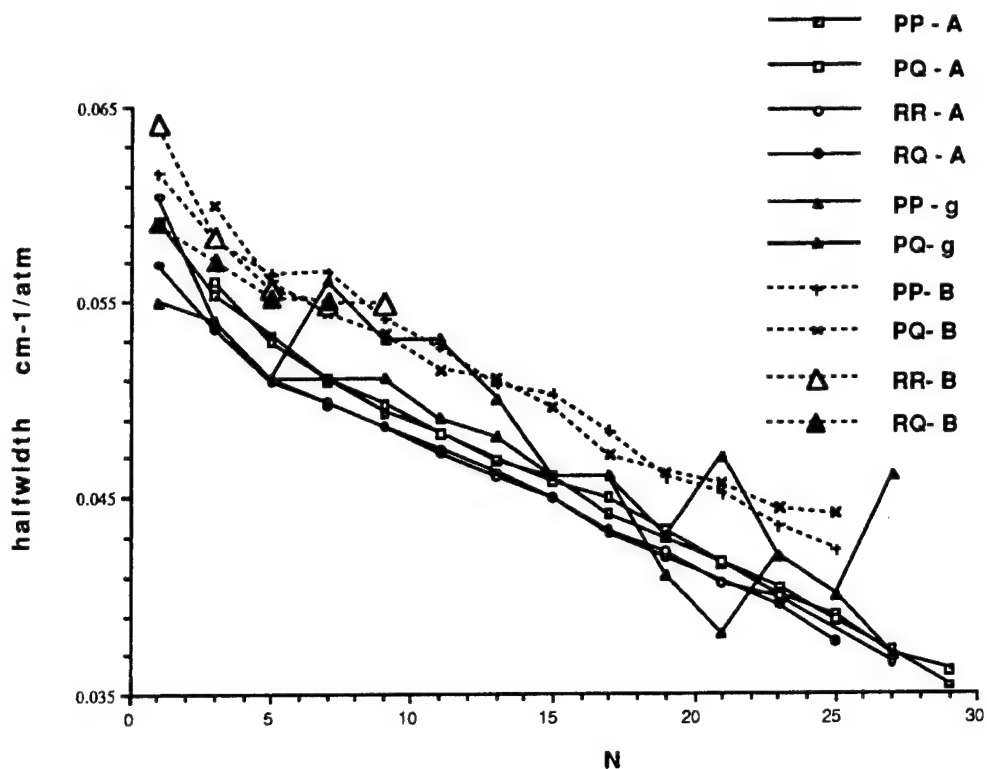


Figure 5. Halfwidth data $\text{cm}^{-1} \text{atm}^{-1}$ at 296K for the A-, B- and γ -bands of O_2 according to branches as a function of N .

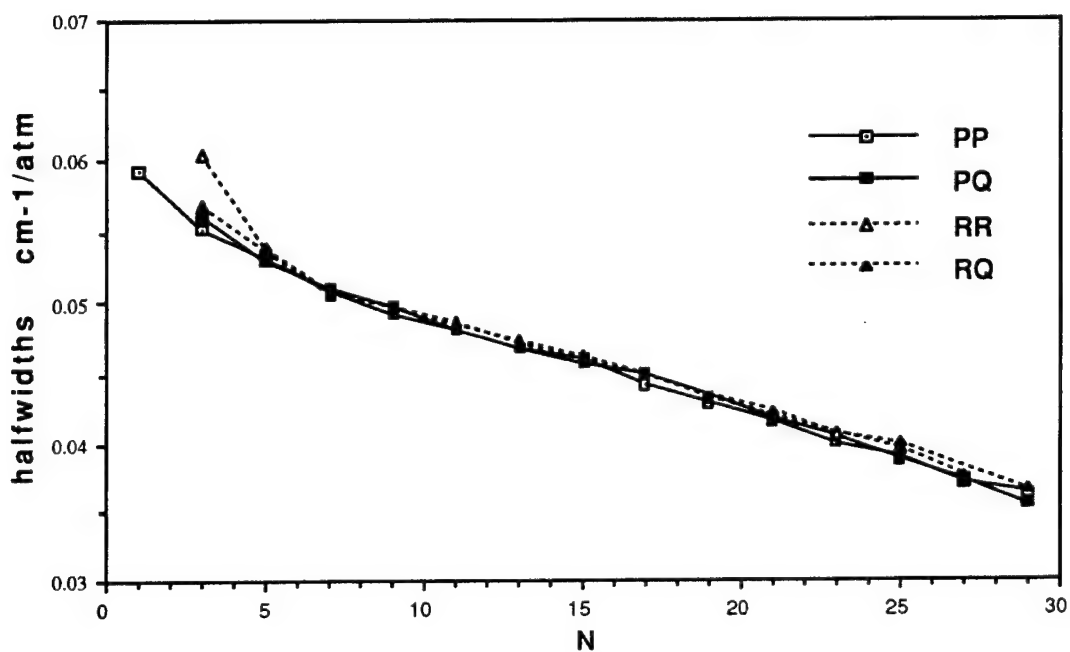


Figure 6. A-band halfwidths $\text{cm}^{-1} \text{atm}^{-1}$ at 296K, RR and RQ values are shifted, $N'' \rightarrow N''+2$.

Comparing the values from Refs. 21,49-50, we find that the A- and γ -band results agree with each other and the B-band results are some 10% larger. The data selected for O₂ on the 1996 HITRAN database use the following procedure for the halfwidths. The X³ Σ^-_g pure rotation band uses the data reported by Krupenie⁵¹ for the 60 GHz lines. The electric quadrupole transitions and the transitions involving the a¹ Δ_g state use the A-band values.²¹ For the A- and γ -bands, the halfwidths of Ritter and Wilkerson²¹ are averaged as a function of N" for the PP and PQ lines together and the RR and RQ lines together. We have calculated transitions to N"=80 and the measurements end at N"=29; thus, it is necessary to extrapolate the data. From the plots, an asymptotic limit of $\gamma=0.032$ cm⁻¹/atm for N"≥40 is estimated. Both the R and P lines use the same asymptotic limit. The values of the halfwidths for the A- and B-bands of O₂ used in HITRAN96 are given in Table 9.

2.4 Updates to the Oxygen Data for the 1996 HITRAN Database

Below, the changes made to the data for the 1996 HITRAN database are discussed for each band of molecular oxygen considered. The line position and energy differences are defined as the HITRAN92 value minus the HITRAN96 value. For the line intensities the ratio computed is HITRAN92/HITRAN96. The average and maximum differences were calculated for the line position and energy parameters. For the line intensities, the average, maximum and minimum ratios were calculated.

Table 9. Halfwidths in $\text{cm}^{-1}/\text{atm}$ for the A- and B-bands of O_2 .

N"	A-P†	A-R††	B‡‡	N"	A-P†	A-R††	B‡‡
1	.0592	.0587	.0616	21	.0417	.0406	.0454
2	.0574	.0562	.0600	22	.0409	.0402	.0447
3	.0557	.0538	.0584	23	.0402	.0397	.0440
4	.0544	.0523	.0571	24	.0395	.0386	.0436
5	.0531	.0509	.0558	25	.0389	.0376	.0432
6	.0520	.0503	.0555	26	.0380	.0371	.0428
7	.0509	.0498	.0552	27	.0371	.0366	.0422
8	.0502	.0492	.0547	28	.0365	.0358	.0418
9	.0495	.0486	.0541	29	.0358	.0358	.0414
10	.0488	.0479	.0531	30*	.0353	.0353	.0410
11	.0482	.0473	.0521	31*	.0349	.0349	.0407
12	.0475	.0467	.0515	32*	.0345	.0345	.0404
13	.0468	.0461	.0509	33*	.0340	.0340	.0400
14	.0464	.0455	.0504	34*	.0337	.0337	.0398
15	.0459	.0449	.0499	35*	.0334	.0334	.0395
16	.0452	.0441	.0488	36*	.0330	.0330	.0394
17	.0445	.0432	.0477	37*	.0328	.0328	.0393
18	.0438	.0426	.0469	38*	.0324	.0324	.0391
19	.0431	.0421	.0461	39*	.0322	.0322	.0390
20	.0424	.0413	.0457	40*	.0320	.0320	.0390

† A-band PP and PQ transitions * Extrapolated

‡ A-band RR and RQ transitions

‡‡ B-band transitions

2.4.1 The principal isotopic species, $^{16}\text{O}_2$.

The $X^3\Sigma^-_g(v=0) \leftarrow X^3\Sigma^-_g(v=0)$ band

The energy levels for the vibrational ground state of the $X^3\Sigma^-_g$ electronic state of $^{16}\text{O}_2$ are calculated using the formalism of Rouillé et al.⁵³ In this work, the Hamiltonian included all rotational terms to second order⁵⁴ and some terms to third order.^{55,56} The molecular constants are those of Rouillé et al.⁵³ These are compared with the energy values from the previous database⁵⁷ in Figure 7. The difference in energy between the two formulations is given as a function of N and J . For the vibrational ground state the difference is near zero for N up to 35 then rapidly goes to -0.3 cm^{-1} at $N=80$. While the transition frequencies from this formulation differ only slightly from the previous results, 0.0039 cm^{-1} maximum difference, $7 \times 10^{-5}\text{ cm}^{-1}$ on average, the formalism of Rouillé et al.⁵³ gives better agreement with measurements.⁵⁸

This band has both magnetic dipole and electric quadrupole transitions. For the electric quadrupole transitions, a newer value of the quadrupole moment derived from far-IR PIA spectra,⁵⁹ $0.34 \times 10^{-26}\text{ esu cm}^2$, has been adopted. There are no data to validate the intensities we obtain. With this value for the quadrupole moment, the line intensities and transition-moments squared are a factor of 5.8 weaker than previous calculations.⁶⁰ Because of this reduction in the line intensities, no electric quadrupole lines survived the cutoff for the 1996 data set. This is further discussed below for the $0 \leftarrow 1$ vibrational band of this electronic band. The 1996 calculations of the magnetic dipole intensities are on average 4% stronger than the 1992

values. This is due to improved energy formulation and partition sums.

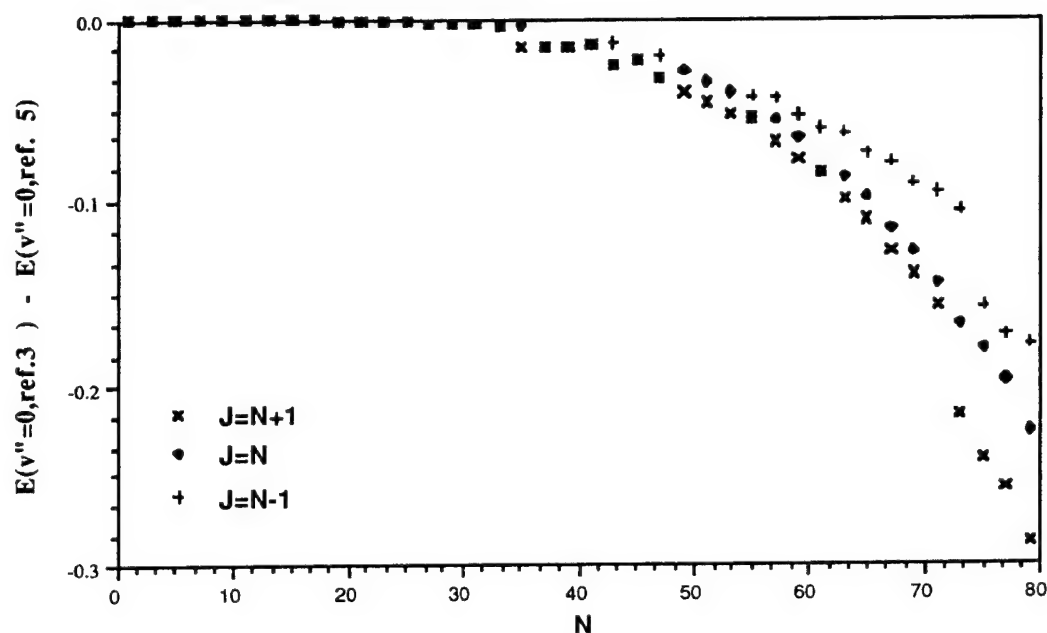


Figure 7. Energy difference in cm^{-1} between the formalism of Rouillé et al.⁵³ and Ref. 57 versus N for the $v''=0$ band of $X^3\Sigma^-_g$ of $^{16}\text{O}_2$.

The $X^3\Sigma^-_g(v=1) \leftarrow X^3\Sigma^-_g(v=0)$ band

The 1992 HITRAN database contained only electric quadrupole (eq) lines for this band. The newer data contain both magnetic dipole (md) and electric quadrupole (eq) transitions.⁶¹ Thus, the comparison made here is for the electric quadrupole lines. The energy levels for the vibrational ground ($v=0$) and first fundamental ($v=1$) of the $X^3\Sigma^-_g$ electronic state of $^{16}\text{O}_2$ are calculated using the formalism and constants of Rouillé et al.⁵³ These energies are

compared with the values from the previous database³⁷ in Figure 8 for the $\nu''=1$ band. The difference is small for N up to ~ 20 then quickly goes to roughly 5 cm^{-1} at $N=80$. For the transitions that make the cutoff criterion, $N \leq 31$, the maximum difference in the energy values is 0.0024 cm^{-1} , 0.0005 cm^{-1} on average. The corresponding average and maximum differences in the line positions are -0.0104 and 0.0850 cm^{-1} . The electric quadrupole transition line intensities are calculated using the formalism of Goldman et al.⁶¹ The absolute intensities are determined by scaling the relative intensities to the measurements of Reid et al.⁶² Comparison of these intensities with the 1992 HITRAN values implies a electric quadrupole moment of $0.145 \times 10^{-26} \text{ esu cm}^2$, not in agreement with the quadrupole moment derived from far-IR PIA spectra⁵⁹ (see previous section). This is under investigation. Comparing the 1996 and 1992 values for the intensities we find an average ratio of 1.0027, with some ratios between 0.740 and 1.31. These large ratios occur for 33 out of the 146 lines and occur only for forbidden (weaker) lines, with $\Delta N \neq \Delta J$ and at low J .

The 1996 calculations for this band are not filtered through a cutoff procedure and many of the lines will have very small intensities. (In fact, one zero intensity magnetic dipole and electric quadrupole transition have been retained in the data for theoretical considerations; it helps to see the effects of assumed parameters on these lines.) There are 254 md transitions and 183 eq transitions for this band.

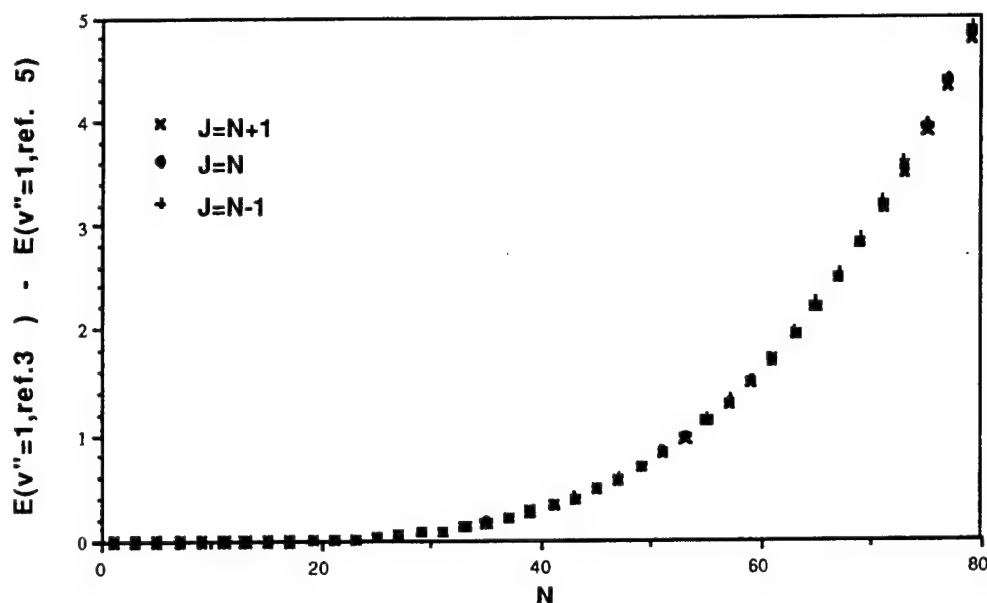


Figure 8. Energy difference in cm^{-1} between the formalism of Rouillé et al.⁵³ and Ref. 57 versus N for the $v''=1$ band of $X^3\Sigma^-_g$ of $^{16}\text{O}_2$.

The $X^3\Sigma^-_g(v=1) \leftarrow X^3\Sigma^-_g(v=1)$ band

As discussed above, the energy differences from the previous calculations and the formulation of Rouillé et al.⁵³ for the $v=1$ level approach 5 cm^{-1} at $N=80$. The maximum energy difference in the lines in the 1996 data is 0.750 cm^{-1} and the average difference is -0.0953 cm^{-1} . The maximum difference in line positions is 0.0457 cm^{-1} with the average difference being -0.00280 cm^{-1} . The intensity ratios are between 0.994 and 0.988 with an average ratio of 0.990. Most of this difference comes from using an improved partition sum in the calculations.

The $a^1\Delta_g (v=0) \leftarrow X^3\Sigma^-_g (v=0)$ band

There are wavenumber differences which arise from a change in the energy formulation of $X^3\Sigma^-_g (v=0)$ to that of Rouillé et al.⁵³ and for $a^1\Delta_g (v=0)$ to that of Scalabrin et al.⁶³ with the constants of Hillig et al.⁶⁴ The maximum difference is 0.0160 cm^{-1} at $N''=37$ and the average difference is -0.00234 cm^{-1} .

The line intensities for this band are calculated using Eq. (14). There are three measurements of the band intensity in the literature (scaled to 296 K) which differ by a factor of about 4.5. The measurement of Badger et al.⁶⁵ gives $S_{00} = 3.6 \times 10^{-24} \text{ cm}^{-1}/(\text{molec}\cdot\text{cm}^{-2})$. The measurement of Lin et al.⁶⁶ is $S_{00} = 9.4 \times 10^{-24} \text{ cm}^{-1}/(\text{molec}\cdot\text{cm}^{-2})$, and Hsu et al.⁶⁷ report a value of $S_{00} = 2.1 \times 10^{-24} \text{ cm}^{-1}/(\text{molec}\cdot\text{cm}^{-2})$. From these values the authors determine the Einstein-A coefficient. Unfortunately, some of the authors have used incorrect statistical degeneracy factors, d_ℓ/d_u ; Badger et al.⁶⁵ used $3/2$ whereas Lin et al.⁶⁶ and Hsu et al.⁶⁷ use $3/1$. It was demonstrated above that in Eq. (14) $d_\ell=3$ and $d_u=2$. Thus, application of Eq. (14) (or Eq. (13)) will only generate consistent line intensities if the statistical degeneracy factors and the derived Einstein-A coefficient are from the same author. Because of the large discrepancy between the measured band intensities, we sought to determine the band intensity from another source. We have obtained unpublished line intensity measurements⁶⁸ of 14 transitions in the $a^1\Delta_g (v=0) \leftarrow X^3\Sigma^-_g (v=0)$ band that were mentioned in the work of Wallace and Livingston.⁶⁹ Using our O₂ program, the Einstein-A coefficient used to calculate the line

intensities was scaled to match the measurements of Ref. 68. The results are in Table 10. This fit gives a band intensity of $S_{00}=3.69 \times 10^{-24} \text{ cm}^{-1}/(\text{molec}\cdot\text{cm}^{-2})$ which is close to the Badger et al.⁶⁵ value. The Einstein-A coefficients, the band intensities, and the statistical degeneracy factors as related by Eq. (13) are listed in Table 11. The calculation of the line intensities for the 1996 database used the Einstein-A coefficient $A=2.59 \times 10^{-4} \text{ sec}^{-1}$ with statistical degeneracy factors of $d_l=3$ and $d_u=2$. The resulting line intensities are larger than HITRAN92 by roughly a factor of 2, this is due to incorrect inversion from Badger et al.'s A to S used in previous versions of HITRAN. Suspicion of such missing factors of 2, and concerns about the interpretation of upper atmosphere emissions, such as inferring ozone from SME (Solar Mesosphere Explorer via the a $^1\Delta_g$ 1.27 μm airglow) were expressed by Mlynczak and Nesbitt⁷⁰ (who conjectured a significant change in A from one of the reported S values in Table 5 (Hsu et al.)) and by Pendelton et al.⁷¹ Recent observations in the mesosphere⁷² confirm the Badger et al.⁶⁵ value of the Einstein-A coefficient. Moreover, new line intensity measurements made at National Institute for Standards and Technology⁷³ and at Rutherford Appleton Laboratory⁷⁴ are roughly 15% larger than the HITRAN96 values. Preliminary comparisons indicate agreement between these two new independent high-resolution studies. When completed, these data will be incorporated into the next edition of HITRAN.

Table 10. Measured intensities (Brault and Brown⁶⁸) of the $a^1\Delta_g$ ($v=0$) \leftarrow $X^3\Sigma^-_g$ ($v=0$) band, final HITRAN96 values, ratios, and final average ratio.

line ^a	Brault & Brown ^{68b}	HITRAN96 ^b	ratio
O23P22	2.44E-27	2.65E-27	0.92145
O19P18	6.47E-27	6.87E-27	0.94205
P23P23	5.67E-27	5.56E-27	1.019234
P23Q22	6.99E-27	6.12E-27	1.142344
O13P12	1.67E-26	1.62E-26	1.030864
P21P21	9.10E-27	9.36E-27	0.972118
P21Q20	1.02E-26	1.04E-26	0.982659
P19P19	1.43E-26	1.47E-26	0.970808
O11P10	1.90E-26	1.78E-26	1.065022
P19Q18	1.70E-26	1.65E-26	1.030303
P17P17	2.06E-26	2.16E-26	0.954588
O 9P 8	1.75E-26	1.72E-26	1.018034
P15P15	2.75E-26	2.93E-26	0.937287
P15Q14	3.45E-26	3.38E-26	1.019805
		average	1.000469

a) Branch symbol for ΔN , N'' , Branch symbol for ΔJ , J''

b) in units of $\text{cm}^{-1}/(\text{molec}\cdot\text{cm}^{-2})$

Table 11. Measured band intensities, derived Einstein-A coefficients, and statistical degeneracy factors for the $a^1\Delta_g (v=0) \leftarrow X^3\Sigma^-_g (v=0)$ band.

Reference	S_{00} $\text{cm}^{-1}/(\text{molec}\cdot\text{cm}^{-2})$	$A_{\epsilon'\Lambda'v'\rightarrow\epsilon''\Lambda''v''}$ sec^{-1}	d_L/d_U
Badger et al. ⁶⁵	3.66×10^{-24}	2.58×10^{-4}	3 / 2
Lin et al. ⁶⁶	9.4×10^{-24}	1.3×10^{-4}	3 / 1
Hsu et al. ⁶⁷	2.1×10^{-24}	2.9×10^{-4}	3 / 1
fit of data ⁶⁸ (†)	3.69×10^{-24}	2.59×10^{-4}	3 / 2

† Adopted for HITRAN 96

The $a^1\Delta_g (v=1) \leftarrow X^3\Sigma^-_g (v=0)$ band

The molecular constants for the $a^1\Delta_g (v=1)$ state are from Brault.⁷⁵ Line positions have changed 0.001302 cm^{-1} on average. The Einstein-A coefficient used is 1/200 of the value of the $a^1\Delta_g (v=0) \leftarrow X^3\Sigma^-_g (v=0)$ band,⁷⁶ hence the line intensities are increased by 1.46 on average. Unfortunately, to our knowledge, no other observations of this band are available to perform a proper test of this adopted ratio. The line positions and energies have only changed by $-0.000273 \text{ cm}^{-1}$ and 0.000388 cm^{-1} on average.

The $a^1\Delta_g (v=0) \leftarrow X^3\Sigma^-_g (v=1)$ band

The wavenumbers have changed due to the reformulation of the energy expressions for both the upper and lower states,^{53,63} resulting in an average change of 0.0157 cm^{-1} . The line intensities are calculated using one-tenth of the Einstein-A coefficient of the $a^1\Delta_g (v=0) \leftarrow X^3\Sigma^-_g (v=0)$ band⁷⁶ and are larger than previous

HITRAN databases³⁷ by an average of 2.04. The same comment as above applies to the adopted ratio used for this band.

The $b^1\Sigma^+_g(v=0) \leftarrow X^3\Sigma^-_g(v=0)$ band (A-band)

The constants for the $b^1\Sigma^+_g(v=0)$ state are from Zare et al.⁷⁷ and those for the $X^3\Sigma^-_g(v=0)$ state are from Rouillé et al.⁵³. The wavenumbers differ by -0.00127 cm^{-1} on average, with the maximum difference being 0.00383 cm^{-1} . The average energy difference is 0.00134 cm^{-1} . Intensity ratios vary from 0.825 to 0.877, with the average ratio being 0.862. The Einstein-A coefficient has been changed from the value of Miller et al.,⁴⁶ 0.077 sec^{-1} to the newer value of 0.0887 from Ritter and Wilkerson.²¹

The $b^1\Sigma^+_g(v=1) \leftarrow X^3\Sigma^-_g(v=0)$ band (B-band)

The constants for the $b^1\Sigma^+_g(v=1)$ state are from Zare et al.⁷⁷ and those for the $X^3\Sigma^-_g(v=0)$ state are from Rouillé et al.⁵³. The wavenumber and energies arise from changes made to the ground state energies. The maximum wavenumber and energy differences are 0.00383 cm^{-1} and 0.00370 cm^{-1} , respectively. The intensity ratios range from 0.782 to 0.822 with an average of 0.811. The value of the Einstein-A coefficient is from Giver et al.,⁴⁸ $A(1-0)=0.00724\text{ sec}^{-1}$, but was incorrectly used in the previous program where it was set to $A(1-0)=0.00591\text{ sec}^{-1}$.

The $b^1\Sigma^+_g(v=2) \leftarrow X^3\Sigma^-_g(v=0)$ band (γ -band)

The constants for the $b^1\Sigma^+_g(v=2)$ state are also from Zare et al.⁷⁷ and those for the $X^3\Sigma^-_g(v=0)$ state are from Rouillé et al.⁵³. The average wavenumber and energy differences are 0.00694 cm^{-1} and 0.00104 cm^{-1} . The intensity ratios range from 1.22 to 1.27. The Einstein-A coefficient of Mélières et al.⁵⁰ is now used, $A(2-0)=2.69 \times 10^{-4} \text{ sec}^{-1}$. Compared with the old value from Miller et al.⁴⁹ of $A(2-0)=3.24 \times 10^{-4} \text{ sec}^{-1}$ (which was incorrectly used as $A(2-0)=2.2 \times 10^{-4} \text{ sec}^{-1}$ in the HITRAN82³⁷ calculations) an average ratio of 0.813 is obtained.

The $b^1\Sigma^+_g(v=1) \leftarrow X^3\Sigma^-_g(v=1)$ band

The molecular constants used in the calculation of energies are from Zare et al.⁷⁷ for the $b^1\Sigma^+_g(v=1)$ state and from Rouillé et al.⁵³ for the $X^3\Sigma^-_g(v=1)$ state. The line positions show a maximum difference of 0.0857 cm^{-1} with an average of 0.0207 cm^{-1} . The difference is due to the change in the ground state energies. The Einstein-A coefficient is from Giver et al.⁴⁸ The intensity ratios range from 0.962 to 0.999. These changes are due to the correct partition sums and removal of some approximations in the formulas.

The $b^1\Sigma^+_g(v=0) \leftarrow X^3\Sigma^-_g(v=1)$ band

The molecular constants are from Zare et al.⁷⁷ for the $b^1\Sigma^+_g(v=0)$ state and from Rouillé et al.⁵³ for the $X^3\Sigma^-_g(v=1)$ state. The changes in the line positions are from the new lower state energies. The maximum value is 0.0333 cm^{-1} and the average is 0.00935 cm^{-1} .

The Einstein-A coefficient is from Galkin.⁴⁷ The resulting intensity ratios range from 0.968 to 1.00.

2.4.2 The $^{16}\text{O}^{18}\text{O}$ species

The $X^3\Sigma^-_g(v=0) \leftarrow X^3\Sigma^-_g(v=0)$ band

The present calculations use the improved molecular constants of Mizushima and Yamamoto.⁷⁸ The resulting energies differ from previous calculations by 0.0174 cm^{-1} on average with a maximum difference of 0.136 cm^{-1} at $N=53$. The average difference in line position is 0.00112 cm^{-1} with the largest difference being 0.00962 cm^{-1} . The line intensities differ only by a few percent maximum which is attributed to the improved partition sums.

The $a^1\Delta_g(v=0) \leftarrow X^3\Sigma^-_g(v=0)$ band

There is a slight change in some of the wavenumbers due to the change in energy formulation for the $X^3\Sigma^-_g(v=0)$ state.⁵³ This gives rise to a maximum difference of 0.00580 cm^{-1} and an average difference of -0.00127 cm^{-1} . Intensity ratios are ~ 0.5 as expected and 49 of the previous lines do not make the intensity cut off.

The $b^1\Sigma^+_g(v=0) \leftarrow X^3\Sigma^-_g(v=0)$ band

The energies of the $X^3\Sigma^-_g(v=0)$ state are calculated using the constants of Mizushima and Yamamoto.⁷⁸ The constants for the $b^1\Sigma^+_g(v=0)$ state are from Babcock and Herzberg.⁷⁹ Wavenumber differences of 0.0242 cm^{-1} at $N''=34$ are observed with an average

difference of -0.00577 cm^{-1} . The average intensity ratio is 0.882 due mostly to the change in partition functions.

The $b^1\Sigma^+_g(v=1) \leftarrow X^3\Sigma^-_g(v=0)$ band

The constants for the $b^1\Sigma^+_g(v=1)$ state are from Benedict.⁸⁰ Those for the $X^3\Sigma^-_g(v=0)$ state are from Mizushima and Yamamoto.⁷⁸ The maximum wavenumber differences is 0.0107 cm^{-1} . This difference is due to the change in the lower state energies. The Einstein-A coefficient is from Giver et al.⁴⁸ The average ratio of the intensities is 0.830.

The $b^1\Sigma^+_g(v=2) \leftarrow X^3\Sigma^-_g(v=0)$ band

The constants for the $b^1\Sigma^+_g(v=2)$ state are from Zare et al.⁷⁷ Those for the $X^3\Sigma^-_g(v=0)$ state are from Mizushima and Yamamoto.⁷⁸ The maximum wavenumber difference is 0.150 cm^{-1} and the average intensity ratio is 0.837. Caution must be used in interpreting these numbers since the comparison is based on only 3 lines.

2.4.3 The $^{16}\text{O}^{17}\text{O}$ species

The $X^3\Sigma^-_g(v=0) \leftarrow X^3\Sigma^-_g(v=0)$ band

The data for this band are taken from the Jet Propulsion Laboratory catalogue.⁸¹ There are 10,787 lines in the JPL file. The data were filtered through the wavenumber dependent cutoff resulting in 2601 lines from 0.000012 cm^{-1} to 186.15 cm^{-1} in the final file. Note the isotopic abundance factor was inadvertently

omitted from the 1996 HITRAN database. Thus, the ratio of the line intensity (S92/S96) is 0.000750 on average. In order to properly use the intensities for these data, they should be multiplied by $I_a = 0.000742235$. The line positions and lower state energies have only changed slightly, 0.000041 cm^{-1} and $-0.000352 \text{ cm}^{-1}$ average difference respectively.

The $b^1\Sigma^+_g(v=1) \leftarrow X^3\Sigma^-_g(v=0)$ band

These data are from Benedict and Braut⁸² and have not changed from the 1982 HITRAN database.

2.5 Other Changes

We have added reference and error codes to the line parameter database. The error code (see HITRAN96 manual⁸³) for the halfwidths is set to 4. The error code for the line positions of $X^3\Sigma^-_g \leftarrow X^3\Sigma^-_g$ electronic band is set to 4 and all other error codes are not utilized on the database (i.e. set to 0). We have also labeled the electric quadrupole and magnetic dipole transitions by the lower case letters q and d, respectively, in the sym field of the rotational quantum number character string, i.e. Br, F", _; Br, N", Br, J", __, Sym.

These data are available in the 1996 HITRAN database.⁸³

2.6 O₂ Continuum Absorption

It is known that the O₂ $X^3\Sigma^-_g(v'') - a^1\Delta_g(v')$ absorption bands exhibit both discrete (rotational) line structure and pressure-induced

continuous absorption.⁶⁵ The most important bands are the $v''=0$, $v'=0$ at $1.27 \mu\text{m}$ (7882 cm^{-1}), $v''=0$, $v'=1$ at $1.06 \mu\text{m}$ (9366 cm^{-1}), and $v''=1$, $v'=0$ at $1.6 \mu\text{m}$ (6326 cm^{-1}). While the rotational lines of the (0-1) band are weaker than those of (0-0) band, and those of (1-0) band are weaker than the (0-1) band, the continuum absorptions are of more similar intensity.

During the update of the (0-0) band line parameters, theoretical calculations were compared with absolute atmospheric transmittance obtained with the University of Denver Absolute Solar Transmittance Interferometer (ASTI).⁸⁴ The results show good agreement of the line structure but a clear indication of the underlying continuum (not modeled), with the P, R (no Q) shape of the envelope under the absorption lines. The continuum is clearer at the higher spectral resolution ($\geq 0.5 \text{ cm OPD}$).

More recent ASTI data in the 9400 cm^{-1} and 6400 cm^{-1} regions also show a strong continuum, similar to that described above. It is thus proposed that this is due to the pressure-induced absorption of the $v''=0$, $v'=1$ and $v''=1$, $v'=0$ bands respectively.⁸⁵ Laboratory data⁸⁶ are consistent with these conclusions, but indicate no pressure-induced absorptions under the $X^3\Sigma^-_g(v'')$ - $b^1\Sigma^+_g(v')$ bands. The pressure-induced absorption in the $X^3\Sigma^-_g(v''=0)$ - $X^3\Sigma^-_g(v'=1)$ has been well documented in previous publications.^{59,87,88}

In the HITRAN database we have included the individual line parameters of these bands, but no cross-sections are provided for the continuum. These cross-sections will be forthcoming on the next version of the HITRAN database.

3.0 HALFWIDTHS AND LINE SHIFTS OF H₂O TRANSITIONS

Water vapor, the most important greenhouse gas in the terrestrial atmosphere, is the principle atmospheric absorber of infrared radiation with some 50,000 spectral transitions ranging from the microwave to the visible portions of the spectrum.³ In order to interpret remote sensing measurements and understand radiative properties of the atmosphere, it is useful to know spectral parameters along with their temperature dependence. For the terrestrial atmosphere, the collisional interaction of water vapor with nitrogen and oxygen must be understood.

A knowledge of the fundamental spectroscopic parameters for H₂O in the presence of other gases (generally referred to as the perturbing gas or buffer gas) is important for applications where these gases are the principal components of the atmosphere or system in question. For example, the Earth's nearest neighbors - Venus and Mars - have atmospheres composed predominantly (at the 95% level) of carbon dioxide. Spectroscopic observations of these atmospheres from spacecraft and ground-based platforms can provide much information about the presence and abundance of water vapor. Water vapor and carbon dioxide are also the principal products of combustion, thus spectroscopic techniques can be used to monitor combustion processes.

The atmospheres of the giant planets are made mostly of H₂ and He, the same constituents that are the dominant constituents of

the Sun. This composition reflects the ability of the massive giant planets to have gravitationally captured large amounts of gases from their birthplace in the primordial solar nebula as well as solids (e.g., water) that were eventually volatilized into heavier gases in their atmospheres. By obtaining accurate estimates of the water abundance in the atmospheres of the giant planets, constraints can be placed on the relative efficiency with which they accumulated gases and solids from the primordial solar nebula. Thus, for these applications it is important to know the spectral parameters for water interacting with hydrogen and helium.

The fundamental spectral parameters needed for a retrieval are the line position, intensity, collision-broadened halfwidth, pressure-induced line shift, and lower-state energy.³ The least well characterized of these parameters are the pressure induced halfwidths and line shifts for the collision partners mentioned above. The need of the spectroscopic and remote sensing communities is to know such parameters to an accuracy of 1-5%.⁸⁹⁻⁹⁰

Theory can contribute to this purpose in two ways. First, the vast spectral range and environmental conditions are difficult to cover exhaustively in the laboratory. Second, nonlinear pressure-broadening effects require a solid theoretical model in order to unravel the sometimes complicated spectra observed. Here we focus on improving the basic theoretical apparatus for calculating halfwidths and line shifts for larger species present in the terrestrial atmosphere, e.g. H_2O , O_3 , CH_4 , etc. The model chosen is a complex implementation of the semiclassical formalism of Robert and Bonamy⁹¹ (RB) for several reasons.

- 1) The formalism is based on the resolvent operator formalism of Baranger,⁹² Kolb,⁹³ and Greim⁹⁴ (BKG). The application of linked-cluster techniques⁹⁵ to the BKG formalism leads to developments^{91,96-98} which eliminate the awkward cutoff procedure that characterized earlier theories.⁹⁹⁻¹⁰² Also, the cumulant⁹⁵ expansion, as incorporated in the RB formalism, provides a better description of the long term dynamics of the collisions.
- 2) The formalism is complex valued, yielding halfwidths and line shifts from a single calculation.
- 3) The intermolecular dynamics are treated more realistically than in earlier theories, i.e. using curved rather than straight line trajectories. This has important consequences in the description of close intermolecular collisions (small impact parameters).
- 4) Connected to item (3) is the incorporation in the RB theory of a short range (Lennard-Jones 6-12¹⁰³) atom-atom component to the intermolecular potential. This component has been shown to be essential for a proper description of pressure broadening, especially in systems where electrostatic interactions are weak.¹⁰⁴ (Here, the notion of strong and weak collisions adopts the definition of Oka.¹⁰⁵)
- 5) This formalism allows the removal of all "adjustable" parameters so as to arrive at a more predictive theory.

While not as rigorous, this formalism has advantages over more exact theories¹⁰⁶⁻¹¹¹ in that it is tractable for molecules of atmospheric interest such as H₂O, O₃ and CH₄. The emphasis has been to develop a formalism which can consider such atmospheric species and produce results at the 5% uncertainty level as required by the spectroscopic and remote sensing communities.

The new feature of this work is the development of the complex Robert-Bonamy formalism (CRBF) which can be applied to larger atmospheric species. Previously, the imaginary components of the resonance functions that arise in the theory were only determined for a small number of terms that occur in the electrostatic potential.^{112,113} We have determined these resonance functions for all integrals that arise in a general spherical tensor expansion of the potential.^{114,115}

It should be noted that within the complex Robert-Bonamy formalism, the imaginary parts of the S matrix expansion affect both the calculation of the line shift and the halfwidth, an effect not achieved in Anderson-Tsao-Curnutte (ATC) theory.⁹⁹⁻¹⁰¹ Calculations based on the complex Robert-Bonamy formalism indicate that the effect of the imaginary terms is very important in determining the halfwidth.¹¹⁴⁻¹¹⁸ The effect of the imaginary components on the halfwidths varies from transition-to-transition and perturber-to-perturber but can be as much as 25%. The change is generally (almost always) in the direction of better agreement with experiment.

In this work, we summarize our CRBF calculations of H₂O pressure-broadened halfwidths and pressure induced line shifts by several perturbing gases: N₂, O₂, CO₂, and H₂, and compare the results with measurements. We have attempted to compare with measurements where both halfwidths and line shifts were made simultaneously, although this was not always possible for the perturbing gases listed above. For N₂ and O₂ as the buffer gases, the data are those of Grossmann and Browell¹¹⁹ for the $3\nu_1 + \nu_3$ and

$2\nu_1+2\nu_2+\nu_3$ bands of H_2O . There are several reasons for this choice: the halfwidths from this work exhibited high quality in a survey of measurements of H_2O halfwidths,¹²⁰ and the line shifts for these ro-vibrational transitions are sufficiently large in magnitude to be measured with reasonable certainty. Measurements of the halfwidth and line shift of transitions in the ν_1 , $2\nu_2$, and ν_3 bands of H_2O in a CO_2 buffer gas are from Gamache et al.^{116,121} Measurements of 630 room-temperature H_2 -broadened halfwidths of H_2O transitions in the pure rotational, and three fundamental bands between 55 and 4045 cm^{-1} are those reported by Brown and Plymate.¹²² Together, these data amount to 772 transitions for which halfwidth data are available and 212 transitions for which line shift data are available. The CRBF calculations are made at a temperature of 296 K and are discussed below. Note, because all measurements are within a few degrees of 296K no temperature correction is applied to the data.

3.1 Complex Robert-Bonamy Formalism

Within the Robert-Bonamy formalism, the line shift, δ , and halfwidth, γ , for the transition $f \leftarrow i$ are given by the real and minus the imaginary parts, respectively, of the diagonal elements of the complex relaxation matrix.¹²³ In computational form, the line shift and halfwidth are usually expressed in terms of the Liouville scattering matrix,^{92,124}

$$\delta_{f \leftarrow i} = \frac{n_2 \bar{\nu}}{2\pi c} \sum_{J_2} \langle J_2 | \rho_2 | J_2 \rangle \int_0^\infty 2\pi b \, db \sin(S_1 + I m\{S_2\}) e^{-Re\{S_2\}} \quad (22)$$

$$\gamma_{f \leftarrow i} = \frac{n_2 \bar{v}}{2\pi c} \sum_{J_2} \langle J_2 | \rho_2 | J_2 \rangle \int_0^\infty 2\pi b [1 - \cos(S_1 + I m\{S_2\}) e^{-Re\{S_2\}}] db \quad (23)$$

where \bar{v} is the mean relative thermal velocity, ρ_2 and n_2 are the density operator and number density of perturbors, and b is the impact parameter. S_1 and S_2 are the first- and second-order terms in successive approximation of the Liouville scattering matrix and depend on the intermolecular potential.

The corresponding equations from Anderson-Tsao-Curnutte theory⁹⁹⁻¹⁰¹ are

$$\delta_{f \leftarrow i} = \frac{n_2 \bar{v}}{2\pi c} \sum_{J_2} \langle J_2 | \rho_2 | J_2 \rangle \int_0^\infty 2\pi b [S_1 + I m\{S_2\}] db \quad (24)$$

$$\gamma_{f \leftarrow i} = \frac{n_2 \bar{v}}{2\pi c} \sum_{J_2} \langle J_2 | \rho_2 | J_2 \rangle \int_0^\infty 2\pi b Re\{S_2\} db \quad (25)$$

where the variables are as in Eqs. (22) and (23). Note, in ATC theory, the halfwidth is the integral over the components of the S_2 term, or equivalently, the sum of the integral of each term. (In general, for each term in the potential the S_2 term is composed of 3 operators, see Ref. 100 and 101 for details.) The similar feature of additivity also holds for the line shift in ATC theory, Eq.(24). This is not true in the theory of Robert and Bonamy because the method of cumulants⁹⁵ places the Liouville scattering matrix in the exponential. More important, when the real and imaginary components of the relaxation operator are taken, one arrives at Eqs. (22) and (23) in

which the real and imaginary components of the expanded S matrix are present in both expressions. All previous RB calculations^{121,125-132} for asymmetric rotor molecules employing the atom-atom and electrostatic potentials have assumed the imaginary contribution to the halfwidth to be negligible. The effects of the imaginary components, the cosine term in Eq. (23), on the halfwidths for the perturbing gases considered here are summarized below.

In the CRBF formalism the intermolecular potential is a combination of three kinds of terms: electrostatic, atom-atom, and induction-dispersion. The first of these is based on the permanent distribution of charge characterizing a given molecule, usually expressed as an expansion in moments (dipole, quadrupole, etc.). Gray and Gubbins^{133,134} have shown that the interaction resulting from two such charge distributions in proximity can be expressed in the form of a spherical tensor expansion, presented here in a slightly modified form for a H₂O-linear system,

$$V = \sum_{\substack{\ell_1 \ell_2 \\ \ell}} \sum_{\substack{n_1 \\ m_1 m_2 \\ m}} \sum_{w,q} \frac{U(\ell_1 \ell_2 \ell, n_1 w q)}{R^{q+\ell_1+\ell_2+2w}} \quad (26)$$

$$\otimes C(\ell_1 \ell_2 \ell; m_1 m_2 m) D_{m_1 n_1}^{\ell_1}(\Omega_1) D_{m_2 0}^{\ell_2}(\Omega_2) Y_{\ell m}(\omega)$$

where $C(\ell_1 \ell_2 \ell; m_1 m_2 m)$ is a Clebsch-Gordan coefficient, $\Omega_1=(\alpha_1, \beta_1, \gamma_1)$ and $\Omega_2=(\alpha_2, \beta_2, \gamma_2)$ are the Euler angles describing the molecular fixed axis relative to the space fixed axis. Subscripts 1 and 2 refer to the radiating and perturbing molecules, respectively, and $\omega = (\theta, \phi)$

describes the relative orientation of the centers of mass (see Figure 9). As stated previously, R is the center of mass separation. The coefficients $U(\dots)$ depend on electrostatic moments of the radiator (H_2O) and perturber gases according to expressions given in appendix A of ref. 115.

Although an electrostatic potential is suitable for large intermolecular separations, it is clearly inadequate at short range for neutral molecules. For example, the electrostatic terms in Eq. (26) are always orientation-dependent, whereas molecules in any orientation must ultimately repel one another at close range. The required terms are isotropic, i.e. with $l_1=l_2=0$, which cannot be supplied by electrostatics.

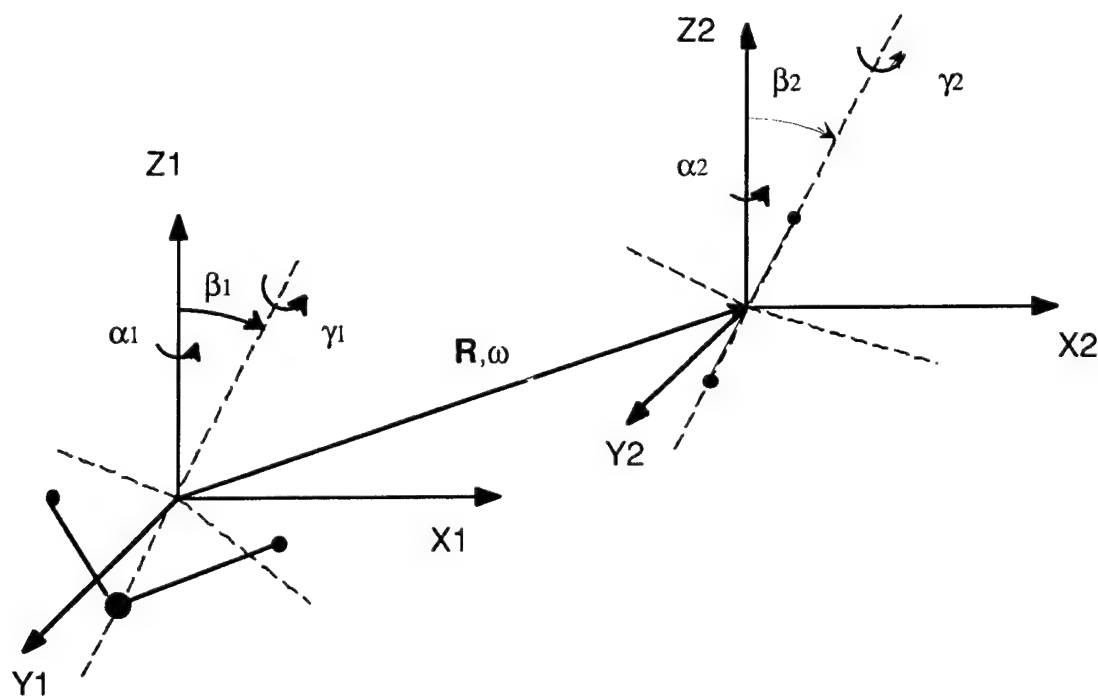


Figure 9 Geometry for $\text{H}_2\text{O}-\text{A}_2$ system. R is the center of mass separation and ω is the relative orientation. The

molecular fixed axes are defined relative to the space fixed axis by Euler angles.

To correct this deficiency, an atom-atom potential is added to the total interaction. This potential is defined as the sum of pairwise Lennard-Jones 6-12 interactions between atoms of molecules 1 and 2,

$$V^{\text{at-at}} = \sum_{i=1}^n \sum_{j=1}^m 4\epsilon_{ij} \left\{ \frac{\sigma_{ij}^{12}}{r_{1i,2j}^{12}} - \frac{\sigma_{ij}^6}{r_{1i,2j}^6} \right\}. \quad (27)$$

The subscripts $1i$ and $2j$ refer to the i th atom of molecule 1 and the j th atom of molecule 2, n and m are the number of atoms in molecules 1 and 2, respectively, and ϵ_{ij} and σ_{ij} are the Lennard-Jones parameters for the atomic pairs. The heteronuclear atom-atom parameters ϵ_{ij} and σ_{ij} are then constructed from homonuclear atom-atom parameters (ϵ_i and σ_i) by the "combination rules"¹³⁵

$$\begin{aligned} \epsilon_{12} &= \sqrt{\epsilon_1 \epsilon_2} \\ \sigma_{12} &= \frac{\sigma_1 + \sigma_2}{2}. \end{aligned} \quad (28)$$

Gray and Gubbins¹³³ have shown how the atom-atom potential may be expressed in the form of Eq. (26), and provide explicit expressions for $U(\dots)$ in terms of ϵ_{ij} and σ_{ij} . With such expressions, CRBF theory can be made to incorporate any combination of

electrostatic and atom-atom components one wishes to employ. The natural choice is simply to add the two, i.e.,

$$V(\text{total}) = V(\text{elec}) + V(\text{atom-atom}) \quad (3.8)$$

using available literature values for all electrostatic and atom-atom parameters. It has been shown^{117,118,136} that the addition of the atom-atom potential to the overall potential does not represent any "over counting" or duplication of potential interactions.

Before taking up discussion of the third interaction (induction-dispersion), three further points should be emphasized with regard to the atom-atom potential.

1. When expressed in the form of Eq. (26), the atom-atom potential can be understood as two simultaneous expansions. One is defined by the tensorial ranks l_1 and l_2 , which determine the symmetry of the interaction. A second expansion is defined by the sum l_1+l_2+2w , which we call the order of the expansion because it is the integer added to q in Eq. (26). It hardly needs to be emphasized that any calculation of halfwidth or line shift should be converged with respect to both order and rank.

2. The atom-atom potential contains an isotropic part ($l_1=l_2=0$) which in general are comprised of terms of the form $1/R^6$, $1/R^8$, $1/R^{10}$, etc. In our implementation, these are used to define the intermolecular trajectory. For the purpose of comparison, however, it is convenient to fit this summation to an effective isotropic (or "hetero-molecular") Lennard-Jones 6-12 potential,

$$V^{iso} = 4e \left[\left(\frac{\sigma}{R} \right)^{12} - \left(\frac{\sigma}{R} \right)^6 \right] \quad (30)$$

The approximation represented by Eq. (30) had no significant impact on our calculations other than to simplify the trajectory calculations somewhat.

3. The remaining parts of the atom-atom potential are anisotropic (non zero l_1 or l_2). These terms may be discussed with the same lexicon that one applies to electrostatic interactions. For example, when $l_1=1$ and $l_2=2$, we refer to a "dipole-quadrupole" interaction. It should be kept in mind that these are symmetry appellations only, and do not refer to electrostatics. Thus, it happens that between H_2O and N_2 , for example, the lowest anisotropic atom-atom term is "dipole-monopole", i.e. with $l_1=1$ and $l_2=0$. Such terms can contribute significantly to the line broadening mechanism.^{117,118,136}

In a third category of interactions relevant to intermolecular collisions are the isotropic induction and dispersion potentials,

$$V_{iso}^{ind} = - \frac{\mu_1^2 \alpha_2}{R^6} \quad (31)$$

and

$$V_{iso}^{dis} = - \frac{3}{2} \frac{E_1 E_2}{E_1 + E_2} \frac{\alpha_1 \alpha_2}{R^6}, \quad (32)$$

where μ_1 is the dipole moment of water vapor and α and E are the polarizability and ionization potentials for water vapor and its perturber. By design, these interactions occur with the same power of $1/R$, and in some sense represent the same forces, as the attractive

part of Eq. (30). Thus, they play no role in our trajectory calculations, although they do serve as a convenient check: we find that the magnitude of the combined induction-dispersion interactions is typically about one-half the value of the corresponding atom-atom term. This is consistent with observations of Gray and Gubbins,¹³³ who point out that Eqs. (31) and (32) are themselves merely the first terms in an expansion, and by Lynch et al.¹¹⁵. In principle, one could arrive at the vibrational dependence of the intermolecular atom-atom potential using contact transformations of Eq. (27) to the appropriate vibrational state. However, the isotropic induction and dispersion potentials provide a convenient, experimentally constrained method of computing the *difference* in isotropic potential for different *vibrational* states, via the vibrational dependence of μ_1 and α_1 (this difference appears in the S_1 term of CRBF theory, as described below). This difference is not accounted for in any other part of the theory, and represents no duplication of potential interactions.

The first order term in Eqs. (22) and (23) depends only on the difference in the isotropic part of the interaction potential between the initial and final vibrational states, v_i and v_f , of the radiator

$$S_1 = \frac{1}{\hbar} \int_{-\infty}^{\infty} dt \left[\langle v_f | V^{\text{iso}} | v_f \rangle - \langle v_i | V^{\text{iso}} | v_i \rangle \right] \quad (33)$$

where the time integral is evaluated along the relative trajectories of the radiator and perturber. The vibrational dependence of the isotropic interaction is approximated from the isotropic induction and

dispersion potentials, Eqs. (31) and (32). The dependence of the dipole moment and polarizability on the vibrational state of the molecule^{137,138} is considered in the calculations. For a ro-vibrational transition of the radiating molecule, the first order term can be written,

$$S_1 = - \frac{\alpha_2}{R_c^5 v_c'} \frac{3\pi}{8} \left[\frac{3}{2} \frac{I_1 I_2}{I_1 + I_2} (\alpha_{1,f} - \alpha_{1,i}) - (\mu_{1,f}^2 - \mu_{1,i}^2) \right], \quad (34)$$

where R_c and v_c' are the distance and effective velocity at the point of closest approach within the parabolic approximation.⁹¹

The vibrational dependence of the dipole moment of water vapor was investigated by Shostak and Muentner¹³⁹ and is given in Debyes by

$$\mu = 1.855 + 0.0051v_1 - 0.0317v_2 + 0.0225v_3, \quad (35)$$

where v_i is the number of quanta in the i^{th} normal mode. The vibrational dependence of the polarizability of water vapor was obtained by Luo et al.¹⁴⁰ and is, in atomic units,¹⁴¹

$$\alpha = 9.86 + 0.29v_1 + 0.03v_2 + 0.28v_3. \quad (36)$$

The second-order term is the complex analog of that appearing in the familiar ATC theory,⁹⁹⁻¹⁰¹

$$S_2 = S_{2,i2}^* + S_{2,f2} + S_{2,\text{middle}} \quad (37)$$

where the notation is that of Anderson.¹⁰⁰ The case in which the imaginary part of S_2 is ignored has been discussed thoroughly in the literature.^{99-101,142,143} Note, $S_{2,\text{middle}}$ only has a real component. The other terms are complex functions and can be written in the form

$$S_{2,f2} = \frac{1}{\hbar^2 [J_f][J_2]} \sum_{\substack{\ell_1 \ell_2 \\ J_2 J_f}} \sum_{\mathbf{n}^a \mathbf{n}^b} D(\ell_1 \ell_2, \mathbf{n}^a \mathbf{n}^b, J_f J_f J_2 J_2) F_{\mathbf{n}^a \mathbf{n}^b}^{\ell_1 \ell_2}(\omega_{f2, f'2'}) \quad (38)$$

where $[J]=2J+1$, $\mathbf{n} = (n_1, n_2)$ and $\omega_{f2, f'2'} = (E_{f'} - E_f + E_{2'} - E_2)$ where E_s is the energy of the state f' , f , $2'$, or 2 . $S_{2,i2}$ is obtained from Eq. (3.17) by replacing f with i . The D terms are reduced matrix elements for the internal states of the radiator and perturber.¹¹⁵ The F terms are the resonance functions and are given by

$$F_{\mathbf{n}^a \mathbf{n}^b}^{\ell_1 \ell_2}(\omega) = \frac{1}{[\ell_1][\ell_2]} \sum_{\substack{\mathbf{w}^a \mathbf{w}^b \\ \mathbf{q}^a \mathbf{q}^b}} \sum_{\substack{\ell^a \ell^b \\ \mathbf{m}_1^a \mathbf{m}_2^b}} C(\ell_1 \ell_2 \ell^a, \mathbf{m}_1 \mathbf{m}_2 \mathbf{m}^a) C(\ell_1 \ell_2 \ell^b, \mathbf{m}_1 \mathbf{m}_2 \mathbf{m}^b) \\ U(\ell_1 \ell_2 \ell^a, \mathbf{n}^a, \mathbf{w}^a \mathbf{q}^a) U^*(\ell_1 \ell_2 \ell^b, \mathbf{n}^b, \mathbf{w}^b \mathbf{q}^b) \quad (39)$$

$$\int_{-\infty}^{\infty} dt e^{i\omega t} \frac{Y_{\ell^a \mathbf{m}^a}[\omega(t)]}{R^{\mathbf{p}^a}(t)} \int_{-\infty}^t dt' e^{-i\omega t'} \frac{Y_{\ell^b \mathbf{m}^b}^*[\omega(t')]}{R^{\mathbf{p}^b}(t')}$$

where $\mathbf{p}^a = \mathbf{q}^a + \ell_1 + \ell_2 + 2\mathbf{w}^a$ (similarly for \mathbf{p}^b) and the other terms are as described earlier. The integration is along the relative semiclassical

trajectory of the molecules involved. All integrals are evaluated, real and imaginary terms,¹¹⁵ for the potential discussed above.

3.2 Calculations

Calculations of the halfwidth and line shift based on the CRBF method are made for transitions of H₂O perturbed by the gases mentioned above. To investigate the contribution of the imaginary components on the halfwidth and line shift, calculations are made with the different imaginary terms and compared. The different calculations are labeled as follows; RRB: the real components of the RB formalism, RS₂: the real components and the imaginary S₂ terms, RS₁: the real components and the S₁ terms, and finally, CRBF: all real and imaginary terms. In addition, the order of the expansion (l_1+l_2+w) of the atom-atom potential is varied. All calculations are made at the HITRAN³ reference temperature, 296 K. No temperature correction is applied to the data since the small difference in the measurement and calculation temperatures is negligible. The CRBF formalism yields the halfwidth and line shift from a single calculation and there are no adjustable parameters or cutoff procedure in the formalism.

All molecular parameters used in this work are the best available values from the literature. *No molecular constants are adjusted to give better agreement with experiment.* The dipole and quadrupole moments of water vapor are taken from Refs. 139 and 144, respectively. The quadrupole moment of nitrogen is from Mulder et al.¹⁴⁵ and that for oxygen is from Stogryn and Stogryn¹⁴⁶

There have been a number of measurements of the quadrupole moment of carbon dioxide¹⁴⁷ which range from 4.0 to roughly 4.6 in units of 10^{-26} esu. The most recent measurement¹⁴⁸ reports a value of $4.02(10) \times 10^{-26}$ esu which is adopted in this work. For hydrogen the value of the quadrupole moment is from Poll and Wolniewicz.¹⁴⁹ The numerical values are listed in Table 12. The vibrational dependence of the dipole moment of H₂O (Eq.(35)) is taken from Shostak and Muentner¹³⁹ and the vibrational dependence of the polarizability of H₂O (Eq.(36)) is taken from the work of Luo et al.¹⁴⁰. The atom-atom parameters, Table 13, were obtained using the combination rules,¹³⁵ (see Eq. 28) and the atom-atom parameters for homonuclear diatomics determined by Bouanich¹⁵⁰ by fitting to second virial coefficient data.

Table 12. Values of electrostatic moments for the water vapor, N₂, O₂, CO₂, H₂.

Molecule	Multipole Moment	Reference
H ₂ O	$\mu = 1.8549 \times 10^{-18}$ esu	139
	$Q_{xx} = -0.13 \times 10^{-26}$ esu	139
	$Q_{yy} = -2.5 \times 10^{-26}$ esu	139
	$Q_{zz} = 2.63 \times 10^{-26}$ esu	139
N ₂	$Q_{zz} = -1.4 \times 10^{-26}$ esu	145
O ₂	$Q_{zz} = -0.4 \times 10^{-26}$ esu	146
CO ₂	$Q_{zz} = -4.02 \times 10^{-26}$ esu	148
H ₂	$Q_{zz} = -0.616 \times 10^{-26}$ esu	149

Table 13. Values of the heteronuclear atom-atom Lennard-Jones (6-12) parameters for the collision pairs considered in this work.

Atomic pair	$\sigma/\text{\AA}$	$\epsilon/k_B / ^\circ\text{K}$
N-O	3.148	43.90
N-H	2.990	20.46
O-O	3.010	51.73
O-H	2.850	24.13
H-C	2.810	32.18
H-H	2.683	11.25
O-C	3.285	40.43

In the parabolic approximation, the isotropic part of the interaction potential is taken into account in determining the distance, effective velocity, and force at closest approach.⁹¹ To simplify the trajectory calculations, the isotropic part of the atom-atom expansion is fit to an isotropic Lennard-Jones 6-12 potential (see Eq. 30) and the resulting parameters are given in Table 14 for the particular collision pairs considered in this work.

Table 14. Values of the isotropic atom-atom parameters used to define the trajectories of the collision systems considered in this work.

Collision System	Order	$\sigma/\text{\AA}$	$\epsilon/k_B (^\circ\text{K})$
H ₂ O-N ₂	8th	3.62	96.6
H ₂ O-O ₂	8th	3.53	105.22
H ₂ O-CO ₂	4th	3.60	164.35
H ₂ O-H ₂	4th	3.838	119.3

To evaluate the reduced matrix elements in Eq. (38), ro-vibrational wave functions are needed. For the $3\nu_1+\nu_3$ and the $2\nu_1+2\nu_2+\nu_3$ bands the constants of Grossmann et al.¹⁵¹ are used. Because of limitations in computing wavefunctions for high J states for the triad, ν_1 , $2\nu_2$, and ν_3 , ground vibrational state wavefunctions are used in the calculations with the Watson-Hamiltonian constants of Flaud and Camy-Peyret.¹⁵² This approximation introduces less than a percent error to the halfwidth for these bands. For the rotation and ν_2 bands, the constants of Flaud and Camy-Peyret¹⁵² are used. The molecular constants for N_2 , O_2 , and H_2 are from Huber and Herzberg.¹⁵³ For carbon dioxide, the molecular constants of Rothman et al.¹⁵⁴ are used.

Finally, the ionization potential of water was taken to be a vibrationally-independent 12.6 eV.¹⁵⁵ The polarizability and ionization potential of the perturbing gases are given in Table 15.

Table 15. Values of the polarizability and ionization potential for N_2 , O_2 , CO_2 , H_2 .

Perturbing gas	Polarizability / 10^{-24} cm ³	Reference	Ionization potential /ev	Reference
N_2	1.740	156	15.576	157
O_2	1.580	156	12.063 ± 0.001	155
CO_2	2.913	156	13.769 ± 0.03	158
H_2	0.806	156	15.427 ± 0.002	159

3.3 Results and Discussion

In this section, we present a summary of the comparison of the calculated and measured halfwidths and line shifts as well as describe some of the general trends observed. There are several important features that stand out from this work. First, we address the expansion of the atom-atom potential and the effects the order of expansion has on both the halfwidth and line shift. The order of the expansion, defined above, is varied from 0 to 8 and the results compared. Note, the electrostatic and induction-dispersion potentials are used in all calculations and are defined as the 0th order calculation, i.e. no atom-atom terms. Figure 10 shows the results of calculations of the halfwidth for transitions belonging to the $3\nu_1 + \nu_3$ band of H₂O for oxygen as a perturbing species. Plotted are the halfwidth versus an energy ordered index, $J''(J''+1) + K_a'' - K_c'' + 1$. These include the measurements of Grossmann and Browell¹¹⁹ with error bars, the calculations for a 0th order (diamond symbols), 4th order (circle symbols), and 8th order (triangle symbols) expansion of the atom-atom potential. What is obvious from the figure is that for oxygen-broadening of H₂O, calculations utilizing only an electrostatic expansion of the intermolecular potential are inadequate. There is an improvement in the agreement between experiment and theory when the 4th order expansion is used. Finally, when calculations are made with the 8th order expansion of the atom-atom potential the best agreement with measurement is obtained. We comment that limitations in our current computational facilities limits us to the 8th order expansion for this system. Similar results are observed for

calculations of the line shift for these transitions. In Figure 11, the measured line shifts from Grossmann and Browell¹¹⁹ with error bars and the 0th, 4th, and 8th order expansion of the atom-atom potential are plotted versus the energy ordered index with the same symbols as Figure 10. There is poor agreement between measurement and calculation with the 0th order calculation, going to best agreement for the 8th order calculation.

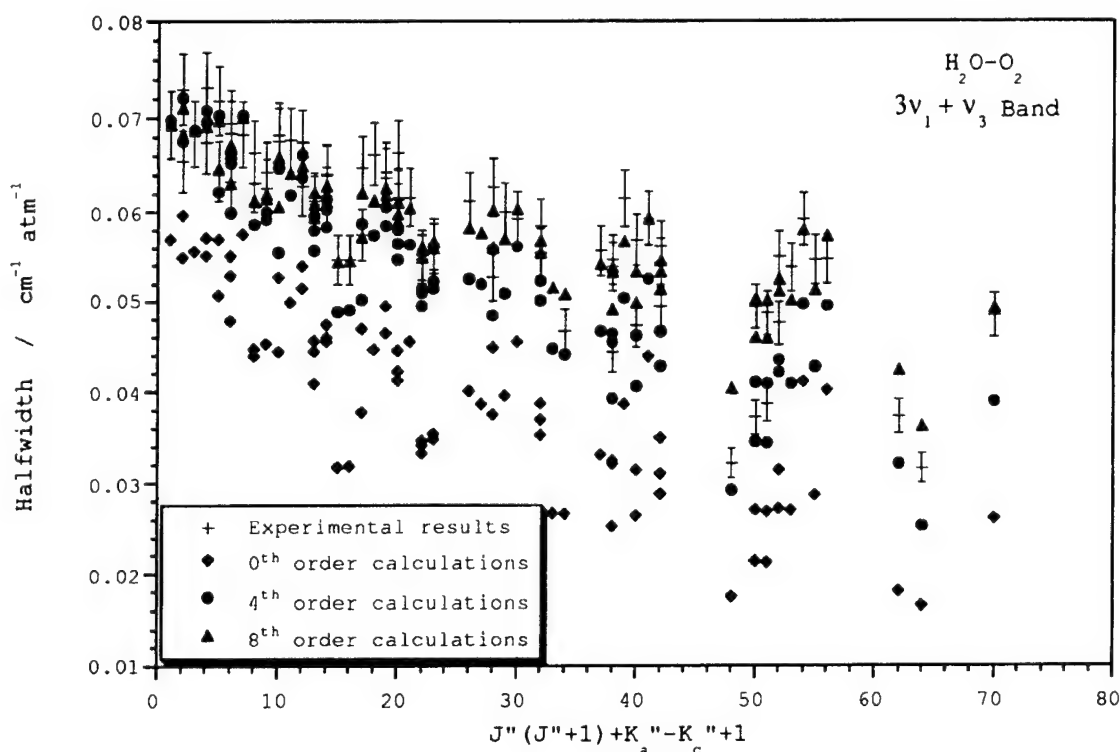


Figure 10 Halfwidth in units of cm⁻¹ atm⁻¹ for water vapor transitions in the 3ν₁+ν₃ vibrational band perturbed by O₂ versus energy ordered index (see text). Measurements of Grossmann and Browell¹¹⁹ are plotted with error bars, 0th order calculations with diamond symbols, 4th order calculations with circle symbols, and 8th order

calculations with triangle symbols (order refers to the expansion of the atom-atom potential).

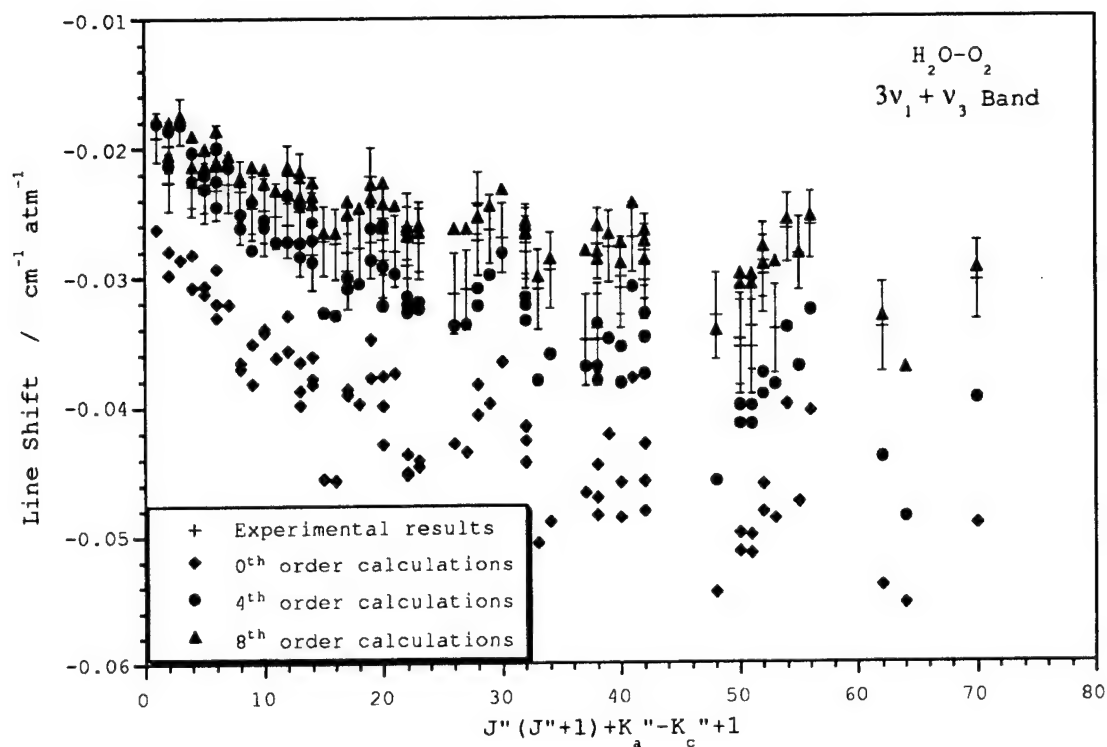


Figure 11 Line shifts in units of $\text{cm}^{-1} \text{ atm}^{-1}$ for water vapor transitions in the $3v_1+v_3$ vibrational band perturbed by O_2 versus energy ordered index (see text). Measurements of Grossmann and Browell¹¹⁹ are plotted with error bars, 0th order calculations with diamond symbols, 4th order calculations with circle symbols, and 8th order calculations with triangle symbols (order refers to the expansion of the atom-atom potential).

The importance of the atom-atom potential varies according to the strength of the electrostatic interaction. In general, we have found that for systems for which the moments of the molecules are

large, e.g. CO_2 , the atom-atom potential has a very small effect on the halfwidth and line shift ($<1\%$). For nitrogen as a perturbing species, the effect is small for many of the transitions, however, there are some transitions where the effect can be 15% of the calculated halfwidth.¹¹⁷ It is found that the transitions where the atom-atom potential has an effect can be classified as weak-collision systems in the definition of Oka.¹⁰⁵ Similar results are found for hydrogen as the perturbing species.¹⁶⁰ For O_2 as the perturbing species, the high-order expansion is necessary to get any reasonable agreement with experimental values. In the calculations presented here, we have expanded the atom-atom potential to 8th, 8th, 4th, and 4th order for N_2 , O_2 , CO_2 , and H_2 as the perturbing species, respectively.

Next, we focus on the line shifts. It is observed that the line shifts for water vapor are both positive and negative depending on the vibrational band in question. This can be understood in terms of the components, S_1 and $Im\{S_2\}$ that contribute to the line shift.¹¹⁵ The S_1 term depends on the vibrational dependence of the polarizability, Eq. (36). Utilizing the coefficients of Ref. 140 this contribution is negative and will increase with the number of quanta in the vibrational state. The imaginary part of the S_2 term can be either positive or negative. For transitions for which the change in the vibrational quantum numbers is small, the line shifts will be both positive and negative. As the change in the number of vibrational quanta for the transition increases, the line shifts become increasingly more negative. Thus, for the transitions considered here, the line shifts for the $3\nu_1+\nu_3$ and the $2\nu_1+2\nu_2+\nu_3$ bands are negative and those for the ν_1 , $2\nu_2$, and ν_3 bands are both positive

and negative. This is demonstrated in Figures 12 and 13 for N₂-induced pressure shifts in the $3\nu_1+\nu_3$ band of H₂O and for CO₂-induced pressure shifts in the ν_1 , $2\nu_2$, and ν_3 bands of H₂O, respectively. In Figure 12, the N₂ induced pressure shifts in the $3\nu_1+\nu_3$ band of H₂O are plotted versus the energy ordered index. Shown are the experimental data of Grossmann and Browell¹¹⁹ with error bars, the RS₂ calculated values are the diamond symbols, the RS₁ calculated values are the circle symbols, and the values from the CRBF calculation are triangles. What is apparent is that as the imaginary terms are included, agreement with experiment improves dramatically. Note, the line shifts from the RS₂ calculation are both positive and negative and the line shifts from the RS₁ calculations are all negative, as discussed above. In Figure 13, the measured line shifts of Gamache et al.¹¹⁶ with error bars are plotted versus the transition number (see Table I of Ref. 116). Included in the plot are the CRBF calculated values as solid circles, the RS₂ calculated values as solid triangles, and the RS₁ values as solid squares. For transitions numbered 17 and 27 there are no measured values thus only the calculated values are plotted. The RS₁ values are all small due to the number of vibrational quanta involved in these transitions and all negative as explained above. Thus, for this system, the line shift is mostly due to the imaginary part of S₂ with small corrections coming from the S₁ terms resulting in line shifts that are both positive and negative. The agreement between the experimental results and the CRBF calculated values is good with most of the calculated values falling within the error estimate of the measurements. This is further summarized below.

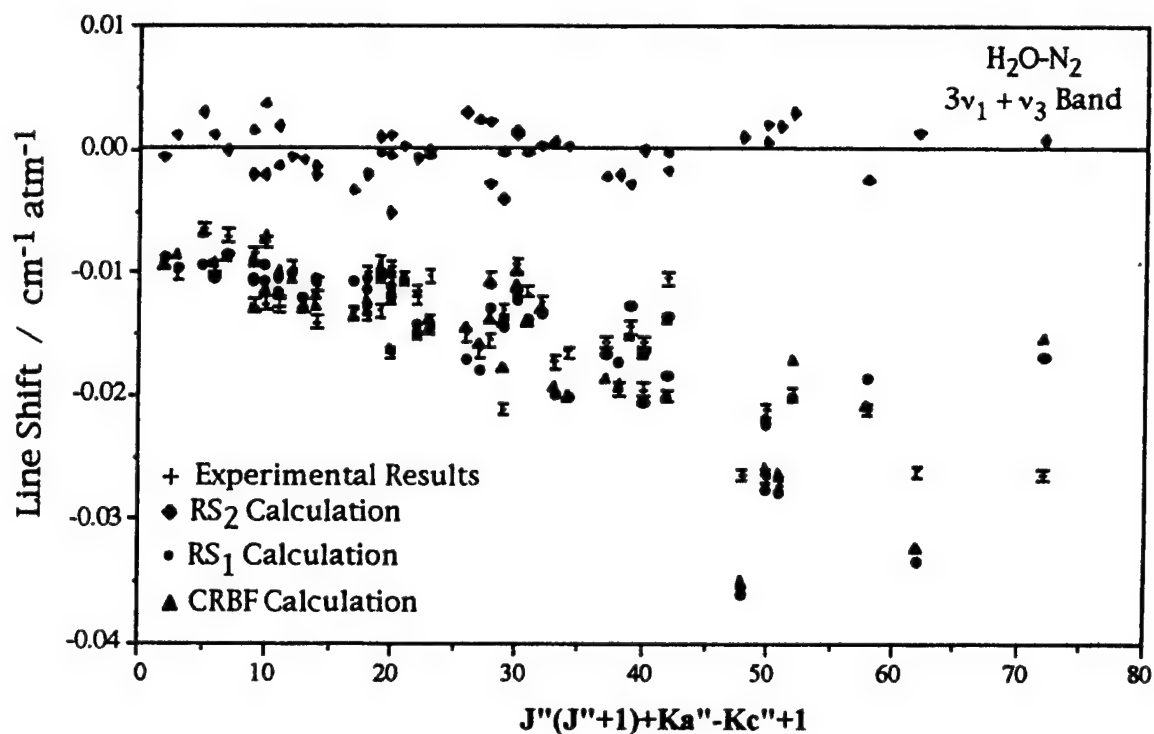


Figure 12 Line shifts in units of $\text{cm}^{-1} \text{ atm}^{-1}$ for water vapor transitions in the $3v_1+v_3$ vibrational band perturbed by nitrogen versus energy ordered index (see text). Calculations with various levels of the imaginary terms: RS_2 calculated values (diamond symbols), RS_1 calculated values (circle symbols), CRBF calculated values (triangle symbols) compared with the experimental data of Grossmann and Browell.¹¹⁹

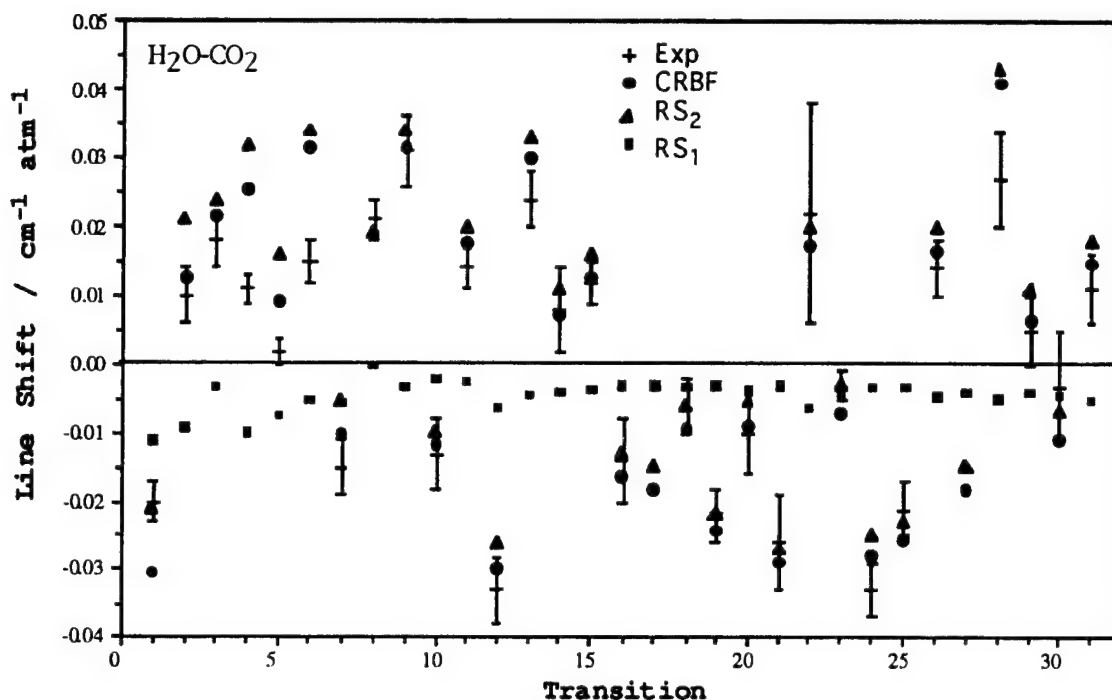


Figure 13 Line shifts for H_2O transitions broadened by CO_2 . Plotted are line shifts in units of $\text{cm}^{-1}/\text{atm}$ versus transition number from Table I of Ref. 116; Measurements with error bars, CRBF as solid circles, RS_2 as solid triangles, and RS_1 as solid squares.

Last, we focus on the imaginary contributions to the halfwidth. As noted, the complex Robert-Bonamy formalism leads to the imaginary components of the expanded S matrix having a contribution to the halfwidth. The contribution of these components to the halfwidth has remained a relatively unexplored facet of the theory because some of the imaginary resonance function integrals have only been derived recently.¹¹⁵ Previous analysis of these contributions for nitrogen and oxygen broadening of water vapor transitions^{114,115,117,118} indicated that the imaginary parts do

contribute to the halfwidth. For the $\text{H}_2\text{O}-\text{N}_2$ system, the difference between the RRB and CRBF calculations are generally small with exceptions up to 10-15% observed. For the $\text{H}_2\text{O}-\text{O}_2$ system, the importance of the imaginary terms is more pronounced, accounting for up to 25% difference between RRB and CRBF calculations. This is shown in Figure 14 where the halfwidth is plotted versus the energy ordered index for transitions in the $3\nu_1+\nu_3$ band of H_2O with O_2 as the perturbing gas. Plotted are the measurements of Grossmann and Browell¹¹⁹ with error bars, the RRB calculated values as circle symbols, and the CRBF calculated results as triangle symbols. In almost all cases, there is a large difference between the RRB and CRBF calculated values with the CRBF values demonstrating good agreement with measurement. Analysis indicates that the transitions for which the imaginary terms make a contribution to the halfwidth are also those for which the atom-atom terms are important (intermediate to weak collisions¹⁰⁵).

The $\text{H}_2\text{O}-\text{CO}_2$ system is characterized by strong collisions, thus one might assume that the imaginary terms are unimportant in the calculation of the halfwidth. This, however, is not what is observed from the calculations.¹¹⁶ In Figure 15 the measured halfwidths with error bars from Ref. 116 are plotted versus the transition number from Table I of Ref. 116 with the calculated CRBF values as solid circles, the RS_2 values as solid triangles, and the RRB values as solid squares. From the figure, it is apparent that as the imaginary components are included in the calculation better agreement with experiment is obtained. The difference between the RRB and CRBF calculation of the halfwidth is greater than the desired accuracy of

the spectroscopic community^{89,90} for more than two-thirds of the lines studied¹¹⁶. This is demonstrated in Figure 16 where the percent differences between the RRB and CRBF calculations, $(\text{CRBF}-\text{RRB})/\text{CRBF}$, are shown versus the transition number (Table I of Ref. 116). For hydrogen broadening of H_2O , we have observed that the imaginary contribution to the halfwidth is very small.¹⁶⁰

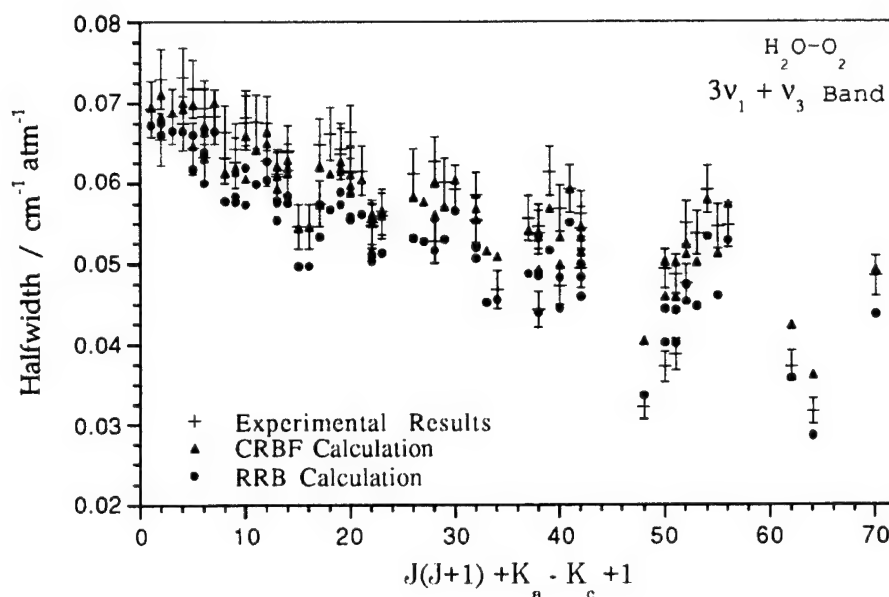


Figure 14. Halfwidths in units of $\text{cm}^{-1} \text{ atm}^{-1}$ for water vapor transitions in the $3\nu_1 + \nu_3$ vibrational band perturbed by oxygen. Measurements of Grossmann and Browell¹¹⁹ are plotted with error bars, results by RRB calculations with circle symbols, and results by CRBF calculations with triangle symbols.

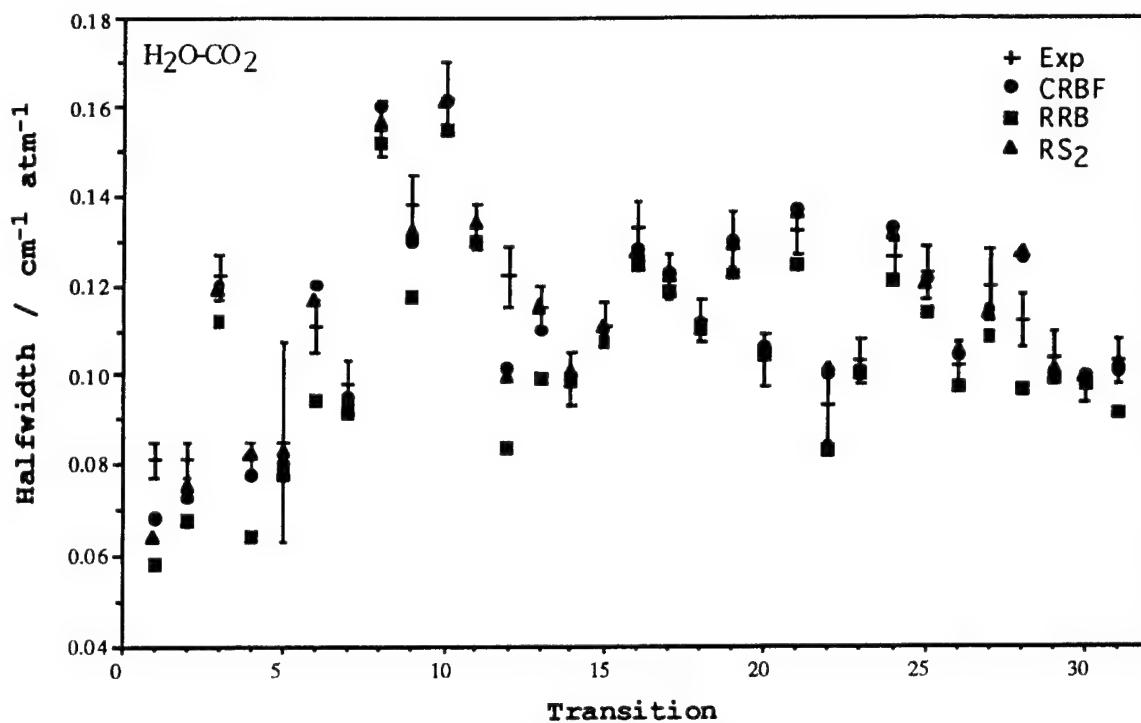


Figure 15. Halfwidths for H₂O transitions broadened by CO₂. Plotted are halfwidths in units of cm⁻¹ atm⁻¹ vs. transition number from Table I of Ref. 116; Measurements with error bars, CRBF as solid circles, RS₂ as solid triangles, and RRB as solid squares.

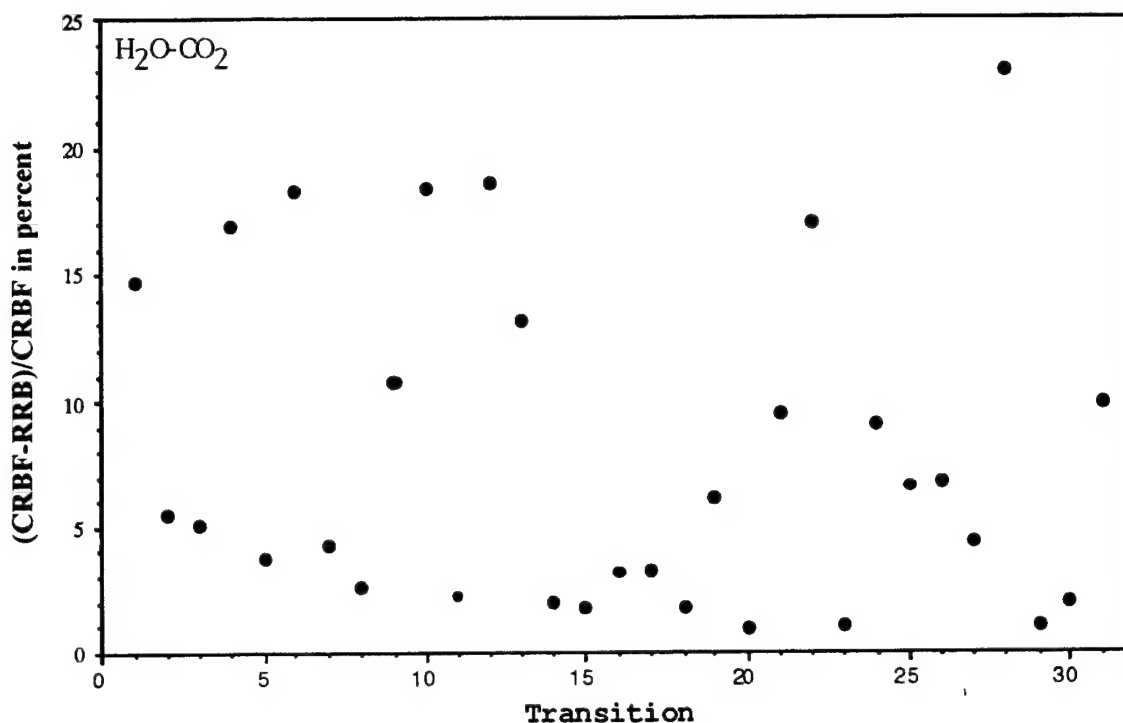


Figure 16. Percent difference between CRBF and RRB calculations, $(CRBF-RRB)/CRBF$, vs. transition number from Table I of Ref 116.

To summarize, we have made CRBF calculations of the pressure-broadened halfwidth for 772 transitions of H_2O perturbed by N_2 , O_2 , CO_2 , and H_2 , and compare these results with measurement. These data are for the rotational, v_1 , v_2 , v_3 , $2v_2$, $3v_1+v_3$ and $2v_1+2v_2+v_3$ bands of H_2O . In addition, pressure-induced line shifts for 212 transitions of water vapor perturbed by N_2 , O_2 , and CO_2 are calculated by the CRBF method and compared to measurements. Tables 16-19 report the average percent differences between the CRBF calculated halfwidth and line shift and the measured values from Refs. 119, 119, 116, and 122, respectively. For hydrogen as the perturbing species there are enough data to calculate a meaningful

standard deviation and this is included in Table 19. We have calculated the average percent difference between the measured and calculated line shifts for the $3\nu_1+\nu_3$ and $2\nu_1+2\nu_2+\nu_3$ bands of H_2O but not for the ν_1 , $2\nu_2$, and ν_3 bands. This is because in the former case the line shifts are large enough in magnitude for a percent difference to be useful. For the later bands, the line shifts are relatively small in magnitude, thus, we are making comparisons of small numbers. In fact, for these data the experimental uncertainty, as small as $0.002 \text{ cm}^{-1}/\text{atm}$, can be as large as 100% of the line shift. Thus, it does not make sense to talk of a percent difference for these comparisons. For the pressure-broadened halfwidths, the overall average percent difference for the 772 comparisons is -0.8 percent. The average percent difference for the 183 comparisons made for the line shift in Tables 16 and 17 is -3.6%. Perhaps it is better to note that for the line shifts, the CRBF calculated values generally fall within or are close to the experimental uncertainties.

Table 16. Average percent differences between the measured¹¹⁹ and CRBF calculated halfwidths and line shifts for the water vapor-nitrogen system.

Band	Parameter	# lines	APD ^a	AAPD ^b
$3\nu_1 + \nu_3$	γ	49	-2.3	3.4
$2\nu_1 + 2\nu_2 + \nu_3$	γ	22	-7.5	10.9
$3\nu_1 + \nu_3$	δ	55	-4.1	11.0
$2\nu_1 + 2\nu_2 + \nu_3$	δ	25	-13.3	18.0

^a Average percent difference

^b Average absolute percent difference

Table 17. Average percent differences between the measured¹¹⁹ and CRBF calculated halfwidths and line shifts for the water vapor-oxygen system.

Band	Parameter	# lines	APD ^a	AAPD ^b
3v ₁ + v ₃	γ	76	-0.2	4.4
2v ₁ + 2v ₂ + v ₃	γ	28	-0.6	4.9
3v ₁ + v ₃	δ	78	7.8	8.4
2v ₁ + 2v ₂ + v ₃	δ	25	-28.2	28.2

^a Average percent difference

^b Average absolute percent difference

Table 18. Average percent differences between the measured¹¹⁶ and CRBF calculated halfwidths and line shifts for the water vapor-carbon dioxide system.

Band	Parameter	# lines	APD ^a
v ₁	γ	8	0.4
2v ₂	γ	1	-0.8
v ₃	γ	22	1.8

^a Average percent difference

Table 19. Average percent differences between the measured¹²² and CRBF calculated halfwidths and line shifts for the water vapor-hydrogen system.

Band	Parameter	# lines	APD ^a	SD ^b
rotation	γ	64	-1.9	4.2
v ₁	γ	92	2.7	4.6
v ₂	γ	273	-2.8	5.4
v ₃	γ	137	2.1	4.2

^a Average percent difference

^b Standard deviation

In conclusion, we give the following comments with respect to calculations of pressure-broadened halfwidths and pressure-induced line shifts for ro-vibrational transitions of water vapor. The effects of the imaginary components, the choice of potential, and the order of expansion of the potential vary from transition to transition. To insure a reasonably correct calculation, the CRBF approach with the leading terms of the electrostatic potential, the atom-atom potential expanded to at least 4th-order, and the isotropic induction and dispersion potentials should be used.

The results of these calculations demonstrate a profound dependence of the halfwidth on the imaginary terms in the calculation for some of the perturbing species considered here. For the 772 transitions studied for 4 perturbing species, the CRBF calculation of the halfwidth is in better agreement with experiment than calculated values based on other theoretical methods. Almost always, as the imaginary components are added and the atom-atom

potential is included to high order, the results move in the direction of measurement. And last, the line shifts calculated by the CRBF method agree very well with experiment.

The CRBF formulation offers a cutoff-free, scaling-parameter-free approach to calculating the halfwidth and line shift. The authors are testing the CRBF formulation on other radiator and perturbing species and investigating the temperature dependence of the halfwidth and line shift. This work will be presented in a future publication. It appears that the CRBF formalism is close to satisfying the spectroscopic community's need to know such parameters to an accuracy of 1-5%.^{89,90}

4.0 PROGRAMS FOR THE HITRAN DATABASE

A new version of the BANDSUM program was written which works with the new .CMN files etc. Also BD-VIBS.FOR was updated again for the Schuman-Runge band information. We have added $v=2$ of $X^3\Sigma^-_g$ and $v=0$ to 19 of $B^3\Sigma^-_g$. The list of vibrational levels of Brown and Urban have been added to BD-VIBS.FOR.

A number of supplemental programs that will accompany the database have been written. These are programs that calculate the natural isotopic abundance, the molecular masses, programs to check the band center list, and similar types of programs. All programs have been delivered to Dr. L. Rothman for use in the maintenance of the database. In addition, updates to several of the BLOCK DATA routines were made.

A new table has also been added to the database which contains the information for the isotopic label, natural isotopic abundance, the partition sum at 296K, the state-independent nuclear degeneracy factor, and the molar mass for each species. This table is called MOLPARAM.TXT and is distributed with the database.

4.1 Transition Moment Squared

The calculation of the transition moment squared for all species on the database was reviewed. Since the last version of the database there have been many changes to the vector indices that control the database. These changes had not been made to the TR-MOM program. In addition to these changes, there were many cases where the transition moment squared could not be calculated due to the partition sums not being present. For the 1995 database, there is also the addition of several new molecules and additional isotopomers for some molecules. All of these factors need to be included in the 1995 version of TR-MOM.

The first changes were to add to the code the correct .CMN files in order to have correspondence with the latest molecule, abundance, isotopomer and vibrational labeling. Next, subroutines were written for all the new molecular species that have been added to the database. The old subroutines were updated for new isotopomers where appropriate. The subroutines that defaulted a value of R^2 equal to zero were also corrected. The individual subroutines were checked for consistent use of partition sums, degeneracy factors, etc. The updates to the transition moment squared program that were

discussed in the last quarterly report were implemented. These include the vector indices (molecule and isotope codes), isotopic abundance, updated partition sums and degeneracies, and other corrections in the codes. One major improvement is the ability to calculate R^2 for all the species on the main database. Thus, the subroutines that defaulted to a zero value of R^2 now correctly calculate the transition moment. For the molecular species new to the database subroutines were written to calculate R^2 . For new isotopomers old subroutines were updated to consider the new species. The individual subroutines were checked for consistent use of partition sums, degeneracy factors, etc. Test calculations unveiled some additional errors which were corrected and the new version of the TR-MOM program was linked with the latest versions of BD-ISO, BD-MOL, BD-VIBS, BD-ABUN, and BD-QT.

4.2 State Independent Degeneracy Factors

Table 20 lists the molecule number, molecule, isotopomer code, species code, and the state independent degeneracy factors that are used for determining the partition function, correct transition moment squared factor, and conversion between intensity, R^2 , Einstein-A coefficients, etc.

Table 20. State Independent Degeneracy Factors

1	H ₂ O	161	1	1	12	HNO ₃	146	45	6		
		181	2	1							
		171	3	6							
		162	4	6							
2	CO ₂	626	5	1	13	OH	61	46	1~		
		636	6	2			81	47	1~		
		628	7	1			62	48	1~		
		627	8	6	14	HF	19	49	4		
		638	9	2			15	HCl	15	50	8
		637	10	12	17	51			8		
		828	11	1	16	HBr	19	52	8		
		728	12	6			11	53	8		
3	O ₃	666	13	1	17	HI	17	54	12		
		668	14	1			18	ClO	56	55	1~
		686	15	1					76	56	1~
		668	16	1	19	OCS	622	57	1		
		686	17	1			624	58	1		
		667	18	6			632	59	2		
		676	19	6	822	60	1				
		4	N ₂ O	446	20	9	623	61	4		
456	21			6	20	H ₂ CO	126	62	1		
546	22			6			136	63	2		
448	23			9			128	64	1		
447	24			54			21	HOCl	165	65	8
5	CO	26	25	1					167	66	8
		36	26	2	22	N ₂			44	67	1
		28	27	1			23	HCN	124	68	6
		27	28	6					134	69	12
		38	29	2	125	70			4		
		37	30	12	24	CH ₃ Cl	215	71	4		
6	CH ₄	211	31	1			217	72	4		
		311	32	2			25	H ₂ O ₂	1661	73	4
		212	33	3	26	C ₂ H ₂			1221	74	1
7	O ₂	66	34	1					1231	75	8
		68	35	1			27	C ₂ H ₆	1221	76	64
		67	36	6	28	PH ₃			1111	77	2
8	NO	46	37	1~					29	COF ₂	269
		56	38	1~			11	NH ₃			4111
		48	39	1~	5111	44					2

Table 20. State Independent Degeneracy Factors

30 SF ₆	29	79	1		7646	87	12
31 H ₂ S	121	80	1	36 NO ⁺	46	88	3
	141	81	1				
	131	82	4	37 HOBr	169	89	8
					161	90	8
32 HCOOH	126	83	4				
				38 H ₄ C ₂	1221	91	1
33 HO ₂	166	84	2		1231	92	32
34 O	6	85	NA				
35 ClONO ₂	5646	86	12				

5.0 SPECTRAL PARAMETERS FOR SPECIES ON THE DATABASE

5.1 Errors in the 1992 data for Hydrogen Halides and Carbon Monoxide

Dr. Curtis Rinsland, of NASA Langley Research Center, reported to us that there were problems with the HCl fundamental ($1 \leftarrow 0$) line positions compared with measurements he has made.¹⁶¹ While investigating this problem, it was suspected that there were errors in the other hydrogen halides and CO. For HCl, comparisons were made with the data of Rinsland, the 1986 HITRAN database data¹⁶² and the 1992 data.¹⁶³ This study revealed errors in the data for the HCl fundamental band on the 1992 database.³ Further investigation showed the data for all bands of HCl on HITRAN92 have some errors.

These problems led us to question whether the data for the other closed shell diatomics are correct. The reference point was taken as the 1986 HITRAN database. The line positions (HITRAN92-HITRAN86) and the ratio in the line intensities (HITRAN92/HITRAN86) were compared for HF, HCl, HBr, HI, and CO.

The comparisons were made and, with the exception of HCl positions, the results indicated that the data for the other diatomics, positions and intensities (HCl included), are not grossly different, except for several typographical errors. These errors were summarized and delivered to Dr. L. Rothman.

For the line positions, we have calculated the energies of the diatomic molecules using the Dunham expansion and compared the values with the 1986 and 1992 databases. This indicated that the 1992 data was in error. From discussions with the author of this data,¹⁶³ we discovered the data files were typed by a secretary from computer output and concluded this to be the source of the typographical errors. This data needs to be corrected for the next version of the database.

5.2 Vibrational Band Centers

We have modified the file of vibrational band centers to be more easily maintainable. The existing file had information about the molecule, isotopic species, vibrational band, band center, and a written reference in an A40 format. It is our intentions to update this file with improved band centers. What we have done is to reformat the file so that it can be read in free format and to eliminate the need for writing the reference. The reference is now the HITRAN reference code and can be found in TABLES.3 of the database. We have gone through the file and cross-referenced with TABLES.3. For the references that existed in TABLES.3 we must use the same numbers, for others we added numbers and references to

TABLES.3 accordingly. The new file of band centers has the structure Mol number, HITRAN isotope code, spectroscopic vibrational quanta (' ← '), the band center in cm^{-1} , reference number.

5.3 Other Species Data for HITRAN

New molecules and isotopic species have been added to the database. The number of molecules is now 36 (up from 32 on the 1992 Edition). The additions include the 667 and 676 isotopic species of ozone and the 37 isotopomer of CO. The new additions with the corresponding molecule number a given in Table 21.

The hydroperoxyl radical, HO_2 has been added as molecule 33, it is an asymmetric rotor and is vibrational Class 6 and in rotation Group 1. The oxygen atom is molecule 34, it has no vibrational structure (an atom) and is a special case. It has been put in vibrational Class 1 and rotational Group 2. Next, molecule 35, is ClONO_2 , this has been placed with the other large species, i.e. vibrational class 10 and in rotational Group 1. NO^+ has been added as molecule # 36 and is in vibrational Class 1.

The new species have the following isotopic species codes; one isotope of HO_2 is present labeled 166 for H^{16}O_2 , oxygen atom (^{16}O) has the code 6, for ClONO_2 there are two isotopes labeled 5646 for $^{35}\text{Cl}^{16}\text{O}^{14}\text{N}^{16}\text{O}_2$ and 7646 for $^{37}\text{Cl}^{16}\text{O}^{14}\text{N}^{16}\text{O}_2$.

There have also been additions to the vibrational tables for some molecules. In particular, the O_2 table has been extended to 29 elements with the additions of the vibrational state labels " B0" to " B19". Dr. Linda Brown has extended the list for NH_3 , this still

needs to be reviewed. A complete list can be found in the routine BD-VIBS.FOR.

Table 21 New Molecules and Isotopomers Added to the HITRAN Database since the 1986 Edition.

Molecule	Molecule Code	Isotope Code
$^{16}\text{O}^{16}\text{O}^{17}\text{O}$	3	667
$^{16}\text{O}^{17}\text{O}^{16}\text{O}$	3	676
$^{16}\text{O}^{12}\text{O}^{33}\text{S}$	19	623
COF_2	29	269
SF_6	30	29
H_2S	31	121
	31	141
	31	131
HCOOH	32	126
HO_2	33	166
O	34	6
ClONO_2	35	5646
		7646
NO^+	36	46
HOBr	37	169
		161
H_4C_2	38	1221
		1231

With the new additions, many changes had to be made to the block data routines that accompany most of the HITRAN programs. A new structure was adopted for these routines. We now use INCLUDE statements for abundance, isotopomers, Q(T), species, and VIBS. All routines were updated with the new information.

5.4 Ozone Data for the 1996 Edition of HITRAN

Nine files of ozone data for the 1994 Edition of HITRAN were obtained from Dr. C. P. Rinsland.¹⁶⁴ The data contained in these files are listed in Table 22. The files were decompressed and run through the ozone halfwidth program which adds the air- and self-broadened halfwidths and the air-broadening temperature exponent to the files along with the reference codes. The data was then transferred to Dr. Rothman for addition to the 1996 HITRAN database.

5.5 NH₃ for HITRAN96

New and updated data were obtained for NH₃ from L. Brown and S. Urban. The changes in the data include new calculated wavenumber, intensity, lower state energies, and self- and air-broadened halfwidths, the notation for the rotational quantum numbers has been changed, and many new vibrational bands have been included. The data sent by both Urban and Brown has used a vibrational labeling scheme that does not agree with the HITRAN system and must be changed to be compatible with the database. The operations were made on the original five data files. These are listed in Table 23. The HINH3.JPL file was data of Brown. NH3_3000.DAT and NH3_4000.DAT were the new data of Urban, and that NH3_HITR.DAT was an incomplete transfer of the file NH3_2500.DAT. Furthermore, the file NH3_2500.DAT is the 1992 HITRAN data for NH3 in the region 0-2154 cm⁻¹. This file was

generated by Urban and contains the new vibrational assignment codes and updated rotational quantum number notation. Other than the quantum codes the data match HITRAN92.

Table 22. Ozone Files for the 1996 HITRAN Compilation

File	ISO	V'	V''	Status	Region	# lines
HITO3941.ARC	666	[(004), (103), (310)]	(000)	N†	2.5μm	4050
HITO3942.ARC	666	[(013), (112)]	(000)	N	2.7μm	2221
HITO3943.ARC	666	[(004), (103), (310)]	(010)	N	3.3μm	476
HITO3944.ARC	666	[(003), (102), (201), (300)]	(000)	R††	3.3μm	9746
HITO3945.ARC	666	[(003), (102), (201), (300)]	[(100), (001)]	R	4.8μm	11262
HITO3946.ARC	666	[(003), (102), (201), (300)]	[(200), (101), (002)]	N	10.0μm	4287
HITO3947.ARC	666	[(004), (103), (310)] [(013), (112)]	[(100), (001)] (010)	N	3.3μm	5179
HITO3948.ARC	667	(010)	(000)	N	14μm	5641
HITO3949.ARC	676	(010)	(000)	N	14μm	2846

† New data, not present on HITRAN 1992.

†† Replace data that are on HITRAN 1992.

Table 23 NH₃ Data Files

File	# Lines	ω_{\min}^{\dagger}	ω_{\max}^{\dagger}
NH3_3000.DAT	836	3118	3675
NH3_2500.DAT	4855	0	2154
NH3_4000.DAT	1130	4036	4710
NH3_HITR.DAT	2570	0	1249
HINH3.JPL	3370	2150	5295

\dagger in cm⁻¹

The data was grouped into 2 files, BROWN.PA1 and URBAN.PA1. The first is the file HINH3.JPL and the second is NH3_2500.DAT, NH3_3000.DAT, and NH3_4000.DAT. A program was written to read these data and make the necessary corrections to the vibrational indices, add references and error codes. The data, which were sent by L. Brown to L. Rothman, were to have updated halfwidths already. Upon inspection, it was found that the JPL file had incorrect halfwidths (changing by 2 orders of magnitude for similar J K transitions). Closer inspection revealed that the Urban data, which looked correct, were also in error by a few percent. This was traced to a units conversion error in L. Brown's program.¹⁶⁵ We took the data of A. Pine¹⁶⁶ for N₂- and O₂-broadening, which are reported in cm⁻¹/MPa and converted these to cm⁻¹/atm. The data were then fitted by the polynomial expression used by Brown¹⁹

$$\gamma(J'',K'') = a_0 + a_1 \cdot J'' + a_2 \cdot K'' + a_3 \cdot J''^2 + a_4 \cdot J'' \cdot K'' \quad . \quad (40)$$

The resulting coefficients are given in Table 24. These are then used with the self-broadening coefficients of Brown¹⁶⁵ to add these to the

two files. The resulting files have been called BROWN.PA2 and URBAN.PA2. These need to be checked and L. Brown suggest the ν_2 - ν_2 data on the database is too intense by a factor of 2. Using a program that identifies the lines of the ν_2 - ν_2 band (labeled 6 and 10, or 10 and 6) the intensities for these lines was divided by 2. There were 199 lines for the 0100s-0100a band and 394 lines for the 0100a-0100s band. After this the halfwidth program was run to add the self- and air-broadened halfwidths to the data. Band sums were made on the final files, called BROWN.PA2 and URBAN.PA3. It was discovered that the labels used for certain vibrational states were incorrect and inverted in cases. Comparing with the "bean counting" program of L. Brown other problems arose in that the states 0000s and 0000a are both labeled 1 and 2.

From Herzberg¹⁶⁷ we find that ν_1 (1000-0000) is a parallel band as well as 11000-0000. For both of these vibrational transitions the selection rules a-s, and s-a apply. This indicated that the band sums sent by L. Brown had the data labeled incorrectly. Checking Urban's original data gives

1000s-0000a called 18 2 in the data

1000a-0000s called 19 1 in the data.

These assignments agree with the correspondence list that has been created for ammonia. This confirmed that the data was correct and the labeling error was only in L. Brown's "bean counting" program. The final data files are BROWN.PA2 and URBAN.PA3. These were delivered to L. Rothman for the 1996 database.

Table 24. Coefficients of Polynomial in Eq. (40) for N₂- and O₂-Broadening of NH₃

System	a ₀	a ₁	a ₂	a ₃	a ₄
NH ₃ -N ₂	.11982	-.94290 10 ⁻²	59746 10 ⁻²	.63050 10 ⁻³	-.61553 10 ⁻³
NH ₃ -O ₂	.69178 10 ⁻¹	-.44293 10 ⁻²	.23350 10 ⁻²	.30747 10 ⁻³	-.31585 10 ⁻³

5.6 Transition Moment Squared for Ozone Molecule

Dr. M. A. H. Smith of NASA Langley Research Center sent email to Dr. Laurence Rothman of Phillips Laboratory (forwarded to me) stating that she noticed that for ozone lines in the 990-1010 cm⁻¹ region on the 1996 HITRAN database the transition moment squared, |R|², is smaller than the 1992 HITRAN database values, yet the other parameters for these lines are exactly the same. To investigate this I considered the calculation of the transition moment squared and what changes could have taken place. The most obvious was the improved partition sums on HITRAN96. Running TIPS92 and TIPS96 gives the results in Table 25. This yields a 1996/1992 ratio of Q₉₆/Q₉₂ = 0.99812.

Table 25. Partition Functions at 296K for Ozone Molecule

Q(296 K) TIPS96	Q(296 K) TIPS92
3481.86	3488.42

Since the transition moment squared is proportional to Q this gives a difference in $|R|^2$ values of $|R|^2(96) = 0.99812 \cdot |R|^2(92)$. I have selected some ozone lines in the 990-1010 cm^{-1} region from the 1992 and 1996 databases. These values are presented along with scaled 1992 values in Table 26. Thus, it appears that the difference is entirely due to the improvements in the partition functions.

Table 26. Transition Moment Squared for O_3 Transitions in the 990-1010 cm^{-1} region from the 1992, scaled 1992, and 1996 HITRAN Databases

position cm^{-1}	$ R ^2(96)$	$0.99812 \cdot R ^2(92)$	$ R ^2(92)$
919.716600	1.699E-2	1.700E-2	1.703E-2
921.309800	2.306E-5	2.3057E-5	2.301E-5
923.02370	1.705E-2	1.7048E-2	1.708E-2
924.956000	1.652E-2	1.6519E-2	1.655E-2
931.375900	8.026E-3	8.02588E-3	8.041E-3

5.7 Halfwidths for Transitions of H_2O_2

We have determined two linear fits to halfwidth data for H_2O_2 . The data are those of Devi et al.¹⁶⁸ There were 18 air-broadened transitions studied from $J''=3$ to 15. The first fit is to all of the data and another fit to the data averaged as a function of J'' was made. There appeared to be no significant difference between the fits so the fit to all the data was chosen as the final one. The data and the fit are shown in Fig 17. Although there is much variation in the data, given the lack of more data this fit is as representative as can be produced.

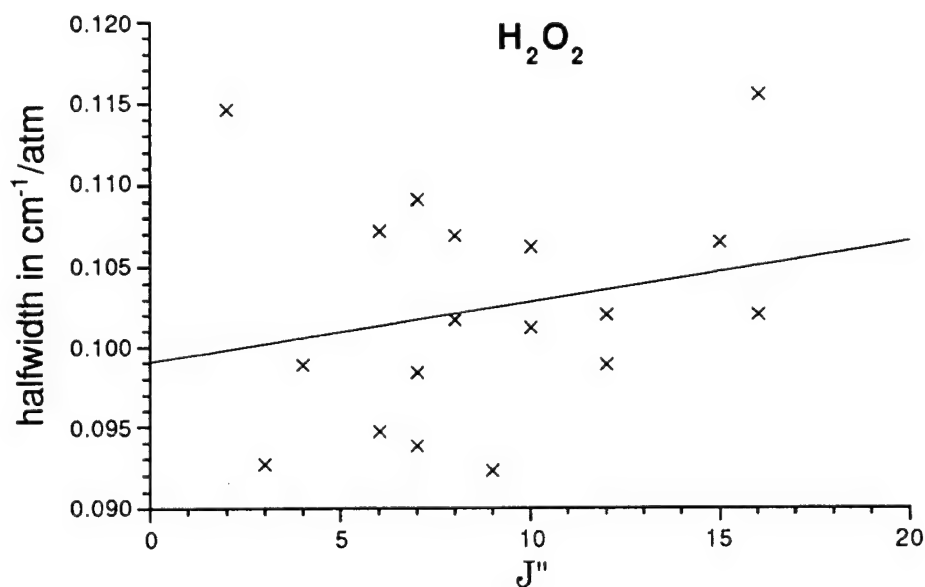


Figure 17. Linear fit in J'' to halfwidths of H_2O_2

The fit of the data yields the following formula to describe the air-broadened halfwidths of hydrogen peroxide;

$$\gamma (\text{cm}^{-1} \text{ atm}^{-1}) = 0.099057 + 3.7703 \times 10^{-4} \times J'' \quad (41)$$

5.8 State Independent Degeneracy Factors for New Species on the Database

Several new species have been added to the database. With the additions, appropriate changes need to be made to a number of programs in order to maintain the indexing structure of the database. This is especially true when one of the added species comes within the current list, as is the case here. The new species are HOBr, C₂H₄, and ¹⁶O¹²C³³S. The last of these species is in the old list so care must be taken to arrange the indices correctly. For HOBr and C₂H₄ there are two species each, H¹⁶O⁷⁹Br and H¹⁶O⁸¹Br; and H₂¹²C₂ and H¹²C¹³CH. The state independent degeneracy factors are given by

$$g_j = \prod_i (2I_i + 1) \quad (42)$$

where the product is over all nuclear spins that do not couple with rotation, hence they are independent of the rotational state. The nuclear spins of the species considered here are: I(¹²C)=0, I(¹⁶O)=0, I(¹H)=1/2, I(⁷⁹Br)=3/2, I(⁸¹Br)=3/2, I(¹³C)=1/2. For ¹⁶O¹²C³³S there is no inversion or rotational symmetry so all nuclei are included in the product, $g_j = (2 \times 0 + 1)(2 \times 0 + 1)(2 \times \frac{3}{2} + 1) = 4$.

For HOBr, because the spins do not change for the two species, g_j is the same for both and is given by $g_j = (2 \times \frac{1}{2} + 1) (2 \times 0 + 1) (2 \times \frac{3}{2} + 1) = 8$.

For hydrogen peroxide the two species are different. The first, $H_2^{12}C_2$, has C_{2v} symmetry so that the spin of the hydrogen atoms couples with the rotational motion to give odd and even states statistical factors of 3 and 1, respectively. For the second species, $H^{12}C^{13}CH$, the presence of the carbon-13 breaks this symmetry so that the state independent degeneracy factor is given by $g_j = (2 \times 0 + 1) \left(2 \times \frac{1}{2} + 1\right)^5 = 32$.

6.0 EINSTEIN A COEFFICIENT, INTEGRATED BAND INTENSITY, AND DEGENERACY FACTORS

The correct use of the nuclear degeneracy factors for relating the Einstein A coefficient to the integrated band intensity has posed a problem to many researchers. The reason is in part due to a casual use (or misuse) of notation. We are currently involved in calculating the line intensities for the $X^3\Sigma^-_g \rightarrow a^1\Delta_g$ band of molecular oxygen from the Einstein A coefficient. In the literature, there are 3 determinations of the integrated band intensity⁶⁵⁻⁶⁷ from which the Einstein A coefficient is deduced. Unfortunately, there are three proposed sets of degeneracy factors. The measurements differ each by roughly a factor of 2, thus the overall spread is a factor of 4. Yet, the derived Einstein A coefficients are close to each other due to the use of incorrect degeneracy factors. (see Table 27)

Table 27. Measured band intensities, derived Einstein-A coefficients, and statistical degeneracy factors for the $a^1\Delta_g (v=0) \leftarrow X^3\Sigma^-_g (v=0)$ band.

Reference	S_{00} $\text{cm}^{-1}/(\text{molec}\cdot\text{cm}^{-2})$	$A_{\varepsilon'\Lambda'v'\rightarrow\varepsilon''\Lambda''v''}$ sec^{-1}	d_ℓ/d_u
Badger et al. ⁶⁵	3.66×10^{-24}	2.58×10^{-4}	3 / 2
Lin et al. ⁶⁶	9.4×10^{-24}	1.3×10^{-4}	3 / 1
Hsu et al. ⁶⁷	2.1×10^{-24}	2.9×10^{-4}	3 / 1

This is an important problem since the Einstein A coefficients are used to determine line intensities in other models. Thus, application of intensity equations will only generate consistent line intensities if the statistical degeneracy factors and the derived Einstein-A coefficient are from the same author.² The line intensities for the $X^3\Sigma^-_g \rightarrow a^1\Delta_g$ band on HITRAN92 are roughly a factor of 2 too small, this is due to incorrect inversion from Badger et al.'s⁶⁵ A to S (i.e. the degeneracy factors). Suspicion of such missing factors of 2, and concerns about the interpretation of upper atmosphere emissions, such as inferring ozone from SME (Solar Mesosphere Explorer via the $a^1\Delta_g$ 1.27 μm airglow) were expressed by Mlynczak and Nesbitt⁷⁰ (who conjectured a significant change in A from one of the reported S values in Table 5 (Hsu et al.)) and by Pendelton et al.⁷¹ Recent observations in the mesosphere⁷² confirm the Badger et al.⁶⁵ value of the Einstein-A coefficient.

The correct equations are discussed in Ref. 2, however a complete derivation was not possible due to space limitations. Below

we derive the relationships between the Einstein A coefficient, the integrated band intensity, the line intensity and degeneracy factors.

The discussion is tailored to the oxygen molecule, however, it can easily be extended to other systems by the appropriate labeling of states. For O₂, which has 2 low-lying excited electronic states and is an open shell electronic system in the ground state the labels needed are an electronic quantum number, e, lambda doubling quantum number, Λ , vibrational quantum number, v, rotational quantum number, J, and the projection of J on the internuclear axis, M. For O₂ the following short hand notation for the Quantum numbers will be used, $\epsilon = e\Lambda v$. The standard spectroscopic notation of double primes for the lower state and a single prime for the upper state will be used and Penner's labeling scheme⁴⁵ will also be used. The degeneracy factors given by the product of the degeneracy factors for the quantized motions, $d_{\eta} = d_{\epsilon} d_{\Lambda} d_v d_J d_{\text{sym}}$ with $d_{\epsilon} = (2S+1)$, $d_{\Lambda} = (2 - \delta_{\Lambda,0})$, $d_v = 1$, $d_J = (2J+1)$, and d_{sym} is one for the heteronuclear species and the (+) states of the homonuclear species and zero for the (-) states of the homonuclear species. This factor accounts for the symmetry restrictions for the homonuclear diatomics (note, this gives an overall factor of 1/2 in the partition sum).

We begin by considering non-degenerate levels. The Einstein A coefficient in sec⁻¹ units is given in terms of the transition moment squared in Debye squared units as⁴⁵

$$A_{\epsilon'J'M' \rightarrow \epsilon''J''M''} = \frac{64\pi^4}{3h} 10^{-36} \omega_{(\epsilon''J''M'')(\epsilon'J'M')}^3 |R_{(\epsilon''J''M'')(\epsilon'J'M')}|^2 \quad (43)$$

In the absence of an E or B field, the states labeled by M are degenerate, so $\omega(\epsilon''J''M'')(\epsilon'J'M') = \omega(\epsilon''J'')(\epsilon'J')$. Ref. 45 tells us that

$$\tilde{A}_{\epsilon'J' \rightarrow \epsilon''J''} = \frac{1}{d_{J'}} \sum_{M'', M'} A_{\epsilon'J'M' \rightarrow \epsilon''J''M''} \quad (44)$$

where $d_{J'}$ is the degeneracy of states summed over, here $2J'+1$. The tilde over the A implies that this is a reduced quantity. Thus, for the problem at hand we get

$$\begin{aligned} \tilde{A}_{\epsilon'J' \rightarrow \epsilon''J''} &= \frac{1}{d_{J'}} \sum_{M'', M'} \frac{64\pi^4 10^{-36}}{3h} \omega_{(\epsilon''J'')(\epsilon'J')}^3 |R_{(\epsilon''J''M'')(\epsilon'J'M')}|^2 \\ &= \frac{64\pi^4 10^{-36}}{3h} \omega_{(\epsilon''J'')(\epsilon'J')}^3 \frac{1}{d_{J'}} \sum_{M'', M'} |R_{(\epsilon''J''M'')(\epsilon'J'M')}|^2 \end{aligned} \quad (45)$$

The line intensity ($\text{cm}^{-1}/\text{mole} \cdot \text{cm}^{-2}$) in terms of the Einstein A coefficients for the non-degenerate case is given by^{45,1}

$$S_{(\epsilon''J''M'')(\epsilon'J'M')} = \frac{c}{8\pi} N_{\epsilon''J''M''} \frac{1}{\nu_{(\epsilon''J''M'')(\epsilon'J'M')}}^2 (1 - e^{-h\nu_{(\epsilon''J''M'')(\epsilon'J'M'')}/kT}) A_{\epsilon'J'M' \rightarrow \epsilon''J''M''} \quad (46)$$

where ν is the frequency in sec^{-1} , c the speed of light. In what follows we adopt a shorthand label for the radiation field part of Eq. (46), i.e. $(1 - e^{-h\nu_{(\epsilon''J''M'')(\epsilon'J'M'')}/kT}) \equiv [\text{rad}]$. For the no-field case, the M states are degenerate so what is measured is the sum over these states,

$$\tilde{S}_{(\epsilon''J'')(\epsilon'J')} = \frac{1}{8\pi c} \sum_{M'',M'} \frac{[\text{rad}]}{\omega_{(\epsilon''J'')(\epsilon'J')}^2} N_{\epsilon''J''M''} A_{\epsilon'J'M' \rightarrow \epsilon''J''M''} \quad (47)$$

The population factors can be written

$$N_{\epsilon J} = \frac{(2J+1) d_{\epsilon JM} e^{-E_{\epsilon J}/kT}}{Q(T)} = \frac{d_{\epsilon J} e^{-E_{\epsilon J}/kT}}{Q(T)} = (2J+1) N_{\epsilon JM} \quad (48)$$

which implies that

$$N_{\epsilon JM} = \frac{N_{\epsilon J}}{(2J+1)}, \quad \text{and} \quad d_{\epsilon JM} = \frac{d_{\epsilon J}}{(2J+1)} \quad (49)$$

Using Eq. (49), the line intensity can be written

$$\tilde{S}_{(\epsilon''J'')(\epsilon'J')} = \frac{1}{8\pi c} \frac{N_{\epsilon''J''}}{d_{J''}} \frac{[\text{rad}]}{\omega_{(\epsilon''J'')(\epsilon'J')}^2} \sum_{M'',M'} A_{\epsilon'J'M' \rightarrow \epsilon''J''M''} \quad (50)$$

From the definition of the reduced Einstein A coefficient, Eq. (44) we get

$$\tilde{S}_{(\epsilon''J'')(\epsilon'J')} = \frac{1}{8\pi c} N_{\epsilon''J''} \frac{1}{\omega_{(\epsilon''J'')(\epsilon'J')}^2} [\text{rad}] \frac{d_{J'}}{d_{J''}} \tilde{A}_{\epsilon'J' \rightarrow \epsilon''J''} \quad (51)$$

which is equivalent to Eq. 2-17 of Penner⁴⁵ for the case of M degeneracy. From Eqs. (45) and (51) we can write the following result

$$\begin{aligned}
\tilde{S}_{(\epsilon''J'')(\epsilon'J')} &= \frac{1}{8\pi c} N_{\epsilon''J''} \frac{1}{\omega_{(\epsilon''J'')(\epsilon'J')}^2} [\text{rad}] \frac{d_{J'}}{d_{J''}} \frac{64\pi^4 10^{-36}}{3 h} \\
&\times \omega_{(\epsilon''J'')(\epsilon'J')}^3 \frac{1}{d_{J'}} \sum_{M'', M'} |R_{(\epsilon''J''M'')(\epsilon'JM')}|^2 \\
&= \frac{8\pi^3 10^{-36}}{3 h c} N_{\epsilon''J''} \omega_{(\epsilon''J'')(\epsilon'J')} [\text{rad}] \frac{1}{d_{J''}} \sum_{M'', M'} |R_{(\epsilon''J''M'')(\epsilon'JM')}|^2 \quad .(52)
\end{aligned}$$

This is Eq. (38) of Gamache and Rothman¹ and Eq. (1) of Ref. 2 without the isotopic abundance factor used in HITRAN.

We now wish to develop the integrated band intensity, $S_{\epsilon}^{\epsilon''}$, for an electronic-vibrational-rotational band. In units of $\text{cm}^{-1}/\text{molec}\cdot\text{cm}^{-2}$ this is given by

$$S_{\epsilon}^{\epsilon''} = \frac{8\pi 10^{-36}}{3 h c} \omega_{(\epsilon'')(\epsilon')} N_{\epsilon''J''} \frac{N_{\epsilon''J''}}{Q_{\epsilon}} |R_{(\epsilon'')(\epsilon')}|^2 \quad . \quad (53)$$

Note, this definition is slightly different than that used by other authors since the radiation field term is not approximated into Eq. (53) as was done previously.⁴⁵ In our formulation it is explicitly retained. Next, we use the approximate separation of energy and the product approximation for the partition function and transition moment squared,

$$Q_{\text{tot}} = Q_{\epsilon} Q_{\text{rot}}$$

$$\sum_{M'', M'} |R_{(\epsilon''J''M'')(\epsilon'JM')}|^2 = |R_{(\epsilon'')(\epsilon')}|^2 |R_{(J'')(J')}|^2$$

$$E_{\epsilon J} = E_{\epsilon} + E_J \quad .$$

and

$$\omega_{(\epsilon'')(\epsilon')} \approx \omega_{(\epsilon'' J'')(\epsilon' J')} \quad (54)$$

Inserting these expressions into Eq. (52) yields

$$\begin{aligned} \tilde{S}_{(\epsilon'' J'')(\epsilon' J')} &= \frac{8\pi^3 10^{-36}}{3hc} \frac{d_{\epsilon''}}{d_{\epsilon''} Q_{\epsilon}} \frac{e^{-E_{\epsilon''}/kT}}{\omega_{(\epsilon'')(\epsilon')}} |R_{(\epsilon'')(\epsilon')}|^2 \\ &\times \frac{d_{J''}}{d_{J''} d_{\text{sym}} Q_{\text{rot}}} \frac{e^{-E_{J''}/kT}}{\omega_{(\epsilon'' J'')(\epsilon' J')}} [\text{rad}] |R_{(J'')(J')}|^2. \end{aligned} \quad (55)$$

Writing $d_{\text{rot}} \equiv d_J D_{\text{sym}}$ gives the following expression for the reduced line intensity

$$\tilde{S}_{(\epsilon'' J'')(\epsilon' J')} = S_{\epsilon''}^{\epsilon''} \frac{d_{\text{rot}}}{d_{\text{rot}} Q_{\text{rot}}} \frac{e^{-E_{J''}/kT}}{\omega_{(\epsilon'')(\epsilon')}} \frac{\omega_{(\epsilon'' J'')(\epsilon' J')}}{\omega_{(\epsilon'')(\epsilon')}} [\text{rad}] |R_{(J'')(J')}|^2 \quad (56)$$

We now go back to $S_{\epsilon''}^{\epsilon''}$, Eq. (53), which contained a factor $|R_{(\epsilon'')(\epsilon')}|^2$. This must be expressed in terms of $\tilde{A}_{\epsilon' \rightarrow \epsilon''}$. Using Eq.(44) we have

$$\begin{aligned} \tilde{A}_{\epsilon' \rightarrow \epsilon''} &= \frac{1}{d_{J' M'}} \sum_{\substack{J'', J' \\ M'', M'}} A_{\epsilon' J' M' \rightarrow \epsilon'' J'' M''} \\ &= \frac{1}{d_{J' M'}} \sum_{\substack{J'', J' \\ M'', M'}} \frac{64\pi^4 10^{-36}}{3h} \omega_{(\epsilon'' J'' M'')(\epsilon' J' M')}^3 |R_{(\epsilon'' J'' M'')(\epsilon' J' M')}|^2. \end{aligned} \quad (57)$$

We now assume that $\omega_{(\epsilon'')(\epsilon')} \approx \omega_{(\epsilon'' J'' M'')(\epsilon' J' M')}$, and we can write

$$\begin{aligned}
\tilde{A}_{\epsilon' \rightarrow \epsilon''} &= \frac{1}{d_{J'M'}} \frac{64\pi^4 10^{-36}}{3h} \omega_{(\epsilon'')(\epsilon')}^3 \sum_{\substack{J'', J' \\ M'', M'}} |R_{(\epsilon'' J'' M'')(\epsilon' J' M')}|^2 \\
&= \frac{64\pi^4 10^{-36}}{3h} \omega_{(\epsilon'')(\epsilon')}^3 |\tilde{R}_{(\epsilon'')(\epsilon')}|^2
\end{aligned} \quad (58)$$

where we have used (e.g. see Penner⁴⁵ top of page 136)

$$|\tilde{R}_{(\epsilon'')(\epsilon')}|^2 = \frac{1}{d_{J'M'}} \sum_{\substack{J'', J' \\ M'', M'}} |R_{(\epsilon'' J'' M'')(\epsilon' J' M')}|^2 \quad (59)$$

Working with this we have,

$$\frac{1}{d_{J'M'}} \sum_{\substack{J'', J' \\ M'', M'}} |R_{(\epsilon'' J'' M'')(\epsilon' J' M')}|^2 = \frac{1}{d_{J'M'}} \sum_{J'', J'} |R_{(\epsilon'')(\epsilon')}|^2 |R_{(J'')(J')}|^2 \quad (60)$$

however $\sum_{J'} |R_{(J'')(J')}|^2 = d_{J''}$ thus

$$|\tilde{R}_{(\epsilon'')(\epsilon')}|^2 = \frac{1}{d_{J'M'}} |R_{(\epsilon'')(\epsilon')}|^2 \sum_{J''} d_{J''} \quad (61)$$

We finally arrive at the result

$$\tilde{A}_{(\epsilon'')(\epsilon')} = \frac{64\pi^4 10^{-36}}{3h} \omega_{(\epsilon'')(\epsilon')} \frac{1}{d_{J'M'}} |R_{(\epsilon'')(\epsilon')}|^2 \sum_{J''} d_{J''} \quad (62)$$

Now, we turn to evaluating the integrated band intensity according to

$$\tilde{S}_{\epsilon'}^{\epsilon''} = \sum_{J'', J'} S_{(\epsilon'' J'')(\epsilon' J')} \quad (63)$$

$$= \sum_{J'', J'} \frac{8\pi^3 10^{-36}}{3hc} N_{\epsilon'' J''} \omega_{(\epsilon'' J'')(\epsilon' J')} [\text{rad}] \frac{1}{d_{J''}} \sum_{M'', M'} |R_{(\epsilon'' J'' M'')(\epsilon' J' M')}|^2 \quad (64)$$

Rearranging gives

$$\tilde{S}_{\epsilon'}^{\epsilon''} = \frac{8\pi^3 10^{-36}}{3hc} \omega_{(\epsilon'')(\epsilon')} \sum_{J'', J'} \frac{d_{\epsilon'' J''} e^{-E_{\epsilon'' J''}/kT}}{Q} \frac{1}{d_{J''}} \sum_{M'', M'} |R_{(\epsilon'' J'' M'')(\epsilon' J' M')}|^2 \quad (65)$$

where we have assumed $\omega_{(\epsilon'')(\epsilon')} \approx \omega_{(\epsilon'' J'' M'')(\epsilon' J' M')}$, $[\text{rad}] \sim 1$, $d_{\epsilon'' J''} = d_{\epsilon''} d_{J''}$. Now using the product approximation for the partition sum, energy additivity, and the separation of the transition moment squared, $\sum_{M'', M'} |R_{(\epsilon'' J'' M'')(\epsilon' J' M')}|^2 = |R_{(\epsilon'')(\epsilon')}|^2 |R_{(J'')(J')}|^2$, we arrive at

$$\tilde{S}_{\epsilon'}^{\epsilon''} = \frac{8\pi^3 10^{-36}}{3hc} \omega_{(\epsilon'')(\epsilon')} \frac{d_{\epsilon''} e^{-E_{\epsilon''}/kT}}{Q_{\epsilon}} |R_{(\epsilon'')(\epsilon')}|^2 \sum_{J'', J'} \frac{e^{-E_{J''}/kT}}{Q_{\text{rot}}} |R_{(J'')(J')}|^2 \quad (66)$$

Next, we use the sum rule $\sum_{J''} |R_{(J'')(J')}|^2 = d_{J''}$ and $\sum_{J''} d_{J''} e^{-E_{J''}/kT} = Q_{\text{rot}}$

and we see the double sum on J'', J' gives $Q_{\text{rot}}/Q_{\text{rot}}=1$. Thus,

$$\tilde{S}_{\epsilon'}^{\epsilon''} = \frac{8\pi^3 10^{-36}}{3hc} \omega_{(\epsilon'')(\epsilon')} \frac{d_{\epsilon''} e^{-E_{\epsilon''}/kT}}{Q_{\epsilon}} |R_{(\epsilon'')(\epsilon')}|^2 \quad (67)$$

Our last step is to relate the integrated band intensity to the reduced Einstein A coefficient. Starting from Eq. (57), assuming that $\omega_{(\epsilon'')(\epsilon')} \approx \omega_{(\epsilon'' J'' M'')(\epsilon' J' M')}$, and $\sum_{M'', M'} |R_{(\epsilon'' J'' M'')(\epsilon' J' M')}|^2 = |R_{(\epsilon'')(\epsilon')}|^2 |R_{(J'')(J')}|^2$

we can arrive at

$$\tilde{A}_{\epsilon' \rightarrow \epsilon''} = \frac{64\pi^4}{3h} \omega_{(\epsilon'')(\epsilon')}^3 |R_{(\epsilon'')(\epsilon')}|^2 \frac{1}{d_{J'M'}} \sum_{J'', J'} |R_{(J'')(J')}|^2 \quad (68)$$

The sum over J' gives the sum rule mentioned above, $\sum_{J'} |R_{(J'')(J')}|^2 = d_{J''}$, and the sum over J'' gives $\sum_{J''} d_{J''} = \sum_{J''} (2J''+1)$ which is just the number of states in the lower electronic-vibrational state. The interpretation of $1/d_{J'M'}$ comes from the meaning of Eq. (44) for the reduced quantity. The reduced Einstein A coefficient is given by a sum over all lower states of the Einstein A coefficient divided by the total number of upper states. Thus, $d_{J'M'}$ is the total number of states in the electronic vibrational band

$$d_{J'M'} = \sum_{J'} d_{J'} = \sum_{J'} (2J'+1) \quad (69)$$

Recall, that for considering the separation of the electronic-vibrational part of the intensity from the rotational part, we assumed the rotational states are degenerate in comparison to the electronic-vibrational states. Finally, we arrive at

$$\tilde{A}_{\epsilon' \rightarrow \epsilon''} = \frac{64\pi^4}{3h} \omega_{(\epsilon'')(\epsilon')}^3 \frac{d_{J''M''}}{d_{J'M'}} |R_{(\epsilon'')(\epsilon')}|^2 \quad (70)$$

We note that

$$\frac{d_{J''M''}}{d_{J'M'}} = \frac{\sum_{J''} (2J''+1)}{\sum_{J'} (2J'+1)} = \text{ratio of states} \quad (71)$$

which for $X^3\Sigma^-_g/a^1\Delta_g$ is 3/2.

The relationship between the line intensity and the reduced Einstein A coefficient is

$$\tilde{S}_{(\epsilon''J'')(\epsilon'J')} = \frac{1}{8\pi c} \frac{d_{\epsilon''}}{Q} \frac{e^{-E_{\epsilon''J''}/kT}}{\omega_{(\epsilon''J'')(\epsilon'J')}^3} [\text{rad}] \frac{1}{d_{J''}} |R_{(J'')(J')}|^2 \frac{d_{J'M'}}{d_{J''M''}} A_{\epsilon' \rightarrow \epsilon''} \quad (72)$$

and the relationship between the integrated band intensity and the reduced Einstein A coefficient is

$$\tilde{S}_{\epsilon''}^{\epsilon'} = \frac{1}{8\pi c} \frac{d_{\epsilon''}}{Q_{\epsilon}} \frac{e^{-E_{\epsilon''}/kT}}{\omega_{(\epsilon'')(\epsilon')}^2} \frac{1}{d_{J''M''}} A_{\epsilon' \rightarrow \epsilon''} \quad (73)$$

7.0 HITEMP

There is a need to add to the HITEMP database the correct halfwidths of water vapor. This can be accomplished by using a group of programs and direct access files, however, this must be set-up for the particular platform that the program will be run on. This is because of the nature of the direct access files. Some time ago the programs were put on the Phillips Laboratory VAX where modifications were made to run in double precision and other VAX specific features were implemented. The addition of the halfwidths to the high temperature water files appeared to have some problems. Some of the air-broadened widths were zero, the extrapolated values were not correct, some self-broadened values were not correct, and

the reference and error codes were not used. To remedy this, I took the necessary codes and installed the ADHW-H₂O.FOR program on a PC at Ontar Corp. This meant that the direct access files needed to be created on this computer from the initial files, etc. This was done and the program was tested and is working fine.

Also for HITEMP, it was found that some of the transition assignments are incorrect. Since this is the only true unique identifier for the transitions, this must be corrected. The list of corrections was supplied to us by Dr. John Selby.¹⁶⁹ A program was written to check this list automatically and search for duplicates.

To correct the transition assignments for H₂O on HITEMP which are incorrect, Dr. R. Wattson has gone through the list supplied from Dr. John Selby with reference to his DND programs and has produced a corrected version of the list.¹⁷⁰ The new list was run through the programs which check the list for duplicates. This is extremely important because of the possibility of dual (or more) changes. The danger here is that since the identification is the label of the transition, once it is changed it is changed forever. We do not want to change an assignment to something else and then find that what we changed it to will then change. Our program found no duplicates. We then wrote a new program that reads the assignment change list and stores the information as a function of the quantum assignments, then reads the HITEMP water database, finds if the assignment read need to be changed and then makes the change while updating the references, etc. This program was tested on a small subset of the data and by me and independently by Dr. Wattson and it appears to work fine. The final program was delivered to Ontar where it was

run on the data and then destroyed (see comments above). The error flags and reference codes were also set by this program. After this, the new files with the correct quantum identifications were run through the ADHWH2O.FOR program to add the air- and self-broadening halfwidths, and the temperature exponent for air-broadening. These operations completed the work on water vapor for the HITEMP database.

8.0 REFERENCES

1. R. R. Gamache and L. S. Rothman, "Extension of the HITRAN Database to Non-LTE Applications," *J. Quant. Spectrosc. Radiat. Transfer* **48**, 519, 1992.
2. R. R. Gamache, A. Goldman, and L. S. Rothman, "Improved Spectral Parameters for the Three Most Abundant Isotopomers of the Oxygen Molecule," in press *J. Quant. Spectrosc. Radiat. Transfer*, 1997.
3. L. S. Rothman, R. R. Gamache, A. Goldman, J.-M. Flaud, R. H. Tipping, C. P. Rinsland, M. A. H. Smith, R. A. Toth, L. R. Brown, V. M. Devi, and D. C. Benner, *J. Quant. Spectrosc. Radiat. Transfer* **48**, 469 (1992).
4. N. Jacquinet-Husson, N. A. Scott, A. Chedin, B. Bonnet, A. Barbe, V. Tyuterev, J.-P. Champion, M. Winnewisser, L. R. Brown, R. R. Gamache, V. Golovko, and A. Chursin, "The GEISA System in 1996: towards an Operational Tool for the Second Generation Vertical Sounder Radiance Simulation," in press *J. Quant. Spectrosc. Radiat. Transfer*, 1997.
5. G. Herzberg, "Molecular Spectra and Molecular Structure II. Infrared and Raman Spectra of Polyatomic Molecules," Van Nostrand, New York, 1960.
6. R. S. McDowell, *J. Chem. Phys.* **88**, 356 (1988).
7. R. S. McDowell, *J. Quant. Spectrosc. Radiat. Transfer* **38**, 337 (1987).
8. R. S. McDowell, *J. Chem. Phys.* **93**, 2801 (1990).
9. J. K. G. Watson, *Mol. Phys.* **65**, 1377 (1988).

10. F. M. Fernández and R. H. Tipping, *Spectrochimica Acta* **48A**, 1283 (1992).
11. K. Fox, *J. Quant. Spectrosc. Radiat. Transfer* **10**, 1335 (1970).
12. J. A. Nelder and R. Mead, *Comput. J.* **7**, 308 (1965).
13. R. L. Poynter and H. M. Pickett, "Submillimeter, Millimeter, and Microwave Spectral Line Catalogue," JPL publication 80-23 Revision 2, June 1, 1984.
14. J. B. Burkholder, P. D. Hammer, C. J. Howard, A. G. Maki, G. Thompson, and C. Chackerian, Jr., *J. Mol. Spectrosc.* **124**, 139 (1987).
15. J.-M. Flaud and C. Camy-Peyret, *J. Mol. Spectrosc.* **55**, 278 (1975).
16. L. Rosenmann, S. Langlois, C. Delaye, and J. Taine, *J. Mol. Spectrosc.* **149**, 167 (1991).
17. L. D. Gray and A. T. Young, *J. Quant. Spectrosc. Radiat. Transfer* **9**, 569 (1969).
18. J.-M. Flaud, C. Camy-Peyret, V. M. Devi, C. P. Rinsland and Mary Ann Smith, *J. Mol. Spectrosc.* **124**, 209 (1987).
19. L. D. Gray-Young, *J. Quant. Spectrosc. Radiat. Transfer* **11**, 1265 (1971).
20. A. G. Robiette and M. Dang-Nhu, *J. Quant. Spectrosc. Radiat. Transfer* **22**, 499 (1979).
21. K. J. Ritter and T. D. Wilkerson, *J. Mol. Spectrosc.* **121**, 1 (1987).
22. A. Goldman, *Appl. Opt.* **21**, 1162 (1982).
23. W. J. Lafferty, A. S. Pine, J.-M. Flaud, and C. Camy-Peyret, *J. Mol. Spectrosc.* **157**, 499 (1993).

24. A. Perrin, J.-M. Flaud, C. Camy-Peyret, B. Carli, and M. Carlotti, *Mol. Phys.* **63**, 791 (1988).
25. N. Husson, A. Goldman, and G. Orton, *J. Quant. Spectrosc. Radiat. Transfer* **27**, 505 (1982).
26. A. Bauer, M. Godon, J. Carlier, and R. R. Gamache, "Continuum in the Window of the Water Vapor Spectrum. Absorption of H₂O-Ar at 239 GHz and Line width Calculations," in press, *J. Quant. Spectrosc. Radiat. Transfer* (1997).
27. S. Urban, D. Papousek, V. Malathy Devi, B. Fridovich, R. D'Chuna, and K. Narahari Rao, *J. Mol. Spectrosc.* **106**, 38 (1984).
28. D. J. W. Kendall and T. A. Clark, *J. Quant. Spectrosc. Radiat. Transfer* **21**, 511 (1979).
29. A. Goldman and J. R. Gillis, *J. Quant. Spectrosc. Radiat. Transfer* **25**, 111 (1981).
30. Classical value from formulas in: G. Herzberg, "Molecular Spectra and Molecular Structure III. Electronic Spectra and Electronic Structure of Polyatomic Molecules," p 505-506, Van Nostrand, New York, 1966.
31. D. Reuter, D. E. Jennings, and J. W. Brault, *J. Mol. Spectrosc.* **115**, 1294 (1986).
32. A. Goldman, C. P. Rinsland, R. D. Blatherwick, and F. S. Bonomo, *Appl. Opt.* **29**, 1860 (1990).
33. J.-M. Flaud and C. Camy-Peyret, J. W. C. Johns, *Can. J. Phys.* **61**, 1462 (1984)
34. R. J. Thomas, C. B. Barth, D. W. Rusch, and R. W. Sanders, *J. Geophys. Res.* **89**, 9569 (1984).

35. M. G. Mlynczak, S. Solomon, and D. S. Zarus, *J. Geophys. Res.* **98**, 18,639 (1993).
36. L. S. Rothman and A. Goldman, *Appl. Opt.* **20**, 2182 (1981).
37. L. S. Rothman, R. R. Gamache, A. Barbe, A. Goldman, J. R. Gillis, L. R. Brown, R. A. Toth, J.-M. Flaud, and C. Camy-Peyret, *Appl. Opt.* **22**, 2247 (1983).
38. E. R. Cohen and B. N. Taylor, *Phys. Today*, August 1995, BG9-BG13.
39. G. Herzberg, *Molecular Spectra and Molecular Structure I. Spectra of Diatomic Molecules*, 2nd edition, Van Nostrand, New York, 1966.
40. M. Tinkham and M. W. P. Strandberg, *Phys. Rev.* **97**, 937 (1955).
41. W. Steinbach and W. Gordy, *Phys. Rev. A* **8**, 1753 (1973).
42. W. Steinbach and W. Gordy, *Phys. Rev. A* **11**, 729 (1975).
43. W. R. Steinbach, "Millimeter and Submillimeter Wave Spectra of the Oxygen Isotopes: $^{16}\text{O}_2$, $^{18}\text{O}_2$, and $^{16}\text{O}^{18}\text{O}$," Ph. D. Thesis, Department of Physics, Duke University, 1974.
44. M. Greenbaum, "The Calculation of Millimeter and Submillimeter Wave Absorption Line Parameters for the Molecular Oxygen Isotopes: $^{16}\text{O}_2$, $^{16}\text{O}^{18}\text{O}$, $^{18}\text{O}_2$," Riverside Research Institute Technical Report T-1/306-3-14, 1975, 80 West End Avenue, New York, NY 10023.
45. S. S. Penner, *Quantitative Molecular Spectroscopy and Gas Emissivities*, Addison-Wesley, Reading, MA 1959.
46. J. H. Miller, R. W. Boese, and L. P. Giver, *J. Quant. Spectrosc. Radiat. Transfer* **9**, 1507 (1969).

47. V. D. Galkin, *Opt. Spectrosc. (USSR)* **47**, 151 (1979).
48. L. P. Giver, R. W. Boese, and J. H. Miller, *J. Quant. Spectrosc. Radiat. Transfer* **14**, 793 (1974).
49. J. H. Miller, L. P. Giver, and R. W. Boese, *J. Quant. Spectrosc. Radiat. Transfer* **16**, 595 (1976).
50. M. A. Mélières, M. Chenevier, and F. Stoeckel, *J. Quant. Spectrosc. Radiat. Transfer* **33**, 337 (1985).
51. P. H. Krupenie, *J. Phys. Chem. Ref. Data* **2**, 423 (1972).
52. R. R. Gamache, R. L. Hawkins, and L. S. Rothman, *J. Mol. Spectrosc.* **142**, 205 (1990).
53. G. Rouillé, G. Millot, R. Saint-Loup, and H. Berger, *J. Mol. Spectrosc.* **154**, 372 (1992).
54. M. Loete and H. Berger, *J. Mol. Spectrosc.* **68**, 317 (1977).
55. W. M. Welch and M. Mizushima, *Phys. Rev. A* **5**, 2692 (1972).
56. L. R. Zink and M. Mizushima, *J. Mol. Spectrosc.* **125**, 154 (1987).
57. The energy levels for O₂ on the 1982-1992 versions of HITRAN used the formulation of Ref. 44.
58. Comparisons were made with the data from Refs. 50 and 66. The different formulations are compared with experiment for 30 lines measured in Ref. 66 and for 2 transitions measured in Ref. 50. The comparison shows the Rouillé et al. formalism to be very slightly better than that of Ref. 44, with the average deviations being 0.00256 cm⁻¹ vs. 0.00259 cm⁻¹, respectively. Note the average deviation is deceptive in that most of the deviations comes from a few large lines. However

on a line-by-line basis the Rouillé et al. data are slightly better than the data of Ref. 44.

59. E. R. Cohen and G. Birnbaum, *J. Chem. Phys.* **66**, 2443 (1977).
60. W. S. Benedict and L. D. Kaplan, *J. Quant. Spectrosc. Radiat. Transfer* **4**, 453 (1964).
61. A. Goldman, C. P. Rinsland, B. Canova, R. Zander, and M. Dang-Nhu, *J. Quant. Spectrosc. Radiat. Transfer* **54**, 757 (1995).
62. J. Reid, R. L. Sinclair, A. M. Robinson, and A. R. W. McKellar, *Phys. Rev. A* **24**, 1944 (1981).
63. T. Scalabrin, R. J. Saykally, K. M. Evenson, H. E. Radford, and M. Mizushima, *J. Mol. Spectrosc.* **89**, 344 (1981).
64. K. W. Hillig II, C. C. W. Chiu, W. G. Read, and E. A. Cohen, *J. Mol. Spectrosc.* **109**, 205 (1985).
65. R. M. Badger, A. C. Wright, R. F. Whitlock, *J. Chem. Phys.* **43**, 4345 (1965).
66. L.-B. Lin, Y.-P. Lee and J. F. Ogilvie, *J. Quant. Spectrosc. Radiat. Transfer* **39**, 375 (1988).
67. Y. T. Hsu, Y. P. Lee, and J. F. Ogilvie, *J. Quant. Spectrosc. Radiat. Transfer* **48A**, 1227 (1992).
68. J. Brault and M. M. Brown, unpublished results.
69. L. Wallace and W. Livingston, *J. Geophys. Res.* **95**, 9823 (1990).
70. M. G. Mlynczak and D. J. Nesbitt, *Geophys. Res. Lett.* **22**, 1381 (1995).
71. W. R. Pendelton, Jr., D. J. Baker, R. J. Reese, and R. R. O'Neil, *Geophys. Res. Lett.* **23**, 1013 (1996).

72. B. J. Sandor, R. T. Clancy, D. W. Rusch, C. E. Randall, R. S. Eckman, D. S. Siskind, and D. O. Muhleman, "Microwave Observations and Modeling of $O_2(^1\Delta_g)$ and O_3 Diurnal Variations in the Mesosphere," submitted to J. Geophys. Res., 1996.
73. W. Lafferty, National Institute of Standards and Technology, private communication, 1996.
74. D. A. Newnham, J. Ballard, and M. S. Page, "Visible Absorption Spectroscopy of Molecular Oxygen," paper A7, Atmospheric Spectroscopy Applications Workshop, Sept. 4-6, Reims, France, 1996.
75. J. Brault, private communication, 1982.
76. A. V. Jones and A. H. Harrison, J. Atmos. Terr. Phys. **13**, 45 (1958).
77. R. N. Zare, A. L. Schmeltekopf, W. J. Harrop, and D. L. Albritton, J. Mol. Spectrosc. **46**, 37 (1973).
78. M. Mizushima and S. Yamamoto, J. Mol. Spectrosc. **148**, 447 (1991).
79. H. Babcock and L. Herzberg, Astrophys. J. **108**, 167 (1948).
80. W. S. Benedict, private communication, 1982.
81. R. L. Poynter, H. M. Pickett, E. A. Cohen, M. L. Delitsky, J. C. Pearson, and H. S. P. Müller, "Submillimeter, Millimeter, and Microwave Spectral Line Catalogue," JPL publication 80-23 Revision 4, March 10, 1996.
82. W. S. Benedict and J. Brault, private communication, 1982.
83. L. S. Rothman, C. P. Rinsland, A. Goldman, S. Massie, J.-M. Flaud, A. Perrin, V. Dana, J.-Y. Mandin, J. Schroeder, A.

- McCann, R. R. Gamache, R. B. Wattson, K. Yoshino, K. Jucks, K. Chance, P. Varanasi, and L. R. Brown, "The 1996 HITRAN Molecular Spectroscopic Database and HAWKS(HITRAN Atmospheric Workstation)," in preparation, 1996.
84. A. Goldman, "The Role of Laboratory Spectroscopy in the Analysis of Atmospheric spectra," Atmospheric Spectroscopy Applications (ASA) Colloquium, Reims, France, Sept. 4-6, 1996.
 85. A. Goldman, "Extended Quantitative Spectroscopy for Analysis of Atmospheric Infrared Spectra," Fourier Transform Spectroscopy OSA -Topical Meeting, Santa Fe, New Mexico, Feb. 10-12, 1997.
 86. G. D. Greenblat, J. J. Orlando, J. B. Burkholder, and A. R. Ravishankara, *J. Geophys. Res.*, **95**, 18, 577 (1990).
 87. J. J. Orlando, G. S. Tyndall, K. E. Nickerson, and J. G. Calvert, *J. Geophys. Res.*, **96**, 20,755 (1991).
 88. C. P. Rinsland, M. A. H. Smith, R. K. Seals, Jr., A. Goldman, F. J. Murcray, D. G. Murcray, J. C. Larsen, and P. L. Rarig, *J. Geophys. Res.*, **87**, 3119 (1982).
 89. M. A. H. Smith, Editor, NASA Conference Publication 2396, NASA, Scientific and Technical Information Branch, 1985.
 90. C. A. Reber, NASA Goddard Space Flight Center Publication 430-1003-001, (1985).
 91. D. Robert and J. Bonamy, *Journal de Physique* **40**, 923 (1979).
 92. M. Baranger, *Phys. Rev.* **112**, 855 (1958).
 93. A. C. Kolb and H. R. Griem, *Phys. Rev.* **111**, 514 (1958).
 94. H. Griem, *Plasma Spectroscopy*, McGraw Hill, N.Y. (1964).

95. R. Kubo, J. Phys. Soc. Japan **17**, 1100 (1962).
96. D. Korff and R. P. Leavitt, Phys. Lett. A **53**, 351 (1975).
97. R. P. Leavitt and D. Korff, J. Chem. Phys. **74**, 2180 (1981).
98. J. P. Looney and R. M. Herman, J. Quant. Spectrosc. Radiat. Transfer **37**, 547 (1987).
99. P. W. Anderson, Dissertation, Harvard University (1949).
100. P. W. Anderson, Phys. Rev. **76**, 647 (1949); **80**, 511 (1950).
101. C. J. Tsao and B. Curnutte, Jr., J. Quant. Spectrosc. Radiat. Transfer **2**, 41 (1962).
102. R. W. Davies, Phys. Rev. A **12**, 927 (1975).
103. J. E. Lennard-Jones, Proc. Roy. Soc. A **106**, 463 (1924).
104. S. P. Neshyba, R. Lynch, R. Gamache, T. Gabard, and J.-P. Champion, J. Chem. Phys. **101**, 9412 (1994.).
105. T. Oka, *Advances in Atomic and Molecular Physics*, Ed. D. R. Bates, Academic Press, New York, 1973.
106. S. Green, J. Boissolès, and C. Boulet, J. Quant. Spectrosc. Radiat. Transfer **39**, 33 (1988).
107. R. Blackmore, S. Green, and L. Monchick, J. Chem. Phys. **88**, 4113 (1988).
108. J. Boissolès, C. Boulet, D. Robert, and S. Green, J. Chem. Phys. **90**, 5392 (1989).
109. R. Blackmore, S. Green, and L. Monchick, J. Chem. Phys. **91**, 3846 (1989).
110. S. Green, J. Chem. Phys. **92**, 4679 (1990).
111. S. Green, J. Chem. Phys. **93**, 1496 (1990).
112. B. S. Frost, J. Phys. B **9**, 1001 (1976).
113. S. Klarsfeld and C. Deutch, Phys. Rev. A **7**, 2081 (1973).

114. R. Lynch, Ph.D. dissertation, Physics Department, University of Massachusetts Lowell, June 1995.
115. R. Lynch, R. R. Gamache, and S. P. Neshyba, *J. Chem. Phys.* **105**, 5711 (1996).
116. R. R. Gamache, R. Lynch, J. J. Plateaux, and A. Barbe, "Halfwidths and Line Shifts of Water Vapor Broadened by CO₂: Measurements and Complex Robert-Bonamy Formalism Calculations," in press, *J. Quant. Spectrosc. Radiat. Transfer* (1997).
117. R. Lynch, R. R. Gamache, and S. P. Neshyba, "Halfwidths and Line Shifts of H₂O Broadened by N₂ and O₂ in the (301)<--(000) and (221)<--(000) Bands," in press, *J. Quant. Spectrosc. Radiat. Transfer* (1997).
118. R. Lynch, R. R. Gamache, and S. P. Neshyba, "Pressure broadening of H₂O in the (301)<--(000) Band: Effects of angular momentum and close intermolecular interactions," in press, *J. Quant. Spectrosc. Radiat. Transfer* (1997).
119. B. E. Grossmann and E. V. Browell, *J. Mol. Spectrosc.* **138**, 562 (1989).
120. R. R. Gamache, J.-M. Hartmann, and L. Rosenmann, in press, *J. Quant. Spectrosc. Radiat. Transfer* (1997). **52**, 481 (1994).
121. R. R. Gamache, S. P. Neshyba, J. J. Plateaux, A. Barbe, L. Régalia, and J. B. Pollack, *J. Mol. Spectrosc.*, **170**, 131 (1995).
122. L. R. Brown and C. Plymate, *J. Quant. Spectrosc. Radiat. Transfer* (1997). **56**, 263 (1996).
123. A word on nomenclature: Since the relaxation matrix is proportional to $-i$ times the Liouville Scattering matrix, the

halfwidth is the real part of the expression in terms of the Liouville scattering matrix and the line shift is the imaginary part of the same expression.

124. A. Ben-Reuven, *Spectral Line Shapes in Gases in the Binary-Collision Approximation*, in Adv. Chem. Phys. **20**, pp. 235, Ed. I. Prigogine and S. A. Rice, Academic Press, New York, 1975.
125. B. Labani, J. Bonamy, D. Robert, J. M. Hartmann, and J. Taine, J. Chem. Phys. **84**, 4256 (1986).
126. J. M. Hartmann, J. Taine, J. Bonamy, B. Labani, and D. Robert, J. Chem. Phys. **86**, 144 (1987)
127. B. Labani, J. Bonamy, D. Robert, and J. M. Hartmann, J. Chem. Phys. **87**, 2781 (1987).
128. A. Bauer, M. Gordon, M. Kheddar, J. M. Hartmann, J. Bonamy, and D. Robert, J. Quant. Spectrosc. Radiat. Transfer **37**, 531 (1987)
129. J. M. Hartmann, C. Camy-Peyret, J.-M. Flaud, J. Bonamy, and D. Robert, in press, J. Quant. Spectrosc. Radiat. Transfer (1997).**40**, 489 (1988).
130. A. Bauer, M. Gordon, M. Kheddar, J. M. Hartmann, in press, J. Quant. Spectrosc. Radiat. Transfer (1997). **41**, 49 (1989).
131. S. P. Neshyba, and R. R. Gamache, in press, J. Quant. Spectrosc. Radiat. Transfer (1997).**50**, 443 (1993).
132. A. Bauer, M. Godon, J. Carlier, and R. R. Gamache, J. Mol. Spectrosc. **176**, 45 (1996).
133. C. G. Gray and K. E. Gubbins, *Theory of Molecular Fluids*, Clarendon Press, Oxford 1984.
134. C. G. Gray, Can J. Phys. **46**,135 (1968).

135. J. O. Hirschfelder, C. F. Curtiss, and R. B. Bird, *Molecular Theory of Gases and Liquids*, Wiley, New York, 1964.
136. R. R. Gamache, R. Lynch, and S. P. Neshyba, "New Developments in the Theory of Pressure-Broadening and Pressure-Shifting of Spectral Lines of H₂O: The Complex Robert-Bonamy Formalism," in press *J. Quant. Spectros. Radiat. Transfer*, 1997.
137. C. Camy-Peyret and J.-M. Flaud, *Vibration-Rotation Dipole Moment Operator for Asymmetric Rotors.*, in *Molecular Spectroscopy: Modern Research*, Vol. III. pp. 69, Ed. K. N. Rao, Academic Press, New York, 1985.
138. M. R. Aliev and J. K. G. Watson, *Higher-Order Effects in the Vibration-Rotation Spectra of Semirigid Molecules*, in *Molecular Spectroscopy: Modern Research*, Vol. III. pp. 1, Ed. K. N. Rao, Academic Press, New York, 1985.
139. S. L. Shostak and J. S. Muentzer, *J. Chem. Phys.* **94**, 5883 (1991).
140. Y. Luo, H. Agren, O. Vahtras, P. Jorgensen, V. Spirko, and H. Hettema, *J. Chem. Phys.* **98**, 7159 (1993).
141. The choice of units for Eqs. (14) and (15) is made to keep the expressions as concise as possible. For conversion to other units see for example Ref. 133, pp. 575.
142. G. Yamamoto and T. Aoki, *JQSRT* **12**, 227 (1972).
143. M. N. Moazzen-Ahmadi and J. A. Roberts, *J. Mol. Spectrosc.* **96**, 336 (1982).
144. W. H. Flygare and R. C. Benson, *Mol. Phys.* **20**, 225 (1971).

145. F. Mulder, G. Van Dijk, and A. Van der Avoird, *Mol. Phys.* **39**, 407 (1980).
146. D. E. Stogryn and A. P. Stogryn, *Molecular Physics* **11**, 371 (1966).
147. See Ref. 133, pp. 580 for a tabulation of older results.
148. C. Graham, J. Pierrus, and R. E. Raab, *Mol. Phys.* **67**, 939 (1989).
149. J. D. Poll and L. Wolniewicz, *J. Chem. Phys.* **68**, 3053 (1978).
150. J.-P. Bouanich, *J. Quant. Spectrosc. Radiat. Transfer* **47**, 243 (1992).
151. B. E. Grossmann, E. V. Browell, A. D. Bykov, V. A. Kapitanov, V. V. Lazarev, Yu. N. Ponomarev, L. N. Sinitsa, E. A. Korotchenko, V. N. Stroinoval, and B. A. Tikhomirov, *Atm. Opt.* **3**, 617 (1990).
152. J.-M. Flaud and C. Camy-Peyret, private communication, University of Pierre and Marie Curie, Paris, France, 1994.
153. K. P. Huber and G. Herzberg, *"Molecular Spectra and Molecular Structure Constants of Diatomic Molecules,"* Van Nostrand, New York, 1979.
154. L. S. Rothman, R. L. Hawkins, R. B. Wattson, and R. R. Gamache, in press, *J. Quant. Spectrosc. Radiat. Transfer* (1997). **48**, 537 (1992).
155. *CRC Handbook of Physics and Chemistry*, 52nd Edition, R. C. Weast, Editor, The Chemical Rubber Company, Cleveland, OH, 1972.
156. M. P. Bogaard and B. J. Orr, *MPT International Review of Science, Physical Chemistry, Series Two, Vol. 2 Molecular*

- Structure and properties* (ed. A. D. Buckingham), Chapter 5, Butterworths, London (1975).
157. A. Lofthus, *The Molecular Spectrum of Nitrogen*, Department of Physics, University of Oslo, Blindern, Norway, Spectroscopic Report No. 2, 1 (1960).
 158. Y. Tanaka, A. S. Jursa, and F. J. LeBlanc, *J. Chem. Phys.* **32**, 1199 (1960).
 159. H. Beutler and H. O. Junger, *Zeit. f Physik* **100**, 80 (1936).
 160. R. R. Gamache, R. Lynch, and L. R. Brown, in press, *J. Quant. Spectrosc. Radiat. Transfer* (1997).**56**, 471 (1996).
 161. C. P. Rinsland, NASA Langley Research Center, Private communication, 1992.
 162. L. S. Rothman, R. R. Gamache, A. Goldman, L. R. Brown, R. A. Toth, H. M. Pickett, R. L. Poynter, J.-M. Flaud, C. Camy-Peyret, A. Barbe, N. Husson, C. P. Rinsland and M. A. H. Smith, "The HITRAN Database: 1986 Edition," *Appl. Opt.* **26**, 4058 (1987).
 163. R. Tipping, University of Alabama, Private communication, 1992.
 164. C. P. Rinsland, NASA Langley Research Center, Private communication, 1994
 165. L. Brown and D. B. Peterson, *J. Mol. Spectrosc.* in press, 1994.
 166. A. S. Pine, V. N. Markov, G. Buffa, and O. Tarrini, *J. Quant. Spectrosc. Radiat. Transfer* **50**, 337 (1993).
 167. G. Herzberg, "Molecular Spectra and Molecular Structure III. Electronic Spectra and Electronic Structure of Polyatomic Molecules," p 505-506, Van Nostrand, New York, 1966.

168. V. Malathy Devi, C. P. Rinsland, M. A. H. Smith, D. C. Benner, and B. Fridovitch, Appl. Opt. **25**, 1844 (1986).
169. John Selby, Northrup-Grumman Corp, private communication, 1996.
170. Richard Wattson, Stewart Radiance Laboratory, private communication, 1996.

9.0 ACKNOWLEDGMENTS

We would like to thank the following individuals for helpful discussions and for providing results prior to publication: (In no particular order) Aaron Goldman, Mary Ann Smith, Curtis P. Rinsland, John Selby, Richard Wattson, James K. G. Watson, Dick Tipping, Jean-Marie Flaud, Claude Camy-Peyret, Wes Cobb, Linda Brown, Bob Hawkins, and Laurence Rothman.